1-1-2010

# Dynamic time-history response of concrete rectangular liquid storage tanks

Amirreza Ghaemmaghami
*Ryerson University*

# DYNAMIC TIME-HISTORY RESPONSE OF CONCRETE RECTANGULAR LIQUID STORAGE TANKS

By

Amirreza Ghaemmaghami

M.A.Sc., Sharif University, Tehran, Iran, 2002

A dissertation

presented to Ryerson University

in partial fulfillment of the

requirements for the degree of

Doctor of Philosophy

In the program of

Civil Engineering

Toronto, ON, Canada, 2010

I hereby declare that I am the sole author of this thesis.

I authorize Ryerson University to lend this thesis to other institutions or individuals for the purpose of scholarly research.

Amirreza Ghaemmaghami

I further authorize Ryerson University to reproduce this thesis by photocopying or by other means, in total or in part, at the request of other institutions or individuals for purpose of scholarly research.

Amirreza Ghaemmaghami

# ABSTRACT

## DYNAMIC TIME-HISTORY RESPONSE OF CONCRETE RECTANGULAR LIQUID STORAGE TANKS

**Doctor of Philosophy 2010**

**Amirreza Ghaemmaghami**

**Civil Engineering**

**Ryerson University**

In this study, the finite element method is used to investigate the seismic behaviour of concrete, open top rectangular liquid tanks in two and three-dimensional spaces. This method is capable of considering both impulsive and convective responses of liquid-tank system. The sloshing behaviour is simulated using linear free surface boundary condition. Two different finite element models corresponding with shallow and tall tank configurations are studied under the effects of all components of earthquake record. The effect of earthquake frequency content on the seismic behaviour of fluid-rectangular tank system is investigated using four different seismic motions including Northridge, El-Centro, San-Fernando and San-Francisco earthquake records. These records are scaled in such a way that all horizontal peak ground accelerations are similar. Fluid-structure interaction effects on the dynamic response of fluid containers are taken into account incorporating wall flexibility. A simple model with viscous boundary is used to include deformable foundation effects as a linear elastic medium. Six different soil types are considered. In addition the application of slat screens and baffles in reducing the sloshing height of liquid tank is investigated by carrying out a parametric study.

The results show that the wall flexibility, fluid damping properties, earthquake frequency content and soil-structure interaction have a major effect on seismic behaviour of liquid tanks and should be considered in design criteria of tanks. The effect of vertical acceleration on the dynamic response of the liquid tanks is found to be less significant when horizontal and vertical ground motions are considered together. The results in this study are verified and compared with those obtained by numerical methods and other available methods in the literature.

## Acknowledgements

Like the waves of the sea, our essence is defined by perpetual motion. This work marks the end to only a part of my journey and hopefully, the beginning of yet another. This journey would not be possible without the help, encouragement, friendship, and guidance of so many people, to all of whom I wish to express my sincere thanks. I am especially grateful to all my teachers, the first of whom were my parents. This thesis is dedicated to them for teaching me the value of education and instilling in me the capacity of reasoning. It is also dedicated to them for their unconditional love, support, and sacrifice over all these years.

I wish to express my deepest gratitude to my supervisor Professor Reza Kianoush whose insight, guidance, meticulous review, and criticism of the work had a significant impact not only on this thesis but also on my perception of research in computational mechanics.

His inspirational attitude toward research, trust in his graduate students, and insight into the problems left a significant impression on this work. I cannot thank him enough as my life will always bear an imprint of his teachings and vision. I would also like to thank the committee for their revisions and suggestions.

Hereby, I take the chance to sincerely thank my previous supervisor, Professor Mohsen Ghaemian who introduced this field to me and was a source of encouragement through my post-graduate studies. I also wish to thank all my colleagues in the Civil Engineering Department at Ryerson University.

Finally, I am very grateful for the financial support provided by Ryerson University in the form of a scholarship.

# Table of contents

# List of Figures

# List of Tables

# List of Symbols

**Roman symbols**

| | |
|---|---|
| a | Length of liquid tank |
| b | Width of liquid tank |
| C | Damping matrix |
| $e_x$, $e_y$, $e_z$ | Unit vectors in x,y and z directions |
| $E_c$ | Modulus of elasticity of concrete |
| $E_f$ | Modulus of elasticity of foundation |
| $F_D$ | Damping force |
| $F_I$ | Inertial force |
| $F_S$ | Stiffness force |
| g | Acceleration gravity |
| $h_0$ | Height of impulsive mass in mechanical model |
| $h_l$ | Fluid height in tank model |
| $h_n$ | Height of convective mass in mechanical model |
| $h_w$ | Tank height |
| K | Stiffness matrix |
| $k_n$ | Equivalent stiffness of spring in simplified mechanical model |
| $L_x$ | Half of the length of liquid tank |
| $L_y$ | Half of the width of liquid tank |
| M | Mass matrix |
| $m_0$ | Equivalent liquid mass attached to tank wall in mechanical model |
| $m_l$ | Mass of contained liquid |
| $m_n$ | Equivalent mass of oscillating liquid in mechanical model |
| N | Shape function matrix |
| $n$ | Sloshing mode number |
| **n** | unit vector normal to the wetted surface |
| $P$ | Fluid pressure |

| | |
|---|---|
| Q | Coupling matrix |
| $t_w$ | Thickness of liquid tank wall |
| *u,v,w* | Components of fluid velocity in x,y and z directions |
| $\ddot{u}$ | Relative acceleration of structure |
| $\ddot{u}_g$ | Ground acceleration |
| $v_p$ | Wave propagation velocity |
| $W_c$ | Convective mass |
| $W_i$ | Impulsive mass |
| $W_L$ | Total mass of liquid |
| *X(t)* | Transient ground displacement |
| x-y-z | Local coordinates |
| X-Y-Z | Global coordinates |

**Greek symbols**

| | |
|---|---|
| $\alpha$ | Angular oscillation of liquid tank model |
| $\beta$ | absolute values of the normal vector on the boundary in the global directions of *Y* |
| $\Phi$ | Velocity potential of fluid motion |
| $\rho_l$ | Fluid density |
| $\delta$ | Displacement of the free surface |
| $\Omega$ | Principle frequency of horizontal ground motion |
| $\omega$ | Natural frequency of liquid wave |
| $\eta$ | absolute values of the normal vector on the boundary in the global directions of *X* |
| $\nu$ | Poisson's ratio |
| $\xi$ | Damping ratio |

# Chapter 1
# Introduction

## 1.1 General overview

The dynamic interaction between fluid and structure is a significant concern in many engineering problems. These problems include systems as diverse as off-shore and submerged structures, biomechanical systems, aircraft, suspension bridges and storage tanks. The interaction can drastically change the dynamic characteristics of the structure and consequently its response to transient and cyclic excitation. Therefore, it is desired to accurately model these diverse systems with the inclusion of fluid-structure interaction (FSI).

One of the critical lifeline structures which have become widespread during the recent decades is liquid storage tank. These structures are extensively used in water supply facilities, oil and gas industries and nuclear plants for storage of a variety of liquid or liquid-like-materials such as oil, liquefied natural gas (LNG), chemical fluids and wastes of different forms.

In addition, liquid tanks have been used as an efficient means of increasing the energy dissipation of structures in recent decades. These tanks can be attached to the structures as an external or auxiliary damping device either during initial construction or at a later stage in order to increase the damping characteristics of the structures.

Liquid tanks are exposed to a wide range of seismic hazards and interaction with other sectors of built environment. Heavy damages have been reported due to strong earthquakes such as Niigata in 1964, Alaska in 1964, Parkfield in 1966, Imperial County in 1979, Coalinga in 1983, Northridge in 1994 and Kocaeli in 1999, some of which are reported by Haroun and Ellaithy (1985), Rai (2002) and Sezen et al. (2006).

The advances in predictive computational simulations help engineers to foresee potential failures and design accordingly. In the past few decades, the desire to efficiently design these systems has resulted in a great surge in creation of mechanical models for predicting FSI effect on liquid tank behaviour. From a numerical perspective, simulation of these systems can be carried out using either frequency domain based or time domain based models. The former method is more convenient for design applications while the latter one is more realistic in predicting the seismic behaviour of tank-fluid interaction under recorded earthquakes.

The focus of this study is on the development of a finite element formulation to investigate the dynamic behaviour of liquid tanks undergoing base excitation. Finite element method (FEM) has been employed widely in predicting the FSI phenomenon in similar systems such as dam-reservoir-foundation models. However, some major differences are noticeable between governing factors of liquid storage tank and concrete dam behaviours due to the amount of contained water and boundary conditions.

Problems associated with liquid tanks involve many fundamental parameters. In fact, the dynamic behaviour of liquid tanks is governed by the interaction between fluid and structure as well as soil and structure along their boundaries. On the other hand, structural flexibility, tank configuration, fluid properties and soil characteristics are the factors which are of great importance in analyzing the tank behaviour. It has been found that hydrodynamic pressure in a flexible tank can be significantly higher than the corresponding rigid container due to the interaction effects between flexible structure and contained liquid. The hydrodynamic pressure induced by earthquake can usually be separated into impulsive and convective terms. The impulsive component is governed by the interaction between tank wall and liquid and is highly

dependent on the flexibility of the wall while the convective component is induced by slosh waves.

At instances, momentum changes of the contained fluid can result in substantial slosh-induced loads, which may adversely affect the dynamic behaviour and structural integrity. The liquid sloshing can result in highly localized pressure on the tank walls (and roofs if presented) which is highly dependent on the tank configuration and seismic characteristics of the applied load.

At present, most of the current design codes such as ACI 350.6 (2006) consider the rigid wall boundary condition to calculate the hydrodynamic pressure. For the case of concrete liquid tanks, the effect of flexibility on dynamic behaviour still needs more investigation. In addition, rectangular liquid tanks are commonly analyzed using a two-dimensional model supported on the rigid foundation. Such assumptions may be unrealistic and need further investigations.

The aim of this study is to gain a better understanding of the actual behaviour of rectangular concrete tanks under earthquake loading. This may lead to some recommendations for possible modifications to the current codes and standards.

### 1.2 Methods of liquid tank analysis

Seismic analysis of concrete rectangular tanks, whenever possible, should start with simplified methods and progress to a more refined analysis as needed. A simplified analysis establishes a baseline for comparison with the refined analyses, as well as providing a practical method to determine if seismic loading controls the design, and thereby offers useful information for making decisions about how to allocate resources. In some cases, it may also provide a preliminary indication of the parameters significant to the structural response. The simplified methods for computation of structural forces consist of the pseudo-static or single – mode

response spectrum analysis. The response spectrum mode superposition is the next level in progressive dynamic analysis. The response spectrum mode superposition fully accounts for the multimode dynamic behaviour of the structure, but it provides only the maximum values of the response quantities.

Finally, the time-history method of analysis is used to compute deformations, stresses and section forces more accurately by considering the time-dependent nature of the dynamic response to earthquake ground motion. This method also better represents the foundation-structure and fluid-structure interaction effects.

### 1.2.1 Simplified procedures

Simplified procedures are used for preliminary estimates of stresses and section forces due to earthquake loading. The traditional seismic coefficient is one such procedure employed primarily for the analysis of rigid or nearly rigid hydraulic structures. In this procedure the inertia forces of the structures and the added mass of water due to the earthquake shaking are represented by the equivalent static forces applied at the equivalent center of gravity of the system. The inertia forces are simply computed from the product of the structural mass or the added mass of water times an appropriate seismic coefficient in accordance with design codes.

If the water is assumed to be incompressible, the fluid-structure interaction for a hydraulic structure can be represented by an equivalent added mass of water. This assumption is generally valid in cases where the fluid responses are at frequencies much greater than the fundamental frequency of structure. These approximations are described by original and generalized Westergaard's methods, velocity potential method for Housner's water sloshing model and Chopra's procedure for intake-outlet towers and submerged piers and shafts (Westergaard (1938), Housner (1957) and Chopra and Liaw (1975)).

### 1.2.2 Response-spectrum modal analysis

The maximum linear elastic response of concrete liquid tanks can be estimated using the response spectrum mode superposition method. The procedure is suitable for the design, but it can also be used for the evaluation of liquid tanks subjected to ground motions which produce linear elastic response. In response spectrum analysis, the maximum values of displacements, stresses and section forces are first computed separately for each individual mode and then combined for all significant modes and multi-component earthquake input. The modal responses due to each component of ground motion are combined using either the square root of the sum of the squares (SRSS) or the complete quadratic combination (CQC) method. The SRSS combination method is adequate if the vibration modes are well separated. Otherwise the CQC method may be required to account for the correlation of the closely spaced modes. Finally the maximum response values for each component of ground motion are combined using the SRSS or percentage methods in order to obtain the maximum response values due to multi-component earthquake excitation. The response spectrum method of analysis, however, has certain limitations that should be considered in the evaluation of the results. All computed maximum response values including displacements, stresses, forces and moments are positive and generally non-concurrent. Therefore, a plot of deformed shapes and static equilibrium checks cannot be performed to validate the results.

Other limitations of the response-spectrum method are that the structure-foundation and structure-water interaction effects can be represented only approximately and that the time-dependent characteristics of the ground motion and structural response are ignored.

### 1.2.3 Time-history analysis

Time-history earthquake analysis is conducted to avoid many limitations of the response spectrum method and to account for the time-dependent response of the structure and better representation of the foundation-structure and fluid-structure interaction effects. The earthquake input for time-history analysis is usually in the form of acceleration time-histories that more accurately characterize many aspects of earthquake ground motion such as duration, number of cycles, presence of high energy pulse and pulse sequencing. Time-history analysis is also the only appropriate method for estimation the level of damage in structures. Response history is computed in the time domain using a step by step numerical integration or in the frequency domain by applying Fourier transformation.

## 1.3 Objectives and scope of the study

The main purpose of the present study is to comprehensively investigate the time-history dynamic response of concrete rectangular liquid storage tanks under earthquake ground motions. In this thesis, a finite element approach is developed to consider the seismic behaviour of liquid tanks incorporating slosh wave, wall flexibility, three-dimensional geometry, earthquake frequency content and soil-foundation interaction. Also, the application of screen slats in increasing the intrinsic damping of the liquid is discussed in this thesis.

The complete system consisting of the structure, the water and the foundation region is modeled and analyzed as a single composite structural system. Similar to substructure approach, the structure is modeled as assemblage of finite elements with appropriate degrees of freedom. The liquid is modeled based on FE discretization of Laplace equation adopted from fluid mechanics. This method is sufficiently accurate to account for the interaction between liquid and

structure. The foundation region is represented by a finite element system accounting for the flexibility of the soil and energy absorption in boundaries using viscous boundary condition.

In order to implement the finite element model, the ANSYS (2004) software which is capable to take the fluid-tank-soil interaction into account is used. Due to some limitation of ANSYS, additional FE subroutines are incorporated into the main program to accurately model the sloshing behaviour. The validity of proposed FEM is considered by comparing the FE results with those obtained by analytical methods for particular conditions. On this basis, the seismic response of liquid tank can be calculated in terms of impulsive and convective components. The scope of this study is summarized below:

(1) Develop a finite element method (FEM) for the purpose of dynamic analysis of rectangular tanks in time domain based on the governing equations of the tank-liquid system and related boundary conditions using ANSYS computer program.

(2) Study the effect of wall flexibility on the structural response and determine the impulsive and convective hydrodynamic pressure distributions for two different tank configurations.

(3) Compare the response of two and three-dimensional liquid tank models. The effect of three-dimensional geometry is investigated in terms of structural responses, hydrodynamic pressure distributions and sloshing heights.

(4) Analyze rectangular tanks under both horizontal and vertical ground motions to investigate the effect of vertical excitation on the dynamic response.

(5) Study the effect of earthquake frequency content on the impulsive and convective components of structural responses using different seismic records applied in finite element procedure.

(6) Investigate the effect of soil-structure interaction on the overall dynamic responses of liquid tanks using simplified elastic soil medium and viscous boundary condition.

(7) Carry out numerical modeling of slat screens as a mean to increase intrinsic damping and to reduce the sloshing height in rectangular tanks for a proposed tank configuration applicable in tall buildings.

It should be noted that this study is limited to open top tanks, linear elastic analysis of walls and soil medium and linear theory of convective behaviour of fluid.

### 1.4 Thesis layout

This thesis is divided into eight chapters. In Chapter 1 the objectives and the scope of thesis is described. A summary of the previous studies done on dynamic response of liquid tanks is presented in Chapter 2.

Chapter 3 discusses mathematical formulation of the dynamic behaviour of rectangular liquid tanks under seismic loads. The basic theory in relation to surface wave or potential flow is presented. Special attention is paid to derivation of response equations for simplified boundary conditions in order to verify the numerical results.

In Chapter 4, finite element formulation of tank-liquid system is derived in two and three-dimensional space. In addition, finite element implementation of fluid damping characteristics is discussed. Moreover, the differences between rigid and flexible wall boundary conditions are highlighted in this Chapter.

Chapter 5 presents the dynamic response of rectangular tanks in two and three-dimensional spaces using finite element method. Both rigid and flexible wall boundary conditions are considered in two-dimensional finite element model to investigate the effect of wall flexibility on

the seismic response of liquid-tank system. In addition, a three-dimensional model of fluid-structure interaction problem incorporating wall flexibility is analysed under the three components of the earthquakes. The results are compared with those obtained for two-dimensional models in order to investigate the effect of three-dimensional geometry on seismic responses of liquid tanks.

In chapter 6, special topics on dynamic response of rectangular concrete tanks are discussed. This chapter is divided into two main parts. First, the dynamic response of liquid tank model is obtained using different ground motions to investigate the effect of earthquake frequency content on both impulsive and convective responses. Second, the effect of deformable foundation on structural responses, sloshing behaviour and dynamic pressure distribution is investigated. The foundation is modelled as a homogeneous flexible media and a viscous boundary condition is used to simulate the energy absorption in truncated boundaries.

Chapter 7 discusses the application of slat screens and baffles in reducing the sloshing amplitude in rectangular tanks. Liquid tanks are used as external dampers to mitigate the seismic responses of various structures such as tall buildings. To reach an optimum design, the amount of inherent damping of liquid should be high enough to reduce the response. In this chapter, the effect of slat screens and baffles on increasing the liquid damping is numerically simulated using finite element method for different configurations.

Finally, a summary and major conclusions reached from the study are described in Chapter 8. In addition, a detailed comparison between current finite elements results and other available methods in literature is given in this chapter. Some recommendations for further studies are also presented.

# Chapter 2
# Literature review

## 2.1 Introduction

The previous research work related to dynamic behaviour of liquid tanks is presented in this chapter. The performance of liquid tanks under earthquakes and some reported damages are presented in section 2.2. Different models used in general analysis of fluid storage tanks are discussed in section 2.3 and the major contributions from past studies are described in this section. Finally, some related information is presented as this subject links to many engineering fields. The design codes and other special topics including soil-structure interaction and application of slat screens in reducing sloshing height are introduced in section 2.4.

## 2.2 Importance of liquid storage tank performance under earthquake

The seismic performance of storage tanks is a matter of special importance, extending beyond the value of the tank and contents. Without an assured water supply, uncontrolled fires subsequent to a major earthquake may cause more damage than the earthquake itself, as occurred in the great 1906 San Francisco earthquake. Safe supplies of drinking water are also essential immediately following destructive earthquakes to avoid outbreak of disease. Consequently, water supply reservoir must remain functional after earthquakes. Failure of tanks containing highly inflammable petroleum products has frequency led to extensive uncontrolled fires as occurred.

Heavy damages have been reported due to strong earthquakes such as Niigata in 1964, Alaska in 1964, Parkfield in 1966, Imperial County in 1979, Coalinga in 1983, Northridge in 1994,

Kocaeli in 1999 and Bhuj in 2001 some of which are reported by Haroun and Ellaithy (1985), Rai (2002) and Sezen et al. (2006).

Damage to steel tanks has frequently reported during past earthquakes. In this case, tank damage or failure generally manifests itself in one of the following ways:

- Buckling of the shell, precipitated by axial compression due to overall bending or beamlike action of the structure which is common in cylindrical steel tanks
- Damage to the roof, caused by sloshing of the upper part of the contained liquid with insufficient freeboard between the liquid surface and the roof
- Fracture of wall-base connection in tanks partially restrained or tanks unrestrained against up-lift

Concrete tanks have also suffered significant damage. For example, many elevated concrete tanks failed, or severely damaged in the 1960 Chilean earthquake and 2001 Bhuj earthquake. In addition, major damages to buried concrete rectangular tanks have been reported by Anshel (1999) during 1995 Kobe earthquake. In general, damages to concrete tanks are categorized as below:

- Leakage in the connection between the reservoir and adjoining walls and vertical cracks in expansion joints
- Failure of the supporting systems for the elevated tanks

Besides, there are many other types of damages to both steel and concrete liquid tanks such as foundation failure or differential settlements.

Based on observations from previous earthquakes, it is concluded that liquid storage tanks can be subjected to large hydrodynamic pressure during earthquakes. In concrete tanks, additional stresses could be resulted from large inertial mass of concrete which could lead to cracking,

leakage or even collapse of the structure. These damages and failures of liquid storage tanks in the past earthquakes attract many practicing engineers and researches to study this problem in order to improve the behaviour of these structures.

It should be noted that very little damage has been reported in concrete rectangular tanks due to poor earthquakes. However, little knowledge on the seismic behaviour of concrete rectangular tanks is available in the literature. The objective of this study is to evaluate the performance of concrete rectangular tanks under seismic loading.

### 2.3 Previous research

Extensive research work on dynamic response of liquid storage tanks commenced in the late 1940's. Originally, this was on dynamic response of the fuel tank in aerospace engineering. The main difference in studies on dynamic response of fuel tanks and those in civil engineering is that the latter is more concerned with response of much larger tanks so the dominant response frequencies are different.

As mentioned before, the dynamic behaviour of liquid tanks is governed by the interaction between fluid and structure as well as soil and structure along their boundaries. On the other hand, structural flexibility, fluid properties, soil characteristics and earthquake frequency content are the factors which are of great importance in analyzing the tank behaviour.

Heavy damages to liquid tanks under earthquakes demonstrated the need for a reliable technique to assess their seismic safety. The Alaska earthquake of 1964 caused the first large-scale damage to tanks and profoundly influenced the research into their vibrational characteristics. Prior to that time, the development of seismic response theories of liquid storage

tanks considered the container to be rigid and focused attention on the dynamic response of contained liquid.

One of the earliest of these studies has been reported by Hoskins and Jacobsen (1934) on analytical and experimental investigation of hydrodynamic pressure developed in rectangular tanks when subjected to horizontal motion.

Later, Housner (1957 and 1963) formulated an idealization, commonly applied in civil engineering practice, for estimating liquid response in seismically excited rigid, rectangular and cylindrical tanks. The fluid was assumed incompressible and inviscid. In this method, the hydrodynamic pressure induced by seismic excitations is separated into impulsive and convective components using lumped mass approximation. The impulsive pressure is caused by the portion of liquid accelerating with the tank and the convective pressure is caused by the portion of liquid oscillating in the tank. On this basis, Housner developed simplified expressions to approximate these pressures by lumped mass approach. The lumped mass in terms of impulsive pressure is rigidly connected with the tank wall and the lumped mass in terms of convective pressure is connected to the tank wall using springs as shown in Figure 2.1. This model has been adopted with some modifications in most of the current codes and standards.

Later, Epstein (1976) presented the design curves according to Housner's model for estimating the bending and overturning moment induced by hydrodynamic pressure for both cylindrical and rectangular tanks.

The first use of a computer program in analyzing fluid-structure interaction problem was reported by Edwards (1969). The finite element method was used with refined shell theory to predict stresses and displacements in a cylindrical liquid-filled container which its height to

diameter ratio was smaller than one. This investigation treated the coupled interaction between elastic wall of the tank and contained fluid.

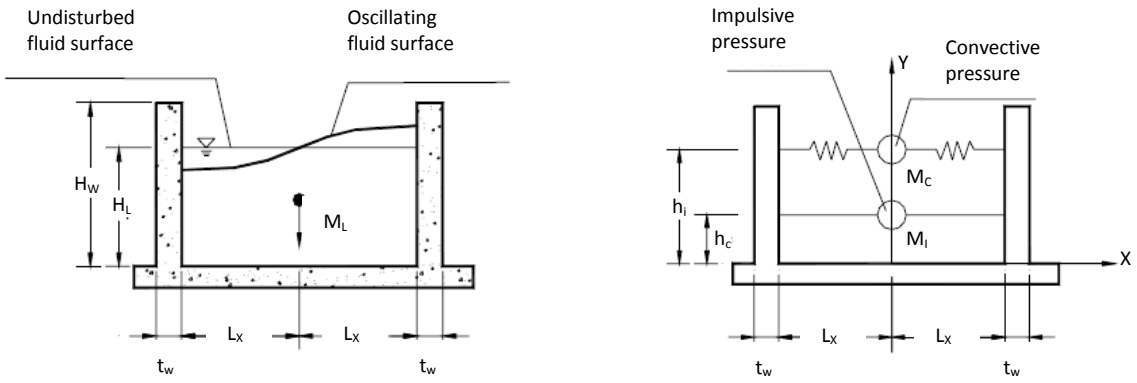


(a) Fluid motion in the tank (b) Mechanical model of liquid

Figure 2.1: Housner's model

Yang (1976) studied the effects of wall flexibility on the pressure distribution in liquid and corresponding forces in the tank structure through an analytical method using a single degree of freedom system with different modes of vibrations. Also, Veletsos and Yang (1977) developed flexible anchored tank linear models and found that the pressure distribution for the impulsive mode of rigid and flexible tanks were similar, but also discovered that the magnitude of the pressure was highly dependent on the wall flexibility.

It was found that hydrodynamic pressure in a flexible tank can be significantly higher than the corresponding rigid container due to the interaction effects between flexible structure and contained liquid.

Minowa (1980 and 1984) investigated the effect of flexibility of tank walls and hydrodynamic pressure acting on the wall. Also, experimental studies were carried out to determine the dynamic characteristics of rectangular tanks.

Haroun (1984) presented a very detailed analytical method in the typical system of loading in rectangular tanks. Seismically induced bending moments in the walls of rectangular concrete liquid storage tanks were evaluated. The tank was assumed to be subjected to simultaneous horizontal and vertical components of earthquake excitations. The liquid was assumed to be homogeneous, inviscid, and incompressible. Hydrodynamic pressures were calculated using the classical potential flow approach and were compared with those obtained from approximate analyses. Typical systems of loadings were identified and applied on the walls which were assumed to behave as elastic plates. Analytical expressions for the computation of internal moments were presented, and numerical values of moment coefficients were tabulated for use in seismic design analysis of tank walls. In addition, Haroun (1983) carried out a series of experiments including ambient and forced vibration tests. Three full scale water storage tanks were tested to determine the natural frequencies and mode shapes of vibrations. Also, Haroun and Tayel (1985) used the finite element method (FEM) for analyzing dynamic response of liquid tanks subjected to vertical seismic ground motions. A method for analyzing the earthquake response of elastic, cylindrical liquid storage tanks under vertical excitations was presented. The method was based on superposition of the free axisymmetrical vibrational modes obtained numerically by the finite element method. The validity of these modes was verified analytically and the formulation of the load vector was confirmed by a static analysis. Two types of ground excitations in the form of step functions and recorded seismic components were used. The radial and axial displacements were computed and the corresponding stresses were presented. Both fixed and partly fixed tanks were considered to evaluate the effect of base fixity on tank behaviour. Finally, tank response under the simultaneous action of both vertical and lateral

excitations was calculated to evaluate the relative importance of the vertical component of ground acceleration on the overall seismic behaviour of liquid storage tanks

Veletsos and Tang (1986) analyzed liquid storage tanks subjected to vertical ground motion on both rigid and flexible supporting media. It was shown that soil-structure interaction reduces the hydrodynamic effects.

Haroun and Abou-Izzeddine (1992) conducted a parametric study of numerous factors affecting the seismic soil-cylindrical tank interaction under both horizontal and vertical excitations using a lumped-parameters idealization of foundation.

Veletsos et al. (1992) presented a refined method for evaluating the impulsive and convective components of response of liquid-storage tanks. They found that the convective components of response are insensitive to the flexibilities of the tank wall and supporting soils, and may be computed considering both the tank and the supporting medium to be rigid.

Kim et al. (1996) further developed analytical solution methods and presented the response of filled flexible rectangular tanks under vertical excitation. Their method is simple and convenient for practical purpose but the flexibility of wall was not thoroughly considered. Park et al. (1992) performed research studies on dynamic response of the rectangular tanks. They used the boundary element method (BEM) to obtain hydrodynamic pressure distribution and finite element method (FEM) to analyze the solid wall.

Subhash and Bhattacharyya (1996) developed a numerical scheme using finite element technique to calculate the sloshing displacement of liquid and pressure developed to such sloshing. Koh et al. (1998) presented a coupled BEM-FEM, including free sloshing motion, to analyze three-dimensional rectangular storage tanks subjected to horizontal ground motion. In

this study, the tank structure was modeled using the finite element method and the fluid domain using the indirect boundary element method.

Dogangun et al. (1997) investigated the seismic response of liquid-filled rectangular storage tanks using analytical methods, and the finite element method implemented in the general purpose structural analysis computer code SAPIV. The liquid was assumed to be linear-elastic, inviscid and compressible. A displacement-based fluid finite element was employed to allow for the effects of the liquid. The effectiveness of the Lagrangian approach for the seismic design of tanks and the effects of wall flexibility on their dynamic behavior were investigated.

Chen and Kianoush (2005) used the sequential method to calculate hydrodynamic pressure in two-dimensional rectangular tanks including wall flexibility effects. However, fluid sloshing of liquid was ignored in their study. Also, Kianoush and Chen (2006) investigated the dynamic behavior of rectangular tanks subjected to vertical seismic vibrations in a two-dimensional space. The importance of vertical component of earthquake on the overall response of tank-fluid system was discussed. In addition, Kianoush et al. (2006) introduced a new method for seismic analysis of rectangular containers in two-dimensional space in which the effects of both impulsive and convective components are accounted for in time domain.

Livaoglu (2008) evaluated the dynamic behaviour of fluid–rectangular tank–foundation system with a simple seismic analysis procedure. In this procedure, interaction effects were presented by Housner's two mass approximations for fluid and the cone model for soil foundation system.

Ghaemmaghami and Kianoush (2009) investigated the seismic behaviour of rectangular liquid tanks in two-dimensional space. Two different finite element models corresponding with shallow and tall tank configurations supported on rigid base were studied under the effects of both

horizontal and vertical ground motions. Fluid-structure interaction effects on the dynamic response of fluid containers were taken into account incorporating wall flexibility. The results showed that the wall flexibility and fluid damping properties have a major effect on seismic behaviour of liquid tanks. The effect of vertical acceleration on the dynamic response of the liquid tanks was found to be less significant when horizontal and vertical ground motions are considered together.

## 2.4 Other related studies

### 2.4.1 Soil-structure interaction

Concrete rectangular liquid tanks are generally assumed to be supported on the rigid foundation. As a result, very limited research has been done on the soil-structure-fluid interaction effect on seismic behaviour of concrete rectangular tanks. In this section, some important previous findings on soil-structure interaction which are applicable in FE analysis of rectangular tanks are discussed.

A brief review on general methods used in modelling interaction among soil-foundation-structure system is given by Dutta and Roy (2002). There are two currently used procedures for analyzing seismic behaviour of structures incorporating soil structure interaction (SSI): (1) Elastic half space theory based on the pioneer study by Sung (1953), and (2) Lumped parameter method (Bowles (1996)). The strengths and limitations of both methods have been discussed in details in the literature by Seed and Lysmer (1975) and Hall et al. (1976).

When modeling a dynamic problem involving soil structure interaction, particular attention must be given to the soil boundary conditions. Ideally, infinite boundary condition should be surrounding the excited zone. Propagation of energy will occur from the interior to the exterior

boundary region. Since the exterior region is non-reflecting, it absorbs all of the incoming energy. Yet, a finite element analysis is constrained into applying finite size boundaries for the foundations. Those boundaries in turn will reflect the elastic waves which is contrary to the physics of the problem. Wolf and Song (1996) simplified foundation as an isotropic homogeneous elastic medium to simulate the interaction between soil and structure. The near field was modeled using finite elements, and the far field was treated by adding some special boundaries such as springs and dampers. The soil in most cases is a semi-infinite medium, and this unbounded domain should be large enough to include the effect of soil structure interaction as performed in some studies by Clough (1993) and Wilson (2002). According to their findings, a foundation model that extends one tank length in the downstream, upstream and downward directions usually suffices in most cases. This approach permits different soil properties to be assigned to different elements, so that the variation of soil characteristics with depth can be considered.

There are different boundary models available in frequency or time domains. First Lysmer and Kuhlmeyer (1969) developed a viscous boundary model using one-dimensional beam theory. This theory has been commonly used with the FE method. Later, more complex boundary types were used and developed such as damping-solvent extraction (Song and Wolf (1994) and Wolf and Song (1996)), doubly-asymptotic multi directional transmitting boundary (Wolf and Song (1995 and 1996)) and paraxial boundary methods (Anrade (1999)).

### 2.4.2 Application of external dampers in reducing sloshing height

The horizontal ground motion causes the liquid tank to oscillate with vertical displacement of the fluid surface. Reducing the sloshing height will result in decreasing the required height of freeboard and consequently the construction cost.

In addition, an efficient means of increasing the energy dissipation of a structure can be achieved using passive damping systems. The function of a passive damper is to alter the dynamic characteristics of the structure. Tuned liquid damper (TLD) is a common passive control device. A TLD consists of a partially filled liquid tank attached to the structure. The liquid sloshing imparts forces that act against the motion of structure and, thus, reduces the structural responses.

However, the performance of a TLD as a dynamic vibration absorber to reduce building response depends on several parameters such as fluid intrinsic damping value. Optimal damping ratio values, expressed in terms of the ratio of fluid mass to structural mass have been determined for a linear system subjected to sinusoidal excitation by Warburton (1982) and Den Hartog (1956).

The value of the TLD damping ratio relating to the energy dissipated in the boundary layer of liquid tanks is often significantly lower than the value required for the TLD to operate optimally (Tait (2007)). An increase in the TLD damping ratio value can be achieved by placing external dampers inside liquid tanks, such as flat screens and baffles. Thus for a particular tank geometry, the designer can determine the required screen configuration in order to achieve the optimal damping ratio.

The additional inherent damping provided by these devices is often determined using experimental methods some of which are reported by Noji et al. (1984) and Fediw et al. (1995).

Warnitchai and Pinkaew (1998) developed a mathematical model of liquid sloshing in rectangular tanks, which included the effects of damper devices. The theoretical study is focused on the first sloshing mode. It was found that the devices introduced non-linear damping to the sloshing mode and also reduced the modal frequency slightly by added mass effect. The findings

were confirmed by free sloshing experiments. In addition, a flat screen device was chosen for further investigation using shaking table experiments and theoretical analysis.

Gedikli and Ergüven (1999) investigated the effects of a rigid baffle on the seismic response of liquid in rigid liquid tanks. Fluid motion was assumed to be irrotational, incompressible and inviscid. The method of superposition of modes was implemented to compute the seismic response. The boundary element method was used to evaluate the natural modes of liquid.

Kaneko and Ishikawa (1999) developed an analytical model for describing the effectiveness of TLD with submerged nets for suppressing horizontal vibration of structures. Dissipation energy due to the liquid motion under sinusoidal excitation was calculated based on nonlinear shallow water wave theory.

Cho et al. (2002) numerically investigated the parametric eigen characteristics of baffled cylindrical liquid-storage tanks using the coupled structural-acoustic FEM. Various combinations of major baffle parameters were intensively examined, in order for the parametric baffle effects on the natural frequency of baffled tanks.

Modi and Akinturk (2002) focused on enhancing the energy dissipation efficiency of a rectangular liquid damper through introduction of two-dimensional wedge-shaped obstacles. The study was complemented by a wind tunnel test program, which substantiated the effectiveness of this class of dampers in regulating both vortex resonance and galloping type of instabilities.

Cho et al. (2005) conducted the numerical analysis of the resonance characteristics of liquid sloshing in a 2D baffled rectangular tank subjected to the forced lateral excitation. Sloshing flow was formulated based on the linearized potential flow theory, while an artificial damping term was employed into the kinematic free-surface condition to reflect the eminent dissipation effect in resonant sloshing. A FEM program was developed for the resonant sloshing analysis in

frequency domain. Through the numerical analysis of sloshing frequency response with respect to the number, location and opening width of baffle, the sloshing damping characteristics by the baffle were parametrically investigated

Tait et al. (2005) estimated the amount of the energy dissipated by a TLD equipped with slat screens. The importance of their experimental study is that it examines TLD behaviour over a wide range of normalized excitation amplitude values. For screens consisting of a number of thin plate slats, a method for determining the loss coefficient was presented. They concluded that the linear model is capable of providing an initial estimate of the energy dissipating characteristics of a TLD. The nonlinear model can accurately describe the response characteristics within the range of excitation amplitudes experimentally tested.

Tait et al. (2007) examined 2D structure-TLD behaviour over a range of excitation amplitude values covering the practical range of serviceability accelerations for buildings subjected to wind loads. Additional slat screens were placed in liquid tanks to increase the intrinsic damping of fluid. Experimental results were used to verify the applicability of a unidirectional structure-TLD numerical model to 2D structure-TLD analysis.

Finally, Panigrahy et al. (2009) carried out a series of experiments in a developed liquid sloshing setup to estimate the pressure developed on the tank walls and the free surface displacement of water from the mean static level. The square tank was attached to a shaking table. Pressure and displacement studies were done on the basis of changing excitation frequency of the shaking table and fill level in the tank. Experiments were carried out without and with baffles, and the consequent changes in the parameters were observed.

### 2.4.3 Design codes and standards

Fluid-structure effects are considered in design of structures which contain, surround or submerge in fluid when subjected to earthquake loading. Therefore, the basics of this study are similar to other hydro or marine facilities. As an example, the behaviour of a concrete gravity dam reservoirs is governed by same equations as liquid storage tanks. However, the fluid is considered as infinite on one side of boundary for dam. In addition, nuclear reactor facilities include numerous liquid containers with different geometries. These tanks were studied by some research groups reported by ASCE (1984).

There are many standards and codes available for design of liquid containing structures. However, most of them are concerned with steel tanks. One of the most common codes for concrete rectangular tank design is ACI350.3-06 (2006). The first edition of this code was published by ACI committee in 2001 entitled "Seismic Design of Liquid-Containing Concrete Structures and Commentary". The design procedure is based on Housner's model in which the boundary condition is considered rigid and hydrodynamic pressure is treated as added masses applied on the tank wall. The dynamic response of tank wall is analyzed by modeling the tank wall as an equivalent cantilever beam. Such model is also used in the New Zealand Code NZS3106 (2010) "Practice for Concrete Structures for the Storage of Liquids".

NZS3106 (2010) uses mechanical model of Veletsos and Yang (1977) for rigid circular tanks and that of Haroun and Housner (1981) for flexible tanks. For rigid rectangular tanks, the rigid circular tank model is used in which, radius is replaced by half length of tank. For flexible rectangular tanks, it suggests the same procedure as that of rigid rectangular tanks.

In these codes and standards, the amplitude of hydrodynamic pressure due to the flexibility of wall is not fully considered.

Eurocode 8 (1998) mentions mechanical model of Veletsos and Yang (1977) as an acceptable procedure for rigid circular tanks. For flexible circular tanks, models of Veletsos (1984) and Haroun and Housner (1981) are used along with the procedure of Malhotra et. al. (2000). Housner's model (1963) is used for rigid rectangular tanks. The procedure given in NZSEE guidelines is also described in Eurocode 8 for evaluating impulsive and convective mass of circular tank.

An important point while using a mechanical model pertains to combination rule used for adding the impulsive and convective forces. Except Eurocode 8, all codes suggest using the SRSS (square root of sum of square) method to combine impulsive and convective forces. However, in Eurocode 8 absolute summation rule is used.

Finally, requirements and provisions for the design and detailing of the earthquake forces in liquid-containing structure are provided in ASCE 7-05 and other codes such as the IBC 2000, UBC 1997, UBC 1994, BOCA 1996 and SBC 1997.

# Chapter 3

# Mathematical background

## 3.1 Introduction

The calculation of hydrodynamic pressure and slosh wave height are key issues in the analysis of rectangular liquid tanks. These problems are studied in this chapter using analytical formulations. There is a need for an accurate analytical method which is capable of predicting the pressure exerted by the liquid on the tank wall and maximum levels of sloshing to be expected under seismic loading. An example of detailed analytical methods is given by NASA SP-106 (1966) which is established for spacecrafts. However, these analytical methods are limited to special boundary conditions such as rigid walls.

The response of body of fluid to an earthquake is a very complex phenomenon and is dependent on many parameters. When earthquake occurs, fluid is excited and gravity waves are generated on its free surface. The fluid motion imparts a force on tank wall which can be divided into impulsive and convective components. The basic formulation of fluid behaviour in a rigid rectangular tank due to the horizontal excitation is presented in this chapter. Also, a brief discussion on general mechanical models of fluid tanks is given. These mechanical models are commonly used in current design codes and standards. The basic theory of linear sloshing for rigid rectangular tank is reviewed in this chapter.

The equations derived in this chapter can be used to obtain a quick estimate of sloshing frequencies or liquid forces in liquid tank system. It should be noted that most of the equations and solution procedures for rigid tanks are adopted from NASA SP-106 guideline and are revised in such a way to make it applicable for rectangular liquid tanks.

### 3.2 Equivalent mechanical models of sloshing

The main dynamical effect of lateral sloshing is a horizontal oscillation of the liquid center of mass relative to the tank. If a tank with liquid free surface is subjected to horizontal ground acceleration, the forces exerted on the tank wall can be divided into two components. First, when the walls of the tank move back and forth a certain fraction of the water participates in motion which exerts a reactive force on the tank wall which is referred to as impulsive force. Second, the free surface oscillations impart an oscillating force on the tank wall which is referred to convective force. These forces can be equally well represented by an equivalent mechanical model as illustrated in Figure 3.1 in which the mass of liquid is divided into two impulsive and convective parts. The convective mass is connected to the rigid walls by two springs, while the impulsive mass is rigidly attached to the walls. This model has been extended for application in liquid tanks by Housner (1957).

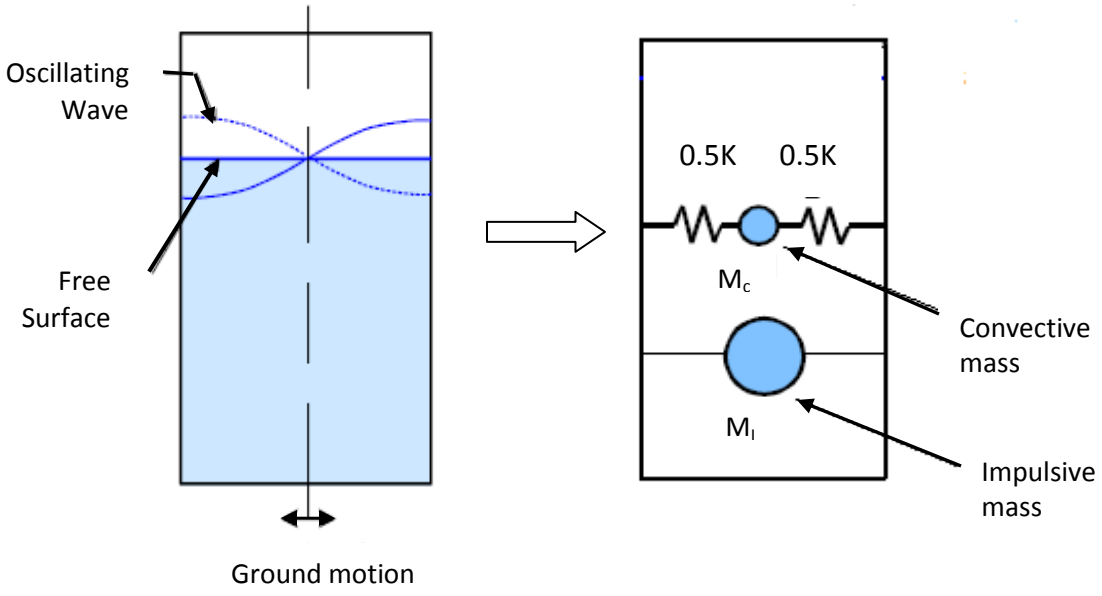


Figure 3.1: Mechanical model of dynamic behaviour of liquid tank

This mechanical model shows that a horizontal motion of the tank causes the liquid to slosh. It also shows that a vertical oscillation of the tank does not generally set the liquid into motion.

The various discussions on dynamic behaviour of liquid-tank system given in this chapter can be more easily understood by keeping in mind the mechanical model as described above.

### 3.2.1 Higher order sloshing response

Figure 3.1 shows a slosh wave that has one peak and one valley. This is the fundamental anti-symmetric wave, and it has the lowest natural frequency. Waves with two or more peaks or valleys with higher natural frequencies can also occur. The mechanical model shown in Figure 3.1 can represent these higher order waves by incorporating an additional sprung mass for each mode. The magnitudes of the sprung mass for these modes are very small compared to the fundamental mode and, thus, higher order modes are usually of little concern.

## 3.3 Mathematical formulation

To explain the basic theory most clearly, the mathematical details of horizontal sloshing are discussed for a rigid tank. It is assumed that the fluid is incompressible, irrotational and inviscid. These assumptions allow classical potential flow theory to be used. The wave motion is also assumed to be linear. In this study, linear motion means that the amplitude of the wave and of the liquid motion is linearly proportional to the amplitude of the applied tank motion, and the natural frequency of the slosh wave is not a function of the wave amplitude. The generalized linear theory is discussed in more details by Fox and Kuttler (1983).

For simplicity, the motion of the tank is assumed to be harmonic, which means that it varies with time as $exp(i\Omega t)$ where $\Omega$ is the frequency of the motion. More complicated time-dependent motions of the tank can be considered by the use of Fourier series or Fourier integrals.

### 3.3.1 Basic differential equations and boundary conditions

Generally, the basic differential equations and boundary conditions for lateral sloshing are most clearly expressed in a Cartesian x,y,z coordinate system, as shown in Figure 3.2. This is therefore the coordinate system used in this section. For a general case, the tank has a translational oscillation along the x, y and z axes as well as rotations around these axes. For clarity, Figure 3.2 shows only one angular oscillation $\alpha_y$ and a roll excitation $\alpha_z$. The x,y,z coordinate system is fixed to and moves with the tank, whereas the inertial X,Y,Z coordinate system is stationary.

Since the liquid is assumed inviscid, irrotational and incompressible, the fluid velocity distribution can be derived from a velocity potential $\Phi$. The x,y,z components of the velocity u,v,w components are computed from the spatial derivative of the potential:

$$u = \frac{\partial \Phi}{\partial x} \quad v = \frac{\partial \Phi}{\partial y} \quad w = \frac{\partial \Phi}{\partial z} \tag{3.1}$$

The basic differential equation that a velocity potential must satisfy everywhere in the liquid volume is the condition of liquid incompressibility, which is given by:

$$\frac{\partial u}{\partial x} + \frac{\partial v}{\partial y} + \frac{\partial w}{\partial z} = 0 \quad \text{or} \quad \nabla^2 \Phi = 0 \tag{3.2}$$

The last form of this equation is written in vector notation and so applies to any coordinate system.

For a potential flow that does not contain vorticity, the fluid dynamics equations of motion can be integrated directly to give the unsteady form of Bernoulli's equation:

$$\frac{\partial \Phi}{\partial t} + \frac{P}{\rho_l} + gz + \frac{1}{2}(u^2 + v^2 + w^2) = f(t) \tag{3.3}$$

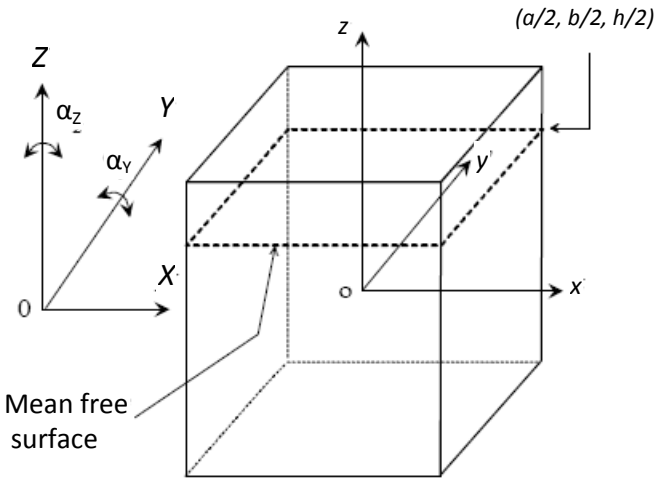


Figure 3.2: Coordinate system used for the derivation of sloshing equations

Where $P$ is the fluid pressure, $\rho_l$ is the fluid density, and $g$ is the acceleration directed in the negative z direction and *f(t)* is the constant of integration.

The velocities *u,v,w* are assumed to be so small that squared and higher power terms of them can be neglected in comparison to linear terms. This means that the equations are linearized. Since only the derivative of the potential has a physical meaning, constants or even functions of time can be added to the definition of $\Phi$ whenever it is convenient. This allows the constant of integration *f(t)* in Eq.3.3 to be absorbed into the definition of $\Phi$. The linearized form of Eq.3.3 is thus:

$$\frac{\partial \Phi}{\partial t} + \frac{P}{\rho} + gz = 0 \tag{3.4}$$

Any mathematical function that is a solution of Eq.3.2 must satisfy the boundary conditions at the tank walls and free surface. Equation 3.4 is used to derive one of the boundary condition at the free surface which is referred to as dynamic boundary condition. The surface is free to move

and the pressure at the surface is equal to zero. Hence, for the liquid at the free surface, the unsteady Bernoulli's equation is written as bellow:

$$\frac{\partial \Phi(x,y,z,t)}{\partial t} + g\delta(x,y,t) = 0 \quad \text{for} \quad z = \frac{h}{2} \tag{3.5}$$

Here, $\delta(x,y,t)$ is the small displacement of the free surface above the undisturbed level *z= h/2*. If the equations were not linearized, Eq.3.5 would have to be evaluated at the actual displaced location z = h/2 + $\delta$ of the surface rather than at the equilibrium location *z = h/2*. The difference between the two conditions (*z = h/2* and *z = h/2 +* $\delta$ ) turns out to be a higher order term in $\delta$ and so can be neglected.

Equation 3.5 is the dynamic condition at the free surface. A kinematic condition is needed to relate the surface displacement $\delta$ to the vertical component of the liquid velocity at the surface. In a linearized form, this condition is simply:

$$\frac{\partial \delta}{\partial t} = w = \frac{\partial \Phi}{\partial z} \quad \text{for} \quad z = \frac{h}{2} \tag{3.6}$$

Equations 3.5 and 3.6 can be combined into a single condition written entirely in terms of $\Phi$ (or $\delta$ ) by differentiating Eq.3.5 with respect to *t*, differentiating Eq.3.6 with respect to z, and combining the two equations to eliminate $\delta$ (or $\phi$ ). The result is:

$$\frac{\partial^2 \Phi}{\partial t^2} + g\frac{\partial \Phi}{\partial z} = 0 \quad \text{for} \quad z = \frac{h}{2} \tag{3.7}$$

Finally, the time derivative of $\Phi$ will involve the natural frequencies of the sloshing. Thus, Eq.3.7 shows that these frequencies are directly related to the gravitational field.

Because viscosity and viscous stresses have been assumed to be negligibly small, the only condition that can be imposed at a wall of the tank is that the liquid velocity perpendicular to the plane of the wall has to be equal to the velocity $V_n$ of the tank wall perpendicular to itself (where

*n* stands for the normal or perpendicular direction). It should be noted that these solutions will allow slipping in a direction parallel to the wall.

If the tank wall is assumed to be rigid, the boundary condition at the wall will therefore just be that the component of the liquid velocity perpendicular to the wall is equal to ground velocity. This condition leads to a unique solution for this boundary value problem. In practice, however, the tank wall is flexible, and the total velocity of the wall is the summation of the ground velocity and its relative velocity due to effect of wall flexibility. This type of boundary value problem can be solved by the using a shape function which should be able to properly estimate the deformation of tank wall.

This chapter will focus on obtaining an analytical solution for impulsive and convective forces assuming rigid wall boundary condition. In addition, the effect of wall flexibility on fundamental periods will be discussed using an analytical approach.

Since the sloshing problem is linear, a series of individual problems can be considered, one for each type of tank motion of interest, and the results added to get the velocity potential for the entire motion. Hence, various kinds of simple tank motion will be considered in turn.

For example, a horizontal ground motion parallel to the x axis is assumed to be applied to the tank-liquid system. For this case, the ground displacement is expressed as $X(t) = -iX_0 \exp(i\Omega t)$. This choice makes the real displacement equal to $X_0 \sin(\Omega t)$. The velocity components of the tank walls are $v = w = 0$ and $u = iX_0\Omega \exp(i\Omega t)$. Thus, the boundary conditions at the wetted surfaces of the tank are expressed as:

$$\mathrm{n}.\nabla\Phi = iX_0\Omega e^{i\Omega t} \tag{3.8}$$

Where **n** is the unit vector normal to the wetted surface. (As an example, for a vertical wall perpendicular to the y-axis, $n.\nabla\Phi$ reduces to $\frac{\partial\Phi}{\partial x}$ and Eq. (3.8) merely states that the x-velocity of the liquid at the wall must equal the imposed x-velocity of the tank).

### 3.3.2 Solution of Equations for a Rectangular Tank

A rectangular tank fits the x,y,z coordinate system shown in Figure 3.2 and since the solutions of Eq.3.2 are familiar trigonometric *sines* and *cosines*, it is used as a detailed example to show how the boundary conditions affect the dynamic behaviour of liquid tank. Initially, the tank is considered to be stationary, and the solutions for this case are conventionally called the eigenfunctions of the problem.

The potential solutions of interest are assumed to be harmonic in time, i.e. $\exp(i\omega t)$. For much of this discussion, the time dependence of $\Phi$ can be ignored, but when time derivatives are needed they are included by multiplying the potential by $i\omega$. The $\Phi(x, y, z)$ Eigen functions are found by the method of separation of variables adopted from NASA SP-106, in which $\Phi(x, y, z)$ is assumed to be the product of three individual functions $\xi(x)$, $\psi(y)$ and $\zeta(z)$ of the coordinates. This assumption is inserted into Eq.3.2 and the entire equation is divided by $\Phi = \xi\psi\zeta$ to give:

$$\frac{1}{\xi}\frac{d^2\xi}{dx^2} + \frac{1}{\psi}\frac{d^2\psi}{dy^2} + \frac{1}{\zeta}\frac{d^2\zeta}{dz^2} = 0 \tag{3.9}$$

Since $\xi$ is only a function of x, $\psi$ is only a function of y, and $\zeta$ is only a function of z, each of the ratios in Eq.3.9 must be independent of any coordinate and so must be equal to a constant.

All the solutions of Eq.3.9 should satisfy the boundary conditions for particular cases. The natural frequencies of the problem, in this case the sloshing frequencies, are determined by the

eigenvalues. Since the natural frequencies will be needed subsequently, they are computed before considering the solutions for cases when the tank is in motion.

The natural frequencies for these two-dimensional waves is found to be:

$$\omega_n^2 = \pi(2n-1)\left(\frac{g}{a}\right)\tanh\left[\pi(2n-1)\left(\frac{h}{a}\right)\right] \tag{3.10}$$

where the subscript *n* indicates that $\omega$ depends on the mode number *n*. The frequency decreases as the depth *h* decreases or the tank width *a* increases. The *n* = 1 mode has the lowest of all natural frequencies.

For a first example, the tank is assumed to oscillate along the x axis. For a rectangular tank, the boundary condition Eq.3.8 therefore reduces to:

$$\frac{\partial\Phi}{\partial x} = \Omega X_0 e^{i\Omega t} \quad \text{for} \quad x = \pm\frac{a}{2}; \quad \frac{\partial\Phi}{\partial \mathrm{y}} = 0 \quad \text{for} \quad y = \pm\frac{b}{2} \tag{3.11}$$

The free surface and bottom boundary conditions are the same as for free oscillations. For this case, the trial solution is assumed to be:

$$\Phi(x,z,t) = \left\{A_0 x + \sum_{n=1}^{\infty} A_n \sin\left[\lambda_n \frac{x}{a}\right]\left\{\cosh\left[\lambda_n \frac{z}{a}\right] + \tanh\left[\lambda_n \frac{h}{2a}\right]\sinh\left[\lambda_n \frac{z}{a}\right]\right\}\right\} e^{i\Omega t} \tag{3.12}$$

For simplicity, the symbol $\lambda_n$ is used for $(2n-1)\pi$ in Eq.3.12 and the product of the integration constants been replaced by another constant $A_n$, where the subscript *n* indicates that the constant depends on the mode in question.

Note that $\partial\Phi/\partial y = 0$ identically and that $\partial\Phi/\partial z = 0$ at the bottom of the tank at $z = -h/2$. So if $A_0$ is chosen to be equal to $\Omega X_0$, the potential $\Phi$ will satisfy all the wall boundary conditions. The requirements for satisfying the free surface condition are now investigated. Substituting $\Phi$ into the free surface condition Eq.3.7 gives:

$$-\Omega^2\left\{\Omega X_0 x+\sum_{n=1}^{\infty}A_n\sin(\lambda_n\frac{x}{a})\left[\cosh(\lambda_n\frac{h}{2a})+\tanh(\lambda_n\frac{h}{2a})\sinh(\lambda_n\frac{h}{2a})\right]\right\}+$$
$$g\left\{\sum_{n=1}^{\infty}A_n(\frac{\lambda_n}{a})\sin(\lambda_n\frac{x}{a})\left[\cosh(\lambda_n\frac{h}{2a})+\tanh(\lambda_n\frac{h}{2a})\sinh(\lambda_n\frac{h}{2a})\right]\right\}=0 \quad (3.13)$$

This equation in effect specifies the integration constants $A_n$ in terms of $X_0$. But to determine them explicitly, the x in the first term of Eq.3.13 has to be written as a Fourier series of $\sin(\lambda_n x/a)$ terms (which is possible because the $\sin(\lambda_n x/a)$ terms are orthogonal over the interval $-a/2 < x < a/2$). This process gives:

$$x=\sum_{n=1}^{\infty}\left(\frac{4a}{\lambda_n^2}\right)(-1)^{n-1}\sin(\lambda_n x/a) \quad (3.14)$$

By replacing the *x* term in Eq.3.13 with this series, terms can be grouped with respect to each $\sin(\lambda_n x/a)$, which allows each $A_n$ to be solved for one at a time (again because the sin terms are orthogonal). The final expression for the velocity potential is found to be:

$$\Phi(x,z,t)=A_0 e^{i\Omega t}\left\{x+\sum_{n=1}^{\infty}\frac{4a(-1)^{n-1}}{\lambda_n^2}\left(\frac{\Omega^2}{\omega_n^2-\Omega^2}\right)\sin\left[\lambda_n\frac{x}{a}\right]\frac{\cosh\left[\lambda_n(z/a+h/2a)\right]}{\cosh\left[\lambda_n\frac{h}{a}\right]}\right\} \quad (3.15)$$

Neglecting the amplitude of the sloshing height will result in a new potential function which is referred to the impulsive behaviour of liquid tank. It should be noted that, in common design practice, the behaviour of liquid tank is usually divided into two parts: convective and impulsive. The convective term is referred to the surface sloshing of the liquid, while the impulsive term is only related to the interaction between wall and liquid without considering the surface sloshing.

Assuming that the amplitude of the sloshing is negligible or $\frac{\partial \Phi}{\partial t} = 0$ at $z = h/2$, the impulsive potential function $\Phi_I$ can be easily obtained:

$$\Phi_I(x,z,t) = A_0 e^{i\Omega t}\left\{ x - \sum_{n=1}^{\infty} \frac{4a(-1)^{n-1}}{\lambda_n^2} \sin\left[\lambda_n \frac{x}{a}\right] \frac{\cosh\left[\lambda_n (z/a + h/2a)\right]}{\cosh\left[\lambda_n \frac{h}{a}\right]} \right\} \tag{3.16}$$

By assuming $\Phi = \Phi_I + \Phi_C$ ,the convective potential function $\Phi_C$ is given:

$$\Phi_C(x,z,t) = A_0 e^{i\Omega t}\left\{ \sum_{n=1}^{\infty} \frac{4a(-1)^{n-1}}{\lambda_n^2} \left( \frac{{\omega_n}^2}{\omega_n^2 - \Omega^2} \right) \sin\left[\lambda_n \frac{x}{a}\right] \frac{\cosh\left[\lambda_n (z/a + h/2a)\right]}{\cosh\left[\lambda_n \frac{h}{a}\right]} \right\} \tag{3.17}$$

### 3.3.3 Resulting forces and moments

The slosh characteristics of most interest in applications are the natural frequencies and the forces and moments exerted on the tank by the sloshing liquid. The forces and moments are determined by integrating the unsteady part of the liquid pressure *p* over the tank wall area. Equation 3.3 (linearized) shows how to determine this pressure in terms of the velocity potential. The differential component of the x-force is $dF_x = \rho dA_x$, where $dA_x$ is the differential element of wall area normal to the x-axis. The x-component of the force, $F_x$, is therefore found by integration:

$$F_x = 2 \int_{-h/2}^{h/2+\delta} \int_{-b/2}^{b/2} p\Big|_{x=a/2} dydz = -2\rho b \int_{-h/2}^{h/2} \frac{\partial \Phi}{\partial t}\Big|_{x=a/2} dz \tag{3.18}$$

Equation (3.18) has been linearized with respect to both the unsteady pressure and the wave amplitude $\delta(x = \pm a/2)$ at the wall, and advantage has been taken of the antisymmetry properties of $\Phi$ to combine the integrals over each wall. Substituting the expression for $\Phi$ from Eq.3.15 and performing the integration gives:

$$\frac{F_{X0}}{-i\Omega^2 X_0 m_l} = 1 + 8\frac{a}{h}\sum_{n=1}^{N}\frac{\tanh[\lambda_n(h/a)]}{\lambda_n^3}\frac{\Omega^2}{\omega_n^2 - \Omega^2} \tag{3.19}$$

Here $F_{X0}$ is the amplitude of the oscillating force, and $m_l = \rho abh$ is the mass of liquid in the tank.

Next, the moment *M* exerted on the tank is computed. This moment acts about the y-axis and is caused by the pressure acting on the x-walls and the bottom of the tank. With the y-axis through the center of mass of the liquid, the differential element of moment is $dM_y = -z(pdA_x) - x(pdA_z)$. Thus the total moment is given by:

$$M_y = 2\left(\int_{-h/2}^{h/2+\delta}\int_{-b/2}^{b/2} zp\Big|_{x=a/2}\, dydz - \int_{0}^{a/2}\int_{-b/2}^{b/2} xp\Big|_{z=-h/2}\, dydx\right) \tag{3.20a}$$

Linearizing and combining terms give:

$$M_y = 2b\int_{-h/2}^{h/2} z\frac{\partial\Phi}{\partial t}\Big|_{x=a/2} dz - 2b\int_{0}^{a/2} x\frac{\partial\Phi}{\partial t}\Big|_{z=-h/2} dx \tag{3.20b}$$

After performing the indicated integrations, simplifying the result with various algebraic and hyperbolic transformations, and rearranging the results to make for easy comparisons with the force, it is found that the moment is given by:

$$\frac{M_{y0}}{-i\Omega^2 X_0 m_l h} = \frac{1}{12}(a/h)^2 + 8(a/h)\sum_{n=1}^{\infty}\frac{\tanh[(\lambda_n(h/a)]}{\lambda_n^3}\times \left\{\frac{1}{2} - \frac{2(a/h)\tanh[\lambda_n(h/2a)]}{\lambda_n} + \frac{g}{h\omega_n^2}\right\}\frac{\Omega^2}{\omega_n^2 - \Omega^2} \tag{3.21}$$

Neglecting the free surface motion, the corresponding x-component of the applied force can be calculated using the potential function in Eq.3.16 as below:

$$\frac{F_{X0}}{-i\Omega^2 X_0 m_l} = 1 - 8\frac{a}{h}\sum_{n=1}^{N}\frac{\tanh[\lambda_n(h/a)]}{\lambda_n^3} \tag{3.22}$$

Similarly, the corresponding moment around y-axis is obtained:

$$\frac{M_{y0}}{-i\Omega^2 X_0 m_l h} = \frac{1}{2} - 8(a/h)\sum_{n=1}^{\infty}\frac{\tanh[(\lambda_n(h/a)]}{\lambda_n^3} \tag{3.23}$$

### 3.4 Analytical derivations of mechanical model parameters

Lateral sloshing was described analytically in the previous sections. Sloshing can have a significant influence on the dynamic behaviour of liquid tanks because the slosh forces and moments interact with the system through a feedback loop. For the purposes of incorporating the dynamic effects of sloshing in the liquid tank analysis, it is convenient to replace the liquid conceptually by an equivalent linear mechanical system. The equations of motion of oscillating point masses and rigid bodies are included more easily in the analysis than are the equations of fluid dynamics. Coupling the equations of motion of a flexible liquid tank to the equations of motion of a continuous liquid is too computationally demanding for ordinary design analyses. However, the interaction between flexible wall and fluid is neglected in these mechanical models. The effect of fluid-structure interaction will be discussed comprehensively using a finite element method in next chapters.

The equations of motion of the model are derived below for the spring-mass form of model. Damping is neglected initially so that a direct comparison can be made with the slosh forces and moments given analytically in previous sections.

Figure 3.3 shows the model and the symbols used in the analysis. The derivation of the model equations given below is independent of tank shape and fluid depth. The system of springs and masses is expected to fit inside the actual tank and replace the liquid. For clarity, only two spring-masses are shown, but there is in fact one spring-mass for each slosh mode.

The spring masses do not have a moment of inertia, so any needed moment of inertia $I_0$ is assigned to the rigidly-attached mass $m_0$. The center of mass of the system is at the same height above the bottom of the tank as the liquid, and the locations $H_n$ of the masses are referenced to the center of mass. The width of the tank is 2*a*. Gravity *g* or an equivalent thrust-induced acceleration acts along the axis of the tank. The tank is excited by a small time-varying linear displacement $X_0$ and the angular rotation $\alpha_0$ is neglected here. The spring masses deflect a distance $x_n$ relative to the tank walls as a result of the tank motion.

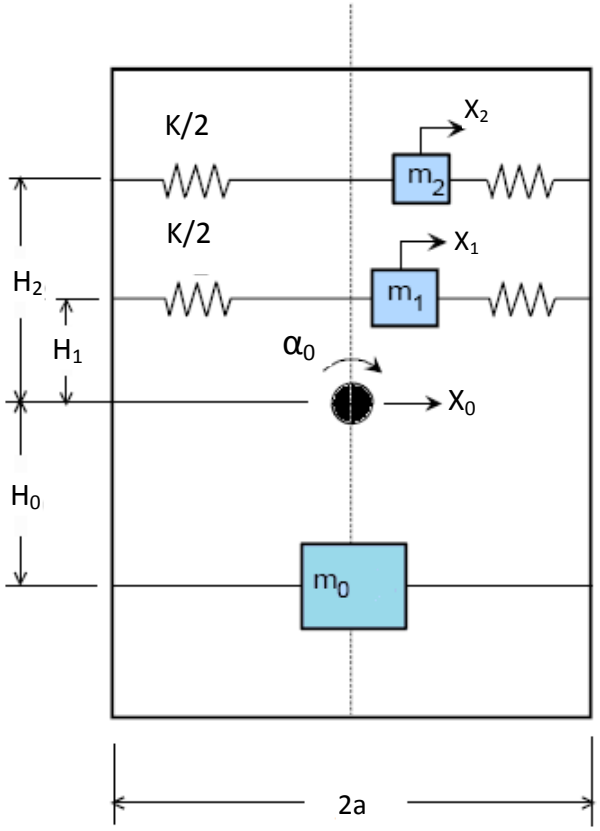


Figure 3.3**:** Schematic of equivalent mechanical model for lateral sloshing

To preserve the static properties of the liquid, the sum of all the masses must be the same as the liquid mass $m_{liq}$, and the center of mass of the model must be at the same elevation as the liquid. These constraints are expressed analytically by:

$$m_0 + \sum m_n = m_{liq} \tag{3.24}$$

$$m_0 H_0 + \sum m_n H_n = 0 \tag{3.25}$$

Equations (3.24) and (3.25) are not sufficient to fix the values of the model parameters. To do that, the model must also duplicate the sloshing forces, moments, and natural frequencies. Duplication of the natural frequencies requires:

$$k_n / m_n = \omega_n^2 \tag{3.26}$$

Where $\omega_n$ is the slosh natural frequency of the *n*th mode. This is a first relation that shows how the spring constant and spring-mass must be chosen; however, the model forces and moments have to be examined to develop other relations.

The net force exerted on the tank in the $+X_0$ direction is given by the reversed inertia forces of the moving masses:

$$-F = m_0 \ddot{X}_0 + \sum m_n (\ddot{X}_0 + \ddot{x}_n) \tag{3.27}$$

Likewise, the net moment exerted on the tank is given by:

$$-M = \sum m_n h_n \ddot{x}_n - g \sum m_n x_n \tag{3.28}$$

Where the last term is the moment caused by the offset of each spring-mass from the tank centerline. The equation of motion for each of the spring-masses is expressed as:

$$m_n (\ddot{X}_0 + \ddot{x}_n) + k_n x_n = 0 \tag{3.29}$$

Just as was done in section 3.3, the tank accelerations are assumed to be oscillatory at frequency $\Omega$. The components of the tank motion are therefore given by $-iX_0 \exp(i\Omega t)$ and Eq.3.39 can be expressed as:

$$x_n = -\frac{i\Omega^2 X_0}{\omega_n^2 - \Omega^2} \tag{3.30}$$

Where Eq.3.26 has also been used to eliminate $k_n$. With these equations, the amplitudes of the force and moment on the tank can be expressed analytically as:

$$\frac{F_{amp}}{-i\Omega^2 X_0 m_{liq}} = \left[ 1 + \sum \frac{m_n}{m_{liq}} \left( \frac{\Omega^2}{\omega_n^2 - \Omega^2} \right) \right] \tag{3.31}$$

$$\frac{M_{amp}}{-i\Omega^2 X_0 m_{liq} h} = \sum \frac{m_n}{m_{liq} h}\left(\frac{H_n\Omega^2 + g}{\omega_n^2 - \Omega^2}\right) \tag{3.32}$$

Since the slosh forces and moments were derived in detail in section 3.3 only for a rectangular parallelepiped tank, that tank shape will be used as an example to demonstrate how model parameters such as $m_n$, $k_n$, and $H_n$ are determined as a function of tank shape and fill level. In this study only the two-dimensional slosh modes that are excited by a translation of the tank in the *x*-direction are investigated as indicated in Figure 3.3.

The lateral force exerted on the tank by the sloshing liquid for a horizontal excitation of the tank parallel to the *x*-axis is given by Eq.3.19.

By comparing Eq.3.19 to the expression for the force created by an *x*-translation of the model (Eq.3.31) it can be seen that the slosh force will be duplicated by the model if the model masses are chosen to be equal to:

$$m_n = m_{liq}\left\{8(\frac{a}{h})\frac{\tanh[\lambda_n h/a]}{\lambda_n^3}\right\} \tag{3.33}$$

Hence, the spring constants of the model must be chosen as:

$$K_n = m_{liq}\left\{8(\frac{g}{h})\frac{\tanh^2(\lambda_n h/a)}{\lambda_n^2}\right\} \tag{3.34}$$

By comparing Eq.3.20 to the expression for the moment created by an *x*-translation of the model [Eq.3.32] and doing some mathematical simplifications, the axial elevation of the masses must be chosen so that:

$$\frac{H_n}{h} = \frac{1}{2} - 2(\frac{a}{h})\frac{\tanh(\lambda_n h/2a)}{\lambda_n} \tag{3.35}$$

As previously mentioned, the horizontal excitation causes the contained fluid to slosh with vertical displacement of the fluid surface. The calculation of the maximum wave height $\delta_{\max}$ generated by earthquake is required to provide the rectangular tanks with sufficient freeboard. According to obtained velocity potential for sloshing motion (Eq.3.15) in rectangular tank and using Bernoulli's equation (Eq.3.5), the sloshing height at the liquid free surface is expressed as following:

$$\delta = -\frac{1}{g} iX_0 \Omega^2 e^{i\Omega t} \left\{ \sum_{n=1}^{\infty} \frac{4a(-1)^{n-1}}{\lambda_n^2} \left( \frac{\omega_n^2}{\omega_n^2 - \Omega^2} \right) \sin\left[ \lambda_n \frac{x}{a} \right] \right\} \tag{3.36}$$

Consideration should now be given to an extension of this equation to the case of an earthquake-induced base motion. As an application to earthquake engineering, the maximum water surface elevation can be estimated using the root of sum of the squares of the maximum modal responses. This may be expressed as:

$$\delta_{\max} = \left( \frac{4a}{\pi^2} \right) \left\{ \sum_{n=1}^{\infty} \left( \frac{1}{(2n-1)^2} \frac{S_a(\omega_n, \xi_n)}{g} \right)^2 \right\}^{1/2} \tag{3.37}$$

Where $S_a(\omega_n, \xi_n)$ is the spectral response acceleration at period $T_n = \frac{2\pi}{\omega_n}$ corresponding with the damping ratio of $\xi_n$. Since the higher modes of sloshing are usually of little concern, the above equation may be simplified using the first fundamental mode of sloshing. Therefore, the Eq.3.37 can be rewritten as following form which is more applicable in design codes:

$$\delta_{\max} = \left( \frac{4a}{\pi^2} \right) C_c \tag{3.38}$$

Where $C_c$ is the seismic response coefficient and can be obtained in accordance with current design codes and practice such as ACI350.3-06 (2006).

### 3.5 Eigen-value solution of flexible liquid tank

As previously mentioned, the potential function of a rigid liquid tank is governed by Eq.3.15. For a flexible liquid tank, the deformation of the tank wall should be considered in developing a new potential function. The harmonic deformation of the wall can be assumed as the following equation:

$$U(z,t) = u(z)e^{iwt} \tag{3.39}$$

The following boundary condition along tank wall should be satisfied by the new potential function:

$$\frac{\partial \Phi}{\partial x} = \frac{\partial U(z,t)}{\partial t} = i\omega u(z)e^{i\omega t} \tag{3.40}$$

In order to consider the effect of wall flexibility on dynamic characteristics of tank-liquid system, the following expression as a solution for the liquid velocity potential which satisfies the Laplace's equation and bottom boundary condition is proposed:

$$\Phi(x,z,t) = e^{i\omega t}\{\sum_{n=1}^{\infty}(A_n \cosh(\varepsilon_n(x+a/2)) + B_n \sinh(\varepsilon_n(x+a/2)))\cos(\varepsilon_n(z+h/2))\} \tag{3.41}$$

Where $\varepsilon_n$ is the root of the below equation:

$$\begin{aligned} &\varepsilon_n h \tan \varepsilon_n h = -\frac{\omega^2 h}{g} && \textit{Convective behaviour} \\ &\cos(\varepsilon_n h) = 0 && \textit{Impulsive behaviour} \end{aligned} \tag{3.42}$$

The equation of the motion of the flexible wall is given by:

$$\frac{\partial^4 U}{\partial z^4} + \frac{\rho_w t_w}{EI}\frac{\partial^2 U}{\partial t^2} = -\frac{\rho_f}{EI}\frac{\partial \Phi}{\partial t} \tag{3.43}$$

Where $\rho_w$ and $t_w$ are wall density and thickness, respectively. The substitutions of equations 3.49 and 3.51 in Eq.3.53 will result in:

$$\frac{d^4u}{dz^4}-\frac{\rho_w t_w \omega^2}{EI}u=-\frac{\rho_f}{EI}(i\omega)\{\sum_{n=1}^{\infty}A_n\cos(\varepsilon_n(z+h/2))\}\quad \text{at}\quad x=-a/2$$
$$\frac{d^4u}{dz^4}-\frac{\rho_w t_w \omega^2}{EI}u=-\frac{\rho_f}{EI}(i\omega)\{\sum_{n=1}^{\infty}(A_n\cosh(a\varepsilon_n)+B_n\sinh(a\varepsilon_n))\cos(\varepsilon_n(z+h/2))\} \quad (3.44)$$
$$\text{at}\quad x=+a/2$$

The general solutions of these equations are:

$$u(z)=C_1\cosh(\lambda_1 z)+C_2\sinh(\lambda_1 z)+C_3\cos(\lambda_1 z)+C_4\sin(\lambda_1 z)$$
$$-\frac{\rho_f}{EI}(i\omega)\sum_{n=1}^{\infty}\frac{A_n}{\varepsilon_n^4-\lambda_1^4}\cos(\varepsilon_n(z+h/2))\quad \text{at}\quad x=-a/2$$
$$u(z)=D_1\cosh(\lambda_1 z)+D_2\sinh(\lambda_1 z)+D_3\cos(\lambda_1 z)+D_4\sin(\lambda_1 z) \quad (3.45)$$
$$-\frac{\rho_f}{EI}(i\omega)\sum_{n=1}^{\infty}\frac{(A_n\cosh(\varepsilon_n h)+B_n\sinh(\varepsilon_n h))}{\varepsilon_n^4-\lambda_1^4}\cos(\varepsilon_n(z+h/2))\quad \text{at}\quad x=a/2$$

In which:

$$\lambda_1^4=\frac{\rho_w h\ \omega^2}{EI} \quad (3.46)$$

Assuming the tank wall is fixed to the ground, the wall motion should satisfy following boundary conditions:

$$u(-h/2)=u'(-h/2)=u''(h/2)=u'''(h/2)=0 \quad (3.47)$$

As a result, the integration constants $C_j$ ($j$=1 to 4) and $D_j$ ($j$=1 to 4) can be expressed in terms of $A_n$ and $B_n$ by applying these boundary conditions.

It is assumed that the liquid remains in contact with the tank wall during the motion. The condition shown in Eq.3.40 must be satisfied at $x=\pm a/2$. This procedure results in a doubly infinite system of equations for the unknown coefficients of $A_n$ and $B_n$:

$$\begin{bmatrix} \alpha_{\mu n}(\omega) & \beta_{\mu n}(\omega) \\ \alpha^*_{\mu n}(\omega) & \beta^*_{\mu n}(\omega) \end{bmatrix} \begin{Bmatrix} A_n \\ B_n \end{Bmatrix} = \begin{Bmatrix} 0 \\ 0 \end{Bmatrix} \tag{3.48}$$

The detailed analytical coefficients are presented by Ibrahim (2005). For non-trivial solution, the determinant of the coefficient matrix of the Eq.3.58 must be equal to zero:

$$\det \begin{bmatrix} \alpha_{\mu n}(\omega) & \beta_{\mu n}(\omega) \\ \alpha^*_{\mu n}(\omega) & \beta^*_{\mu n}(\omega) \end{bmatrix} = 0 \tag{3.49}$$

In order to illustrate the results of analysis, a numerical subroutine using MATLAB program was developed to solve the Eq.3.49. The infinite order determinant of this equation was truncated to a twentieth order one for the calculation of first coupled natural frequency. The analysis results will be presented and compared with FE results in Chapter 5.

### 3.6 Summary

This chapter demonstrates how a velocity potential is derived under specific boundary conditions and seismic excitations for rectangular tanks. The analysis is similar for other tank shapes, but the potential functions may not be *sines* and *cosines*.

In addition, the analytical pressure distribution along the side walls of rigid rectangular tanks can be easily calculated for actual earthquake records. This will be discussed in the next chapter as a mean to verify the proposed finite element method in this study.

The mechanical model described in this chapter is the basis for most of the design codes and standards such as ACI 350.3-06. However, it should be noticed that these unique analytical solutions are only valid for rigid rectangular tanks which are supported on rigid foundations.

# Chapter 4
# Finite element formulation of liquid tank system

## 4.1 Introduction

The first step in dynamic analysis of a system is to properly model the actual system. In mathematical modelling, the equation of the motion is formulated and can be subsequently solved using an appropriate method. In previous chapter, the equation of the motion of the fluid was formulated. Here, the structural equation of the motion is derived and its corresponding finite element equation in addition to that of fluid domain is presented.

Computation of earthquake response history for concrete rectangular tanks involves solution of coupled sets of equations of motion that include large number of equations or degrees of freedom. The main objective of this chapter is to demonstrate the solution procedure for this system using finite element formulation in the time domain. Also, problems associated with damping characteristics, free surface motion and wall boundary conditions are discussed in this chapter. As mentioned before, the ANSYS (2004) computer program along with some additional computer subroutines are used for the purpose of liquid-tank analysis. This chapter describes the analysis method and solution procedures.

## 4.2 Analysis in the time domain

As mentioned before, in linear response analysis the system equation of motion can be formulated either in the time domain or in the frequency domain.

In practice, time domain response analyses are generally based on some forms of step-by-step methods using numerical integration procedures to satisfy the equations of motion. In all the step-by-step methods the loading and the response history are divided into a sequence of time

intervals or steps. The response during each step is computed from initial conditions and the beginning of the step and from history of loading during the step. The structural properties during each step are assumed to be constant, but could vary from one step to another (nonlinear behaviour) or remain the same during all time steps (linear behaviour). The step-by-step method may be classified as explicit or implicit. In an explicit method, the new response values calculated in each step depend only on the response quantities available at the beginning of the step. The analysis therefore proceeds directly from one step to the next. In an implicit method, on the other hand, the new response values for a given step include one or more values pertaining to the same step, so that trial values and successive iterations are necessary. The iteration within a step makes implicit formulation inconvenient.

In this study, direct integration scheme is chosen which is appropriate for coupled system of equations. In this method, the step-by-step integration is applied directly to the original equations of motion with no need to obtain natural mode shapes and frequencies or to limit damping to proportional type.

Following is a description of how finite element method (FEM) is applied in the solution of earthquake response behaviour in the time domain using a direct method.

### 4.3 Finite element modeling of the structure

In a multi-degree-of-freedom (MDOF) system, it is required to know the values of the displacement in more than one point in order to define its motion at any instant of time. Consider a system with *n* degrees of freedom which accelerates in the *y* direction as shown in Figure 4.3.

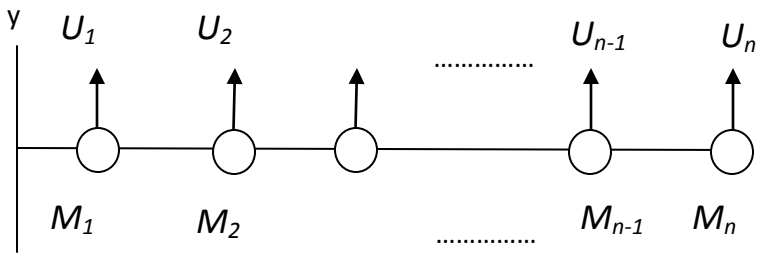


Figure 4.1: An example of multi-degree-of-freedom (MDF) with degrees of freedom in *y* direction

The inertial forces can be written as:

$$F_I = \begin{Bmatrix} F_{I1} \\ F_{I2} \\ . \\ . \\ F_{I(n-1)} \\ F_{I(n)} \end{Bmatrix} = \begin{bmatrix} M_1 & . & . & . & . & . \\ . & M_2 & . & . & . & . \\ . & . & . & . & . & . \\ . & . & . & . & . & . \\ . & . & . & . & M_{n-1} & . \\ . & . & . & . & . & M_n \end{bmatrix} \begin{Bmatrix} \ddot{u}_1 \\ \ddot{u}_2 \\ . \\ . \\ \ddot{u}_{n-1} \\ \ddot{u}_n \end{Bmatrix}^t \tag{4.1}$$

Or it can be written as:

$$F_I = [M]\{\ddot{U}\}^t \tag{4.2}$$

The mass matrix $[M]$ is a diagonal matrix and in general it can be a non-diagonal symmetric matrix. The forces due to elasticity can be written as:

$$F_S = \begin{Bmatrix} F_{S1} \\ F_{S2} \\ . \\ . \\ F_{S(n-1)} \\ F_{S(n)} \end{Bmatrix} = \begin{bmatrix} K_{11} & K_{12} & . & . & . & K_{1n} \\ K_{21} & K_{22} & . & . & . & K_{2n} \\ . & . & . & . & . & . \\ . & . & . & . & . & . \\ . & . & . & . & . & . \\ K_{n1} & K_{n2} & . & . & . & K_{nn} \end{bmatrix} \begin{Bmatrix} u_1 \\ u_2 \\ . \\ . \\ u_{n-1} \\ u_n \end{Bmatrix} \tag{4.3}$$

Or it can be written as:

$$F_S = [K]\{U\} \tag{4.4}$$

Where $[K]$ is the stiffness matrix. The damping matrix can be written as:

$$F_D = \begin{Bmatrix} F_{D1} \\ F_{D2} \\ . \\ . \\ F_{D(n-1)} \\ F_{D(n)} \end{Bmatrix} = \begin{bmatrix} C_{11} & C_{12} & . & . & . & C_{1n} \\ C_{21} & C_{22} & . & . & . & C_{2n} \\ . & . & . & . & . & . \\ . & . & . & . & . & . \\ . & . & . & . & . & . \\ C_{n1} & C_{n2} & . & . & . & C_{nn} \end{bmatrix} \begin{Bmatrix} \dot{u}_1 \\ \dot{u}_2 \\ . \\ . \\ \dot{u}_{n-1} \\ \dot{u}_n \end{Bmatrix} \tag{4.5}$$

Or it can be written as:

$$F_D = [C]\{\dot{U}\} \tag{4.6}$$

Where $[C]$ is the damping matrix.

Equating of the external forces and internal forces will result in:

$$[M]\{\ddot{U}_t\} + [C]\{\dot{U}\} + [K]\{U\} = \{f(t)\} \tag{4.7}$$

Where $\{f(t)\}$ is the external force acting on the structure and can be written as:

$$\{f(t)\} = \begin{Bmatrix} f_1(t) \\ f_2(t) \\ . \\ . \\ . \\ f_n(t) \end{Bmatrix} \tag{4.8}$$

If there is a base acceleration applied on the system, the equation of the motion is written as:

$$[M]\{\ddot{U}_t\} + [C]\{\dot{U}\} + [K]\{U\} = \{f(t)\} - [M]\{\ddot{U}_g\} \tag{4.9}$$

In the case of liquid tanks, $\{f(t)\}$ can be separated into hydrodynamic pressure $\{f\}$ and resultant of all the other forces, $\{f_1\}$, that act on the structure. Thus, the final form of the equation of the motion can be written as:

$$[M]\{\ddot{U}_t\}+[C]\{\dot{U}\}+[K]\{U\}=\{f\}+\{f_1\}-[M]\{\ddot{U}_g\} \tag{4.10}$$

In a MDOF system, a system is discretized into its degrees of freedom (DOF). The number of degrees of freedom depends on the number of elements and the degree of freedom for each element. Usually in the case of liquid tanks isoparametric solid elements are used. These types of elements are also used for two dimensional problems as plain strain or plain stress elements.

In 3-D analysis the simplest case is the case of tetrahedron element. Based on the nature of the problem each node may have 3 different components *u*, *v* and *w* in the direction of X, Y and Z. For more complex type of element, more rotational degrees of freedom are added to each node. Three dimensional analysis of concrete rectangular tank requires a large number of DOF. For this reason, two dimensional analysis, which is more simple, is common in engineering practice.

### 4.3.1 Coupling matrix of the tank-liquid system

As previously mentioned, the fluid pressure applies an equivalent structural force on the tank wall. The coupling matrix relates the pressure of the liquid and the forces on the tank-liquid interface as following:

$$[Q]\{P\}=\{f\} \tag{4.11}$$

Where $\{f\}$ is the force vector acting on the structure due to the hydrodynamic pressure.

Figure 4.2 shows a line element on the interaction boundary of the tank-liquid system. The work done by the hydrodynamic pressure on the interaction surface of the structure must be

equal to the work of the equivalent nodal forces on the interface boundary of an element. Thus, for unit thickness elements as shown in Figure 4.4, the following expression can be written:

$$\int pU_n ds = \left\{f^e\right\}^T \{\delta\} = \left\{f_{x1} \quad f_{y1} \quad f_{x2} \quad f_{y2}\right\} \begin{Bmatrix} u_1 \\ v_1 \\ u_2 \\ v_2 \end{Bmatrix} \tag{4.12}$$

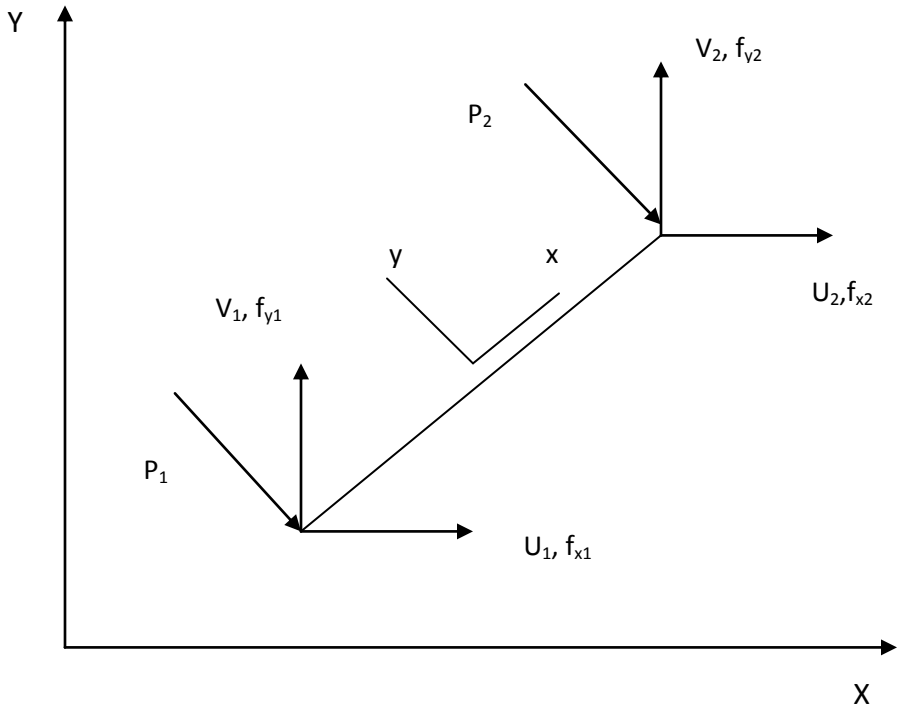


Figure 4.2: Interface element on the tank-fluid interaction boundary

Where $p$ and $U_n$ are the values of the hydrodynamic pressure and normal displacement along the element interface, respectively. $\{\delta\}$ and $\left\{f^e\right\}$ are the displacement and force vector of an interface element. $u_i$ and $v_i$ ( $f_{xi}$ and $f_{yi}$ ) are the displacements (forces) at node *i* of the interface

element along the global X and Y coordinates, respectively. The integration is performed along each element on the tank-liquid interface. The superscript '*e*' refer to the element on the tank-liquid interface. Writing *u* and *v*, displacements along the *X* and *Y* coordinates of the interface element, in terms of structural shape functions, then:

$$\begin{aligned} u &= N_1 u_1 + N_2 u_2 \\ v &= N_1 v_1 + N_2 v_2 \end{aligned} \tag{4.13}$$

Where $N_i$ is the structure shape function at node *i* of the interface element. For the normal displacement along the element surface, $U_n$, we have:

$$U_n = u_n + v_n = \eta N_1 u_1 + \eta N_2 u_2 + \beta N_1 v_1 + \beta N_2 v_2 \tag{4.14}$$

In Eq.4.14, $\eta$ and $\beta$ are the absolute values of the normal vector on the boundary in the global directions of *X* and *Y*, respectively. Eq.4.14 can be written in the following form:

$$U_n = \begin{bmatrix} \eta N_1 & \beta N_1 & \eta N_2 & \beta N_2 \end{bmatrix} \{\delta\} = \left\{ N_n^s \right\}^T \{\delta\} \tag{4.15}$$

The hydrodynamic pressure can be expressed as shape function of the fluid in the form:

$$p = \left\{ N^f \right\}^T \left\{ p^e \right\} = \begin{bmatrix} N_1^f & N_2^f \end{bmatrix} \left\{ p^e \right\} \tag{4.16}$$

Where $N_i^f$ is the fluid shape function at node *i* of the interface element. Combining equations 4.12, 4.15 and 4.16, there is obtained:

$$\left\{ f^e \right\} = \int_{s_e} \left\{ N_n^s \right\} \left\{ N^f \right\}^T ds \left\{ p^e \right\} = \left[ Q^e \right] \left\{ p^e \right\} \tag{4.17}$$

Where $\left[ Q^e \right]$ and $\left\{ p^e \right\}$ are the coupling matrix and hydrodynamic pressure vector of an element on the tank-liquid interface. The total coupling matrix [*Q*] is obtained by assembling all element coupling matrices. From Eq.4.17, $\left[ Q^e \right]$ is written as:

$$\{Q^e\} = \int_{s_e} \{N_n^s\}\{N^f\}^T ds \tag{4.18}$$

For an interface element as shown in Figure 4.2, then:

$$[Q]^e = \int_{s_e} \begin{bmatrix} \eta N_1^s N_1^f & \eta N_1^s N_2^f \\ \beta N_1^s N_1^f & \beta N_1^s N_2^f \\ \eta N_2^s N_1^f & \eta N_2^s N_2^f \\ \beta N_2^s N_1^f & \beta N_2^s N_2^f \end{bmatrix} ds \tag{4.19}$$

Eq.4.19 is valid for a two-dimensional tank-liquid system. For three-dimensional system with four-node interface elements with *x* and *y* and *z* tranlational degree of freedom (DOF) at each node on the face of the container wall, and corresponding four-node interface elements with pressure DOF at each node attached to the liquid elements, the coupling matrix is given as:

$$[Q]^e = \varpi \int_{-1}^{1}\int_{-1}^{1} \begin{bmatrix} \alpha_1 N_1^s N_1^s N_1^f & \alpha_1 N_1^s N_1^s N_2^f & \alpha_1 N_1^s N_1^s N_3^f & \alpha_1 N_1^s N_1^s N_4^f \\ \beta_1 N_1^s N_1^s N_1^f & \beta_1 N_1^s N_1^s N_2^f & \beta_1 N_1^s N_1^s N_3^f & \beta_1 N_1^s N_1^s N_4^f \\ \gamma_1 N_1^s N_1^s N_1^f & \gamma_1 N_1^s N_1^s N_2^f & \gamma_1 N_1^s N_1^s N_3^f & \gamma_1 N_1^s N_1^s N_4^f \\ \cdot & \cdot & \cdot & \cdot \\ \cdot & \cdot & \cdot & \cdot \\ \cdot & \cdot & \cdot & \cdot \\ \alpha_1 N_1^s N_1^s N_1^f & \alpha_1 N_1^s N_1^s N_2^f & \alpha_1 N_1^s N_1^s N_3^f & \alpha_1 N_1^s N_1^s N_4^f \\ \beta_1 N_1^s N_1^s N_1^f & \beta_1 N_1^s N_1^s N_2^f & \beta_1 N_1^s N_1^s N_3^f & \beta_1 N_1^s N_1^s N_4^f \\ \gamma_1 N_1^s N_1^s N_1^f & \gamma_1 N_1^s N_1^s N_2^f & \gamma_1 N_1^s N_1^s N_3^f & \gamma_1 N_1^s N_1^s N_4^f \end{bmatrix}_{24\times 4} \times \left\| t_\xi \times t_\eta \right\| d\xi d\eta \tag{4.20}$$

In which

$$t_\xi = \left\{ \frac{\partial x}{\partial \xi}, \frac{\partial y}{\partial \xi}, \frac{\partial z}{\partial \xi} \right\}$$

$$t_\eta = \left\{ \frac{\partial x}{\partial \eta}, \frac{\partial y}{\partial \eta}, \frac{\partial z}{\partial \eta} \right\} \tag{4.21}$$

$$\varpi = \frac{\int_{A_e} \left\| t_\xi \times t_\eta \right\| d\xi d\eta}{\sum_{i=1}^{8} \int_{A_e} N_i^s N_i^s \left\| t_\xi \times t_\eta \right\| d\xi d\eta}$$

Where $N^f$ and $N^s$ are the shape function in fluid and the structure domain, respectively. Also, $\alpha_1$, $\beta_1$ and $\gamma_1$ are the direction cosines of the nodes of the surface element on the wet face of the structure.

### 4.4 Finite element formulation of the fluid system

In liquid domain, the hydrodynamic pressure distribution is governed by the pressure wave equation described in Chapter 3. Because of the small volume of containers, the velocity of pressure wave assumed to be infinity. Assuming that water is incompressible and neglecting its viscosity, the small-amplitude irrotational motion of water is rewritten in terms of fluid pressure using Eq.3.2 in general three-dimensional space:

$$\nabla^2 P(x, y, z, t) = 0 \tag{4.22}$$

Where $P(x, y, z, t)$ is the hydrodynamic pressure in excess of hydrostatic pressure.

The hydrodynamic pressure in Eq.4.22 is due to the horizontal and vertical seismic excitations of the walls and bottom of the container. The motion of these boundaries is related to hydrodynamic pressure by boundary conditions. For earthquake excitation, the appropriate boundary condition at the interface of liquid and tank is governed by:

$$\frac{\partial P(x,y,z,t)}{\partial n} = -\rho a_n(x,y,z,t) \tag{4.23}$$

Where $\rho$ is the density of liquid and $a_n$ is the component of acceleration on the boundary along the direction outward normal $n$. No wave absorption is considered in the interface boundary condition. It should be noticed that for rigid tanks the value of $a_n$ is equal to base acceleration while for flexible tanks this value is equal to the summation of ground acceleration and wall relative acceleration.

Relative acceleration of tank wall is highly dependent on its flexibility. On the other hand, Eq.4.23 mainly differentiates rigid tank behaviour from flexible tank behaviour.

Accounting for the small-amplitude gravity waves on the free surface of the liquid, the resulting boundary condition is given as:

$$\frac{1}{g}\frac{\partial^2 P}{\partial t^2} + \frac{\partial P}{\partial z} = 0 \tag{4.24}$$

In which $z$ is the vertical direction and $g$ is the gravitational acceleration.

As mentioned in chapter 3, applying the small-amplitude wave boundary condition will lead to an evaluation of convective pressure distribution in the liquid domain which is of great importance in liquid containers. However, due to the large amplitude of sloshing under the strong seismic excitations and turbulence effects in liquid tanks, more complicated boundary conditions on the surface of liquid are needed to accurately model the convective motions. This is especially the case in shallow tank models which may not completely follow the linearized boundary condition equations. In a recent study done by Virella et al. (2008), the influence of nonlinear wave theory on the sloshing natural periods and their modal pressure distribution for rectangular tanks with $H_L$/a ratios ranging from 0.2 to 0.82 was investigated. They concluded that the

nonlinearity of the surface wave does not have a major effect on the pressure distribution on the walls and on natural sloshing frequencies. In the present study, two different tank configurations namely a shallow and a tall tank are analyzed as will be discussed later. The ratios of $H_L/a$ are 0.19 and 0.63 for the shallow and tall tanks, respectively. In this case, the linearized boundary condition is appropriate particularly for practical applications. Neglecting the gravity wave effects leads to the free surface boundary condition which is appropriate for impulsive motion of liquid. The related governing equation is given as:

$$P(x, y, \frac{H_l}{2}, t) = 0 \tag{4.25}$$

Where $H_l$ is the height of liquid in the container and the same coordinate system shown in Figure 3.3 is used here.

Using finite element discretization and discretized formulations of equations 4.22, 4.23 and 4.24 the fluid pressure equation can be written as the following matrix form:

$$[G]\{\ddot{P}\}+[H]\{P\}=\{F\} \tag{4.26}$$

In which $G_{i,j} = \sum G^e_{i,j}$, $H_{i,j} = \sum H^e_{i,j}$ and $F_i = \sum F^e_i$. The coefficients $G^e_{i,j}$, $H^e_{i,j}$ and $F^e_i$ for an individual element are determined using the following expressions:

$$\begin{aligned} G^e_{i,j} &= \frac{1}{g}\int_{A_e} N_i N_j dA \\ H^e_{i,j} &= \int_{V_e} (\frac{\partial N_i}{\partial x}\frac{\partial N_j}{\partial x} + \frac{\partial N_i}{\partial y}\frac{\partial N_j}{\partial y} + \frac{\partial N_i}{\partial z}\frac{\partial N_j}{\partial z})dV \\ F^e_i &= \int_{\bar{A}_e} N_i \frac{\partial P}{\partial n} d\bar{A} \end{aligned} \tag{4.27}$$

The force $\{F\}$ depends on the tank-liquid boundary conditions and can be obtained using Eq.4.23 as following:

$$\{F\} = -\rho[Q]^T (\{\ddot{U}\} + \{\ddot{U}_g\}) \tag{4.28}$$

In the above equations, $N_i$ is the shape function of the *i*th node in the liquid element, $\{\ddot{U}\}$ is the acceleration vector of nodes in the structure domain, $\{\ddot{U}_g\}$ is the ground acceleration vector applied to the system and $[Q]$ is the coupling matrix. $A_e$ and $V_e$ are the integrations over free surface and volume of the fluid element, respectively. $\overline{A}_e$ is the integration over interface between structure and fluid.

In the above formulation, matrices $[H]$ and $[G]$ are constants during the analysis while the force vector $\{F\}$, pressure vector $\{P\}$ and its derivatives are the variable quantities. In the coupling system of liquid–structure the pressures are applied to the structure surface as the loads on the container walls. The general equation of fluid–structure can be written in the following form:

$$\begin{aligned} &[M]\{\ddot{U}\} + [C]\{\dot{U}\} + [K]\{U\} = \{f_1\} - [M]\{\ddot{U}_g\} + [Q]\{P\} = \{F_1\} + [Q]\{P\} \\ &[G]\{\ddot{P}\} + [C']\{\dot{P}\} + [H]\{P\} = -\rho[Q]^T (\{\ddot{U}\} + \{\ddot{U}_g\}) = \{F_2\} - \rho[Q]^T \{\ddot{U}\} \end{aligned} \tag{4.29}$$

Where $[M]$, $[C]$ and $[K]$ are mass, damping and stiffness matrices of structure. The term $[C']$ is the matrix representing the damping of liquid which is dependent on the viscosity of liquid and wave absorption in liquid domain and boundaries and is rigorously determined. As previously discussed, the matrix $[Q]$ transfers the liquid pressure to the structure as well as structural acceleration to the liquid domain.

The direct integration scheme is used to find the displacement and hydrodynamic pressure at the end of time increment *i+1* given the displacement and hydrodynamic pressure at *i*. The $\alpha$

method is used for discretization of both equations. In this method $\{\dot{U}\}_{i+1}, \{U\}_{i+1}, \{\dot{P}\}_{i+1}$ and $\{P\}_{i+1}$ can be written as follows:

$$
\begin{aligned}
\{\dot{U}\}_{i+1} &= \{\dot{U}\}^{p}_{i+1} + \gamma\Delta t\{\ddot{U}\}_{i+1} \\
\{\dot{U}\}^{p}_{i+1} &= \{\dot{U}\}_{i} + (1-\gamma)\Delta t\{\ddot{U}\}_{i} \\
\{U\}_{i+1} &= \{U\}^{p}_{i+1} + \beta\Delta t^{2}\{\ddot{U}\}_{i+1} \\
\{U\}^{p}_{i+1} &= \{U\}_{i} + \Delta t\{\dot{U}\}_{i} + (0.5-\beta)\Delta t^{2}\{\ddot{U}\}_{i} \\
\{\dot{P}\}_{i+1} &= \{\dot{P}\}^{p}_{i+1} + \gamma\Delta t\{\ddot{P}\}_{i+1} \\
\{\dot{P}\}^{p}_{i+1} &= \{\dot{P}\}_{i} + (1-\gamma)\Delta t\{\ddot{P}\}_{i} \\
\{P\}_{i+1} &= \{P\}^{p}_{i+1} + \beta\Delta t^{2}\{\ddot{P}\}_{i+1} \\
\{P\}^{p}_{i+1} &= \{P\}_{i} + \Delta t\{\dot{P}\}_{i} + (0.5-\beta)\Delta t^{2}\{\ddot{P}\}_{i}
\end{aligned}
\tag{4.30}
$$

Where $\gamma$ and $\beta$ are integration parameters. The terms with superscript *p* represent quantities at time step *i+1* that can be calculated from quantities of time step *i*. The governing field equations at time *i+1* can be written as follows:

$$
\begin{aligned}
[M]\{\ddot{U}\}_{i+1} + [C]\{\dot{U}\}_{i+1} + (1+\alpha)[K]\{U\}_{i+1} &= \{F_1\}_{i+1} + [Q]\{P\}_{i+1} + \alpha[K]\{U\}_{i} \\
[G]\{\ddot{P}\}_{i+1} + [C']\{\dot{P}\}_{i+1} + (1+\alpha)[H]\{P\} &= \{F_2\}_{i+1} - \rho[Q]^{T}\{\ddot{U}\}_{i+1} + \alpha[H]\{P\}_{i}
\end{aligned}
\tag{4.31}
$$

Where $\alpha$ is the integration parameter which is used in coupled field equations. The coupled field equations can be solved using staggered method (Ghaemian and Ghobara (1999)). The equations of motion of structure can be approximated as:

$$
[M]\{\ddot{U}\}^{*}{}_{i+1} = \{F_1\}_{i+1} + [Q]\{P\}^{p}{}_{i+1} - [C]\{\dot{U}\}^{p}{}_{i+1} - (1+\alpha)[K]\{U\}^{p}{}_{i+1} + \alpha[K]\{U\}_{i} \tag{4.32}
$$

Combining Eq. 4.32, 4.31 and 4.30 gives:

$$
[M]\{\ddot{U}\}_{i+1} = [M]\{\ddot{U}\}^{*}_{i+1} + \beta\Delta t^{2}[Q]\{\ddot{P}\}_{i+1} - \gamma\Delta t[C]\{\ddot{U}\}_{i+1} - (\alpha+1)\beta\Delta t^{2}[K]\{\ddot{U}\}_{i+1} \tag{4.33}
$$

Using the diagonal properties of mass matrix, Eq. 4.33 is modified as follows:

$$[M]\{\ddot{U}\}_{i+1} = [M]\{\ddot{U}\}^*_{i+1} + \beta\Delta t^2[Q]\{\ddot{P}\}_{i+1} \tag{4.34}$$

Substituting Eq. 4.34 into Eq. 4.31 yields:

$$\begin{aligned}&([G] + \rho\beta\Delta t^2[Q]^T[M]^{-1}[Q])\{\ddot{P}\}_{i+1} + [C']\{\dot{P}\}_{i+1} + (1+\alpha)[H]\{P\}_{i+1} = \{F_2\}_i \\ &-\rho[Q]^T\{\ddot{U}\}^*_{i+1} + \alpha[H]\{P\}_i\end{aligned} \tag{4.35}$$

In Eq.4.35, the right hand side terms are known, thus pressure value at time step *i+1* can be obtained and used to calculate the corresponding displacement values.

The method of staggered displacement is unconditionally stable for linear coupled equations of liquid-tank system when $\alpha = 0$. The procedure of staggered displacement method is summarized as:

- $\{\ddot{U}\}^*_{i+1}$ can be obtained from Eq.4.32 by knowing the displacement, velocity and pressure at time *i*. The terms with superscript *p* in Eq.4.32 can be calculated from quantities at time *I* using Eq.4.30.
- $\{\ddot{U}\}^*_{i+1}$ is introduced in Eq.4.35 to calculate $\{P\}_{i+1}$
- $\{P\}_{i+1}$ is substituted in Eq.4.31 to calculate $\{U\}_{i+1}$ and its derivatives

In this study, the values of 0.505 and 0.252 are chosen as input data in ANSYS compute program for parameters $\beta$ and $\gamma$, respectively. Further descriptions regarding the direct integration method can be found in the studies done by Bathe (1996) and Zienkiewicz (1977). As described by Zienkiewicz (1977).

The accuracy of the proposed methods is based on the selection of the appropriate time step. According to a study done by Mirzabozorg et al. (2003), the integration time interval equal to 0.005 second is appropriate for dynamic analysis of liquid-structure interaction and is used in this study.

### 4.5 Damping characteristics of liquid sloshing

Under free oscillations, the motion of free liquid surface decays due to damping forces created by viscous boundary layers. Basically, the damping factor depends on the liquid height, liquid kinematic velocity and tank dimensions. From this point of view, evaluation of damping characteristic for a fluid–tank system needs more considerations. However, due to lack of sufficient data in this field, the classical damping scheme is used in the finite element model. Considering impulsive and convective parts of liquid domain, damping matrix can be given as:

$$\lfloor C_f \rfloor = a[G] + b[H] \tag{4.36}$$

In which $a$ and $b$ are computed by Rayleigh damping method. In this equation, coefficient $a$ is calculated based on fundamental frequency of liquid sloshing to present the convective part of the response while, coefficient $b$ is computed based on fundamental frequency of the tank which is related to the impulsive term. The fundamental frequencies of tank-liquid system are calculated using both finite element method and analytical equations adopted from ACI 350.3-06 (2006). The convective frequencies are exactly the same but some differences are seen for impulsive values. In this study, the values corresponding to finite element method is used to calculate the damping coefficients which will be discussed later.

Sloshing in a tank without any anti-sloshing device is usually damped by viscous forces. The investigations done by Mikishev and Dorozhkin (1961) showed that in a storage tank with rational dimensions viscous damping is less than 0.5%. In addition, ACI 350.3-06 (2006) indicates that the damping of the sloshing water is approximately between 0.5 to 1 percent of the critical damping.

In the proposed FE procedure, Rayleigh damping as mentioned previously is used in the direct step-by-step integration method. The stiffness proportional damping equivalent to 5% of critical

damping is assumed as structural damping. For sloshing behavior of liquid 0.5 percent of critical damping is applied. Damping values associated with horizontal and vertical motions are dependent on earthquake shear wave velocity and the ratio of $H_L$ /$R$ in which $R$ is the equivalent radius of a cylindrical tank with the same plan area as the rectangular tank. These values can be drawn based on studies done by Veletsos and Tang (1986) and Veletsos and Shivakumar (1997) for each tank configuration. In their study, the tank was analyzed approximately by application of Galerkin's method considering the tank-liquid system to respond as a SDOF system with a fixed base boundary condition. Comprehensive numerical analyses including different tank configurations were carried out to investigate the behaviour of both rigidly and flexibly supported tanks, and the effects of the numerous parameters that influence the response. It was shown that the wave shear velocity affects the hydrodynamic distribution and that the consequences of such phenomenon may be approximated with good accuracy by a change in the natural frequency of the tank-liquid system and damping ratio.

In this study, the value of 5 percent of critical damping is applied for liquid domain as a conservative damping ratio.

### 4.6 Finite element implementation

A schematic configuration of a rectangular concrete tank which is more common in design codes is shown in Figure 4.3. In this study, two different model configurations associated with shallow and tall tanks are investigated in both two and three-dimensional spaces. These tanks have also been used in some previous investigations by Kianoush and Chen (2006), Chen and Kianoush (2005) and Kim et al. (1996). The dimensions and properties of shallow and tall tank are as follows:

Shallow Tank:

$\rho_w = 2300kg/m^3$ $\rho_l = 1000kg/m^3$ $E_c = 26.44GPa$ $\nu = 0.17$
$L_x = 15m$ $L_z = 30m$ $H_w = 6.0m$ $H_l = 5.5m$ $t_w = 0.6$

Tall Tank:

$\rho_w = 2300kg/m^3$ $\rho_l = 1000kg/m^3$ $E_c = 20.77GPa$ $\nu = 0.17$
$L_x = 9.8m$ $L_z = 28m$ $H_w = 12.3m$ $H_l = 11.2m$ $t_w = 1.2$

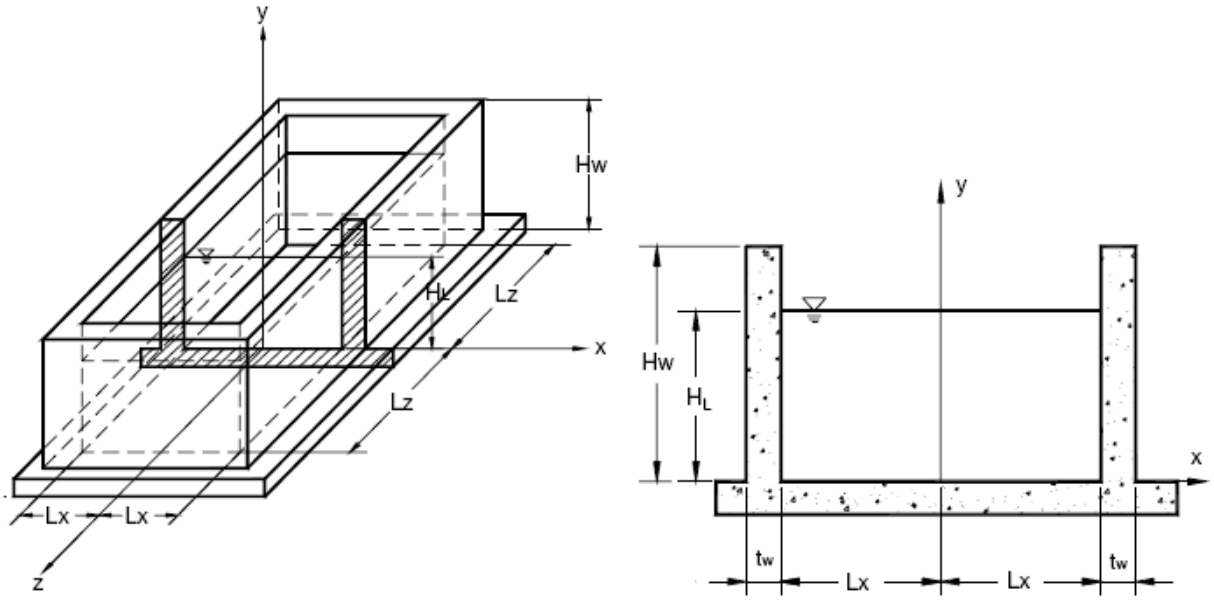


Figure 4.3: Schematic configuration of a rectangular liquid tank

A 1 m strip of the tank at the middle of longer dimension is modeled to simulate the two-dimensional behaviour of the system. In current design code, it is generally assumed that the tank is supported on a rigid foundation and the effect of soil-structure interaction is indirectly considered using site coefficient factors $F_a$ and $F_v$ in accordance with ASCE 7-05 (2205). It is

also assumed that the tank is anchored at its base and the effects of uplift pressure are not considered.

In this study, to accurately simulate the interaction among soil, structure and fluid, an eight node isoparametric solid element (Solid 45 in ANSYS program) with three translational degrees of freedom in each node is used in the three-dimensional FE procedure to model the tank walls, base slab and soil foundation. For two-dimensional analysis, a four node isoparametric solid element with two translational degrees of freedom (Solid 42 in ANSYS program) is used. The liquid domain is modeled using 8-node isoparametric fluid elements in 3D space and 4-node isoparametric fluid elements in 2D space with pressure degree of freedom in each node (3D Acoustic 30 and 2D Acoustic 29 in ANSYS program).

Due to limitation of ANSYS program in applying free surface sloshing boundary condition, additional numerical algorithms are incorporated into the main program to account for the dynamic sloshing behaviour. In addition, this numerical algorithm is able to simulate the damping properties of the liquid domain as presented in previous section. The proposed numerical approach is adopted from NSAD program developed by Ghaemian and Ghobarah (1999) for 2D nonlinear seismic analysis of concrete gravity dams including dam-reservoir interaction.

In this study, the FLUID algorithm is developed for the purpose of 2D and 3D analysis of concrete rectangular liquid tanks. An example of main subroutine file is given in Appendix A.

The finite element (FE) model configurations for both shallow and tall tanks are shown in Figure 4.4. Letters A, B and C shown in the figures refer to locations where the results of sloshing are presented. The 2D model consists of 182 solid elements and 110 fluid elements for shallow tank configuration and 149 solid elements and 165 fluid elements for tall tank

configuration. In 3D model, the shallow tank model is generated using 2592 solid elements and 2200 fluid elements while tall tank model includes 3420 solid elements and 3300 fluid elements.

The longitudinal, transversal and vertical components recorded for 1940 El-Centro earthquake are used as primary excitations of the tank–liquid system. The components are scaled in such a way that the peak ground acceleration in the longitudinal direction is 0.4g, as shown in Figure 4.5.

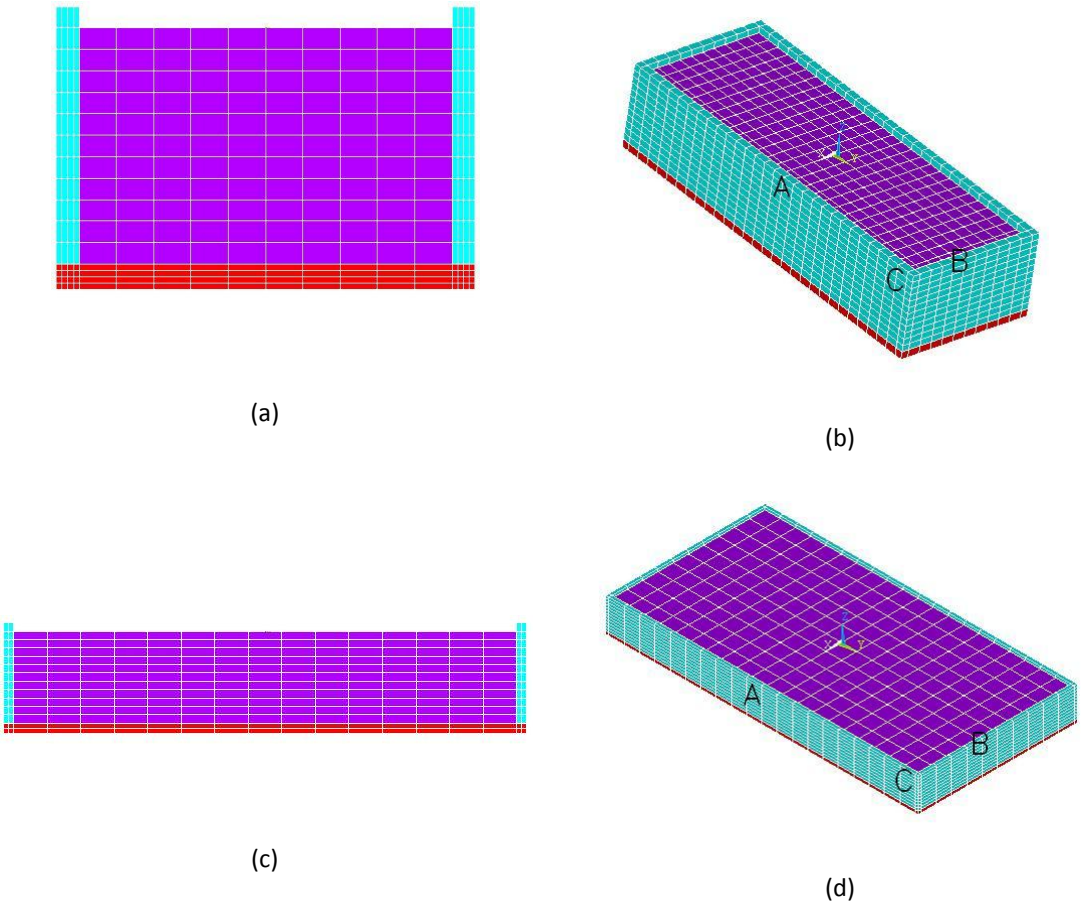


(a) (b)

(c) (d)

Figure 4.4: Finite element model of rectangular tank: (a) 2D tall tank model (b) 3D tall tank model (c) 2D shallow tank model (d) 3D shallow tank model

Two rectangular concrete liquid container models given in Figure 4.4 are used basically for the example analyses in time-domain. To investigate the effect of three-dimensional geometry on dynamic behaviour of liquid tanks, both two and three-dimensional tank responses have been obtained. The cross-section parallel to short side wall is adopted for 2D FE models. It should be noticed that both longitudinal and transversal components of earthquake perpendicular to longer and shorter tank wall are simultaneously applied in three-dimensional modeling and are referred to as horizontal excitation. In addition, both rigid and flexible boundary conditions are applied to investigate the effect of wall flexibility on the seismic response of liquid tanks including both impulsive and convective components.

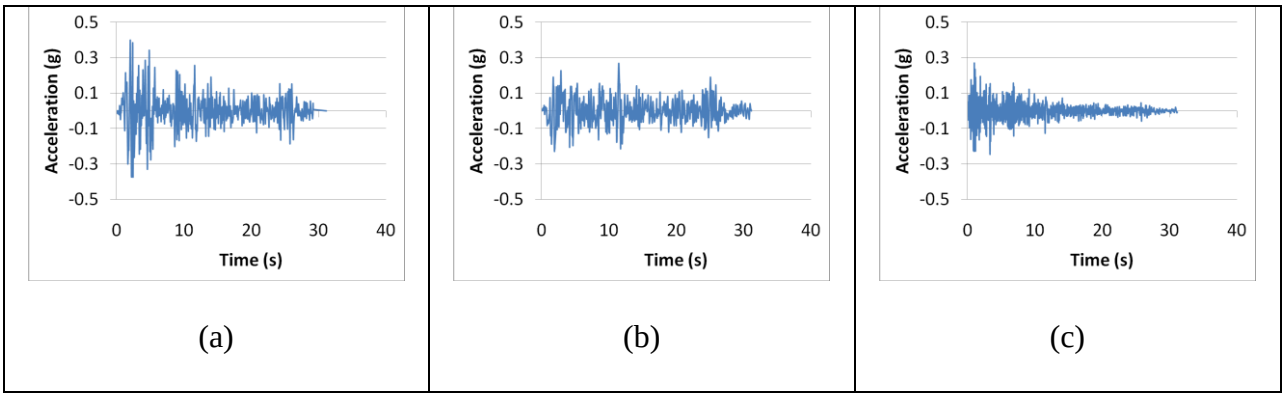


Figure 4.5: Scaled components of the 1940 El-Centro earthquake: (a) longitudinal component (b) transverse component (c) vertical component

Since the sloshing height variation is a matter of concern in design of rectangular tanks, its value is measured at three different locations (points A, B and C in Figure 4.4) of three-dimensional model and then compared to two-dimensional model. In Figure 4.4, points A, B and

C are located at the fluid surface at the middle of longer length, middle of shorter length and the corner of tank model, respectively.

Finally, special topics such as soil-structure interaction and effect of earthquake frequency content are considered using appropriate boundary conditions and various earthquake records.

### 4.6.1 Mesh sensitivity and error estimation

The first step in a finite-element analysis is to estimate the possible error by selecting a mathematical model to represent the object being analyzed. The mathematical target for this study was derived in Chapter 3 for a rigid rectangular tank and can be selected as the maximum pressure at the bottom of rigid tank.

The analysis goal is to compute the exact solution of bottom pressure named $P_{EX}$ and then calculate its value using FEM which is $P_{FE}$. The term $P_{EX}$ depends only on the definition of the mathematical model and not on the method used for finding an approximate solution. Therefore, it does not depend on mesh quality, type, and size of elements. The difference between $P_{EX}$ and the physical property it represents is called the modeling error.

As a result, discretization error is defined by:

$$e = \frac{(P_{EX}) - (P_{FE})}{(P_{EX})} \tag{4.37}$$

The variations of ratio of FE bottom pressure to the analytical pressure with the number of mesh divisions are shown in Figure 4.6 for both rigid shallow and tall tank models. It is found that the discritization errors are equal to 1.66 and 0.03 percent for proposed shallow and tall tank models respectively when subjected to an earthquake ground motion. This range of error is acceptable for numerical analyses. A detailed comparison between analytical and FE results will be discussed in Chapter 5.

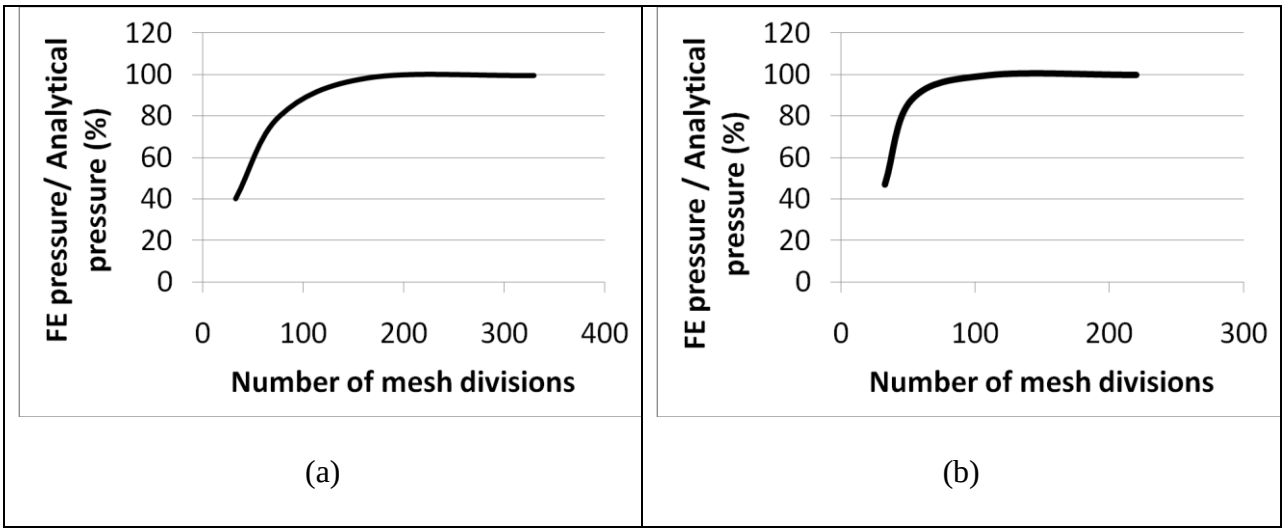


Figure 4.6: Finite element discritization error: (a) 2D shallow tank model (b) 2D tall tank model

## 4.7 Foundation modelling

### 4.7.1 Wave equation

In this study, a viscous boundary method is used in three-dimensional space which was successfully employed in FE modeling of elevated liquid tanks done by Livaoglu and Dogangun (2007). The wave propagation in the x-direction is considered to calculate the properties of this boundary condition. The forces that cause the wave propagation are shown acting on a unit cube in Figure 4.7. For this cube, the one dimensional equilibrium equation in the x-direction is:

$$\rho \frac{d^2u}{dt^2} - \frac{d\sigma_x}{dx} = 0 \tag{4.38}$$

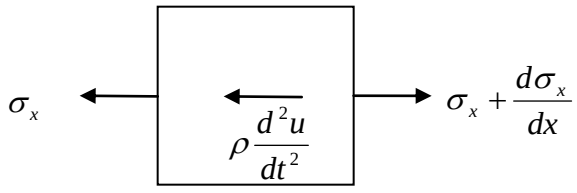


Figure 4.7: Applied forces on a unit cube

Where $\rho$, $u$ and $\sigma_x$ represent mass density, displacement and the stress in the x-direction, respectively. The one-dimensional partial differential equation is written in the classical wave propagation form as:

$$\frac{d^2u}{dt^2} - v_p^2 \frac{d^2u_x}{dx^2} = 0 \tag{4.39}$$

Where $v_p$ is the wave propagation velocity and is given by $v_p = \sqrt{E_f / \rho_f}$, in which $\rho_f$ is the mass density and $E_f$ is the bulk modulus of soil. The strain in the same direction and corresponding stress can be expressed in the following simplified form: (Lysmer and Kuhlmeyer (1969))

$$\varepsilon(t,x) = \frac{du}{dx} = -\frac{\dot{u}(x,t)}{v_p} \tag{4.40}$$
$$\sigma_x = E_f \varepsilon(t,x) = -\rho_f v_p \dot{u}(x,t)$$

These viscous boundaries can be used with the FE mesh as shown in Figure 4.8 for a generalized three-dimensional model (Livaoglu and Dogangun (2007)). In this figure, $A_n$, $A_{t1}$ and $A_{t2}$ are the fields controlling the viscous dampers, $\sigma$ and $\tau$ are the normal and shear stresses occurring in the boundaries of the medium, and the subscripts *n* and *t* represent normal and tangent directions in the boundary. When the viscous boundary is taken into consideration, an additional damping matrix is applied to the system as below:

$$\left[C_i^*\right] = \begin{bmatrix} A_n \rho v_p & 0 & 0 \\ 0 & A_{t1} \rho v_s & 0 \\ 0 & 0 & A_{t2} \rho v_s \end{bmatrix} \tag{4.41}$$

Where $v_p$ and $v_s$ are dilatational and shear wave velocity of the considered medium. It should be noticed that in two-dimensional analysis, the third row and column are eliminated.

Using Lysmer's method, additional springs with the stiffness of $K_{Spring}=E_f A_f / h_f$ are set along truncated boundaries to account for the elastic properties of the far-field soil. $E_f$ is the Young's modulus of the foundation, $A_f$ is the tributary area of the node connected to the spring, and $h_f$ is the width or depth of foundation.

It is assumed that the tank structure is anchored to the foundation. Considering the effects of soil-structure interaction, Eq.4.29 can be re-written as below:

$$[M]\{\ddot{U}\}+([C]+[C_i^*])\{\dot{U}\}+([K]+[K_i^*])\{U\}=\{f_1\}-[M]\{\ddot{U}_g\}+[Q]\{P\}=\{F_1\}+[Q]\{P\}$$
$$[G]\{\ddot{P}\}+[C']\{\dot{P}\}+[H]\{P\}=\{F\}-\rho[Q]^T(\{\ddot{U}\}+\{\ddot{U}_g\})=\{F_2\}-\rho[Q]^T\{\ddot{U}\} \quad (4.42)$$

Where $[C_i^*]$ and $[K_i^*]$ are the damping and stiffness matrices associated with the foundation-structure interaction.

$N_n = A_n\sigma_n;\ N_{t1} = A_{t1}\tau_{t1};\ N_{t2} = A_{t2}\tau_{t2}$
$N_n + C_n\dot{u}_n = 0$
$N_{t1} + C_{t1}\dot{u}_{t1} = 0$
$N_{t2} + C_{t2}\dot{u}_{t2} = 0$

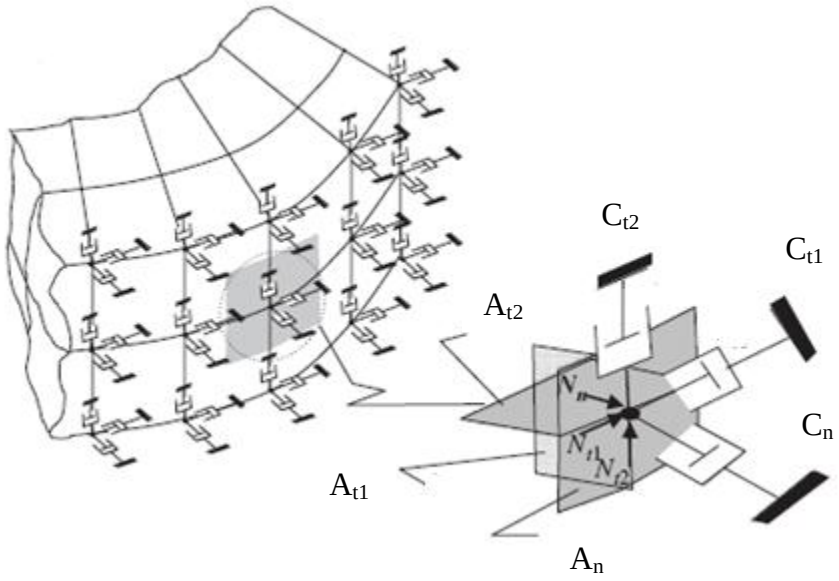


Figure 4.8: Viscous boundary condition in the 3D finite element model (Livaoglu and Dogangun 2007)

### 4.8 Summary

In this Chapter, the solution procedure for coupled system of liquid-tank-foundation using finite element method in the time domain was described. Also, problems associated with damping characteristics, free surface motion and wall boundary conditions were discussed.

In addition, a brief description of FE error estimation was given. It is found that the proposed FE mesh patterns for both shallow and tall tank configurations are able to accurately simulate the fluid dynamic behaviour.

Finally, a simplified foundation model using viscous boundary condition was presented to account for the effect of soil-structure interaction on the dynamic behaviour of liquid tanks.

# Chapter 5
# Dynamic response of concrete rectangular liquid tanks in 2D and 3D spaces

## 5.1 Introduction

In this chapter, the effects of wall flexibility and three-dimensional geometry on the dynamic behaviour of liquid concrete rectangular tanks are discussed. This chapter is divided into two parts. In the first part, liquid tank models are analyzed in 2D space including both rigid and flexible wall boundary conditions. The results are then compared to investigate the effect of wall flexibility on the impulsive and convective response of tank models. Both horizontal and vertical components of earthquake are applied.

Additional boundary conditions including walls with a linear distribution of moment of inertia along their heights which represents an estimation of the level cracking of the tank walls are considered in numerical analyses. It should be noted that the modelling of nonlinear behaviour of concrete is beyond the scope of this study and this additional boundary condition is merely applied to investigate the effect of varying wall flexibility on liquid tank behaviour.

In the second part, the response of flexible liquid tank models are obtained in 3D space and a comparison is made with 2D results to investigate the effect of three-dimensional geometry on the dynamic behaviour of tank models. All the three components of earthquake record including vertical are applied in the analyses.

Finally, the results of this study are compared with those available in literature as well as analytical approaches to verify the proposed method. In addition, some recommendations are proposed to be considered in liquid tank design procedures based on findings of this study.

### 5.2 Effect of wall flexibility on dynamic behaviour of liquid tank models

Two rectangular concrete liquid container models presented in section 4.6 are used basically for the example analyses in two-dimensional space. The cross-section parallel to short side wall is adopted for 2D FE models as shown in Figures 4.6(a) and 4.6(c) including both impulsive and convective responses. To investigate the effect of wall flexibility on dynamic behaviour of liquid tanks, both flexible and rigid tank responses have been obtained. Seismic analyses are performed using both horizontal and vertical components of ground acceleration and the results are compared with other relevant methods available in literature.

Prior to conducting the time-history analyses, the natural periods of sloshing as well as impulsive and convective mass ratios are calculated using both finite element and analytical method. According to ACI 350.3-06 (2006), for a given rectangular prismatic tank shown in Figure 3.2, the fundamental sloshing period and frequency of liquid depending on fill depth are given by:

$$f_\omega = \frac{1}{2\pi}\sqrt{(n\pi g/a)\tanh(n\pi H_L/a)} \quad T_\omega = \frac{1}{f_\omega} \tag{5.1}$$

The impulsive and convective mass ratios are calculated using the following equations according to Housner (1957):

$$\frac{W_c}{W_L} = \frac{1}{3}\sqrt{\frac{5}{2}}\left(\frac{a}{2H_L}\right)\tanh\left[\sqrt{\frac{5}{2}}\left(\frac{2H_L}{a}\right)\right] \tag{5.2a}$$

$$\frac{W_i}{W_L} = \frac{\tanh\left(\frac{\sqrt{3}}{2}\left(\frac{a}{H_L}\right)\right)}{\frac{\sqrt{3}}{2}\left(\frac{a}{H_L}\right)} \tag{5.2b}$$

Where $W_i$ and $W_c$ are impulsive and convective masses and $W_L$ is the total mass of fluid, respectively.

A comparison among FE, ACI Code and analytical results is shown in Table 5.1 which indicates that the FE results are in agreement with ACI code values in terms of convective values especially for shallow tank model. This is mainly because of the linearized wave equation which is used in both methods. However, some discrepancies are found between impulsive terms. In the ACI Code procedure, the impulsive mass of fluid is assumed as a lumped mass rigidly attached to the cantilever wall. On this basis, the impulsive behaviour is calculated. Figure 5.1 shows the mode shape related to first fundamental frequency of sloshing. In FEM, the coupled systems of equations are solved to obtain the fundamental frequencies. As a result, different impulsive responses in terms of both natural frequencies and mass ratios are expected when comparing FE results with those of ACI code approach.

Table 5.1: Natural sloshing periods and mass ratios of 2D shallow and tall tank models

| | Analytical | | FEM | | | | ACI code | | | |
|---|---|---|---|---|---|---|---|---|---|---|
| | Fundamental period (sec) | | Fundamental period (sec) | | Effective mass ratio | | Fundamental period (sec) | | Effective mass ratio | |
| | $T_i$ | $T_c$ | $T_i$ | $T_c$ | $m_i/m$ | $m_c/m$ | $T_i$ | $T_c$ | $m_i/m$ | $m_c/m$ |
| Shallow tank | 0.14 | 8.60 | 0.15 | 8.58 | 0.10 | 0.68 | 0.10 | 8.56 | 0.21 | 0.75 |
| Tall tank | 0.33 | 5.29 | 0.33 | 5.30 | 0.43 | 0.30 | 0.22 | 5.50 | 0.59 | 0.44 |

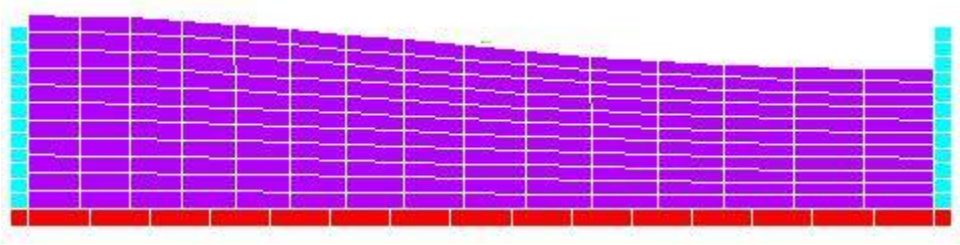

Figure 5.1: Mode shape related to first fundamental frequency of sloshing

In addition, FE values are consistent with those of analytical approach described in Chapter 3 for a flexible tank. Further details on the calculation of sloshing frequencies and masses are given by Karamanos et al. (2006) and Patkas & Karamanos (2007).

### 5.2.1 Behaviour of liquid tanks with rigid walls

#### 5.2.1.1 Response of 2D shallow tank model

Once the ground accelerations are defined, time history analyses are performed to compute the response of the structure at each of the time steps specified in the computer program. In this study, the variations of impulsive and convective structural responses with time are obtained to consider the time-dependent response characteristics of the fluid-structure system.

The transient base shear and base moment for rigid shallow tank model due to horizontal and vertical ground excitations of El-Centro record corresponding to peak ground acceleration of 0.4g are calculated by proposed method. The related diagrams are shown in Figures 5.2 and 5.3 for base shear and base moment, respectively.

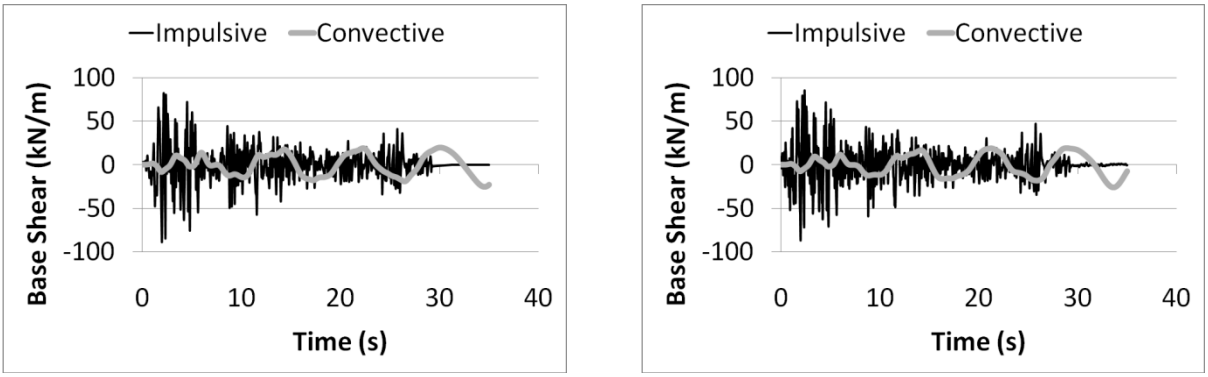


(a) (b)

Figure 5.2: Time history of base shear for shallow tank model with rigid side walls: (a) Horizontal excitation (b) Horizontal and vertical excitation

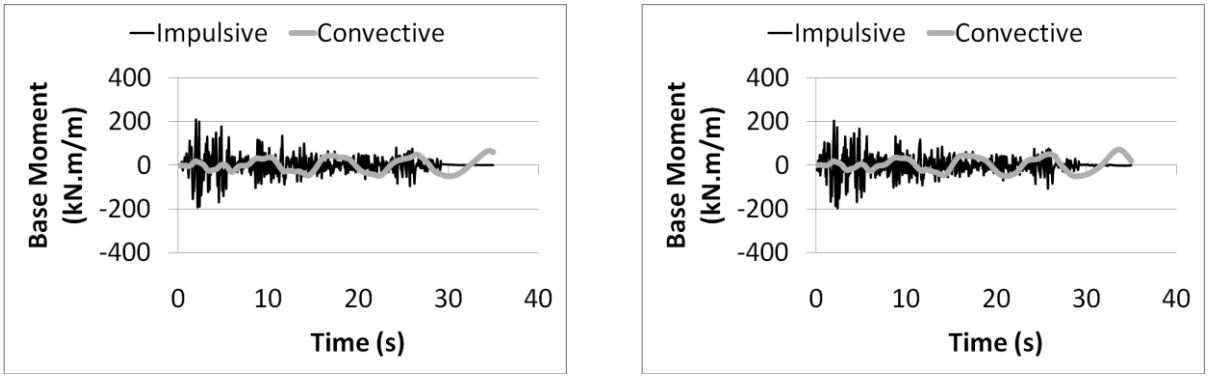


(a) (b)

Figure 5.3: Time history of base moment for shallow tank model with rigid side walls: (a) Horizontal excitation (b) Horizontal and vertical excitation

The absolute maximum values of the impulsive response resulting base shear and base moment due to the horizontal excitations are 89 kN/m and 209 kNm/m, respectively. In this case, the absolute peak values of convective base shear and base moment responses are 25 kN/m and 67 kNm/m which have occurred around 30 seconds after peaks of impulsive responses. On the other hand, when the impulsive response reaches its peak, the convective response is at the beginning stage and has not yet fully developed. Therefore, as seen in Figures 5.2 and 5.3, the forces due to liquid fluctuations have insignificant effect on the overall dynamic responses of liquid tank model. As a result, in this case the base shear and base moment responses are governed by impulsive components.

Considering the combined effect of vertical and horizontal ground motions, the impulsive base shear and base moment responses decrease slightly about 3 and 2 percent, respectively while the absolute maximum values of convective base shear and base moment slightly increase by 4 and 6 percent, respectively. It is found that in this case vertical acceleration of earthquake has an insignificant effect on seismic response. A summary of the peak response values are provided in Table 5.2.

In addition, the time history diagram of surface sloshing height at the top of the wall is shown in Figure 5.4. Due to effect of vertical acceleration, the absolute maximum values of sloshing has increased from $\delta_{max} = 527$ mm at t=33.98 s to $\delta_{max} = 548$ mm at t=33.04 s which represents about 4 percent increase over that under horizontal ground motion.

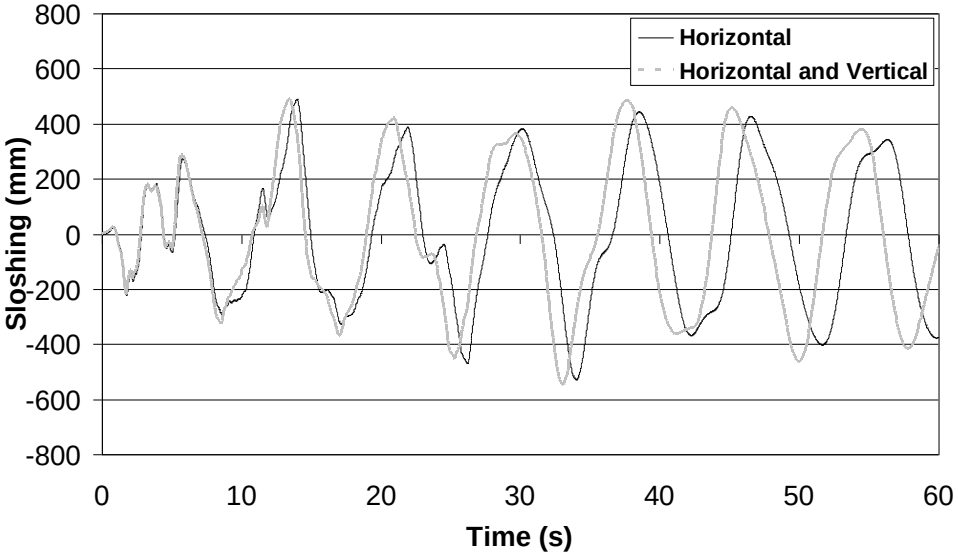


Figure 5.4: Time history of sloshing height at the top of the wall for rigid shallow tank model

#### 5.2.1.2 Response of 2D tall tank model

Figures 5.5 and 5.6 present the diagrams of structural response in terms of base shear and base moment time history for rigid tall tank model. The absolute maximum values of the resulting base shear and base moment of the impulsive component due to the horizontal excitations are 328 kN/m and 1575 kNm/m, respectively. Considering the free surface motion, the obtained absolute maximum values of convective base shear and base moment responses are 39 kN/m and 202 kNm/m respectively which have occurred at around 5 seconds following peaks of the

impulsive responses. In this case, the absolute maximum values of convective response are about 10 percent of those values associated with impulsive response. However, this ratio was found to be much higher in shallow tank model. As a result, the convective term is more significant in the shallow tank than the tall tank.

Table 5.2: Summary of dynamic responses of 2D shallow and tall tank models

| | | | Impulsive response | | | Convective response | | |
|---|---|---|---|---|---|---|---|---|
| | | | H | H+V | (H+V)/H | H | H+V | (H+V)/H |
| Shallow tank | Rigid | Base Shear (kN/m) | 89 | 86 | 0.97 | 25 | 26 | 1.04 |
| | | Base Moment (kNm/m) | 209 | 205 | 0.98 | 67 | 71 | 1.06 |
| | | Sloshing (mm) | - | - | - | 527 | 548 | 1.04 |
| | Flexible | Base Shear (kN/m) | 142 (60%)* | 148 (72%) | 1.04 | 22 (-12%) | 24 (-8%) | 1.09 |
| | | Base Moment (kNm/m) | 415 (99%) | 437 (113%) | 1.05 | 55 (-18%) | 62 (-13%) | 1.13 |
| | | Sloshing (mm) | - | - | - | 488 (-7%) | 490 (-11%) | 1.04 |
| Tall Tank | Rigid | Base Shear (kN/m) | 328 | 324 | 0.99 | 39 | 40 | 1.02 |
| | | Base Moment (kNm/m) | 1575 | 1555 | 0.99 | 202 | 210 | 1.04 |
| | | Sloshing (mm) | - | - | - | 636 | 708 | 1.11 |
| | Flexible | Base Shear (kN/m) | 588 (79%) | 563 (74%) | 0.96 | 43 (10%) | 47 (17%) | 1.09 |
| | | Base Moment (kNm/m) | 3630 (130%) | 3626 (133%) | 1.00 | 228 (13%) | 254 (21%) | 1.11 |
| | | Sloshing (mm) | - | - | - | 689 (8%) | 786 (11%) | 1.14 |

*The values in the bracket indicate percentage increase over 2D rigid model

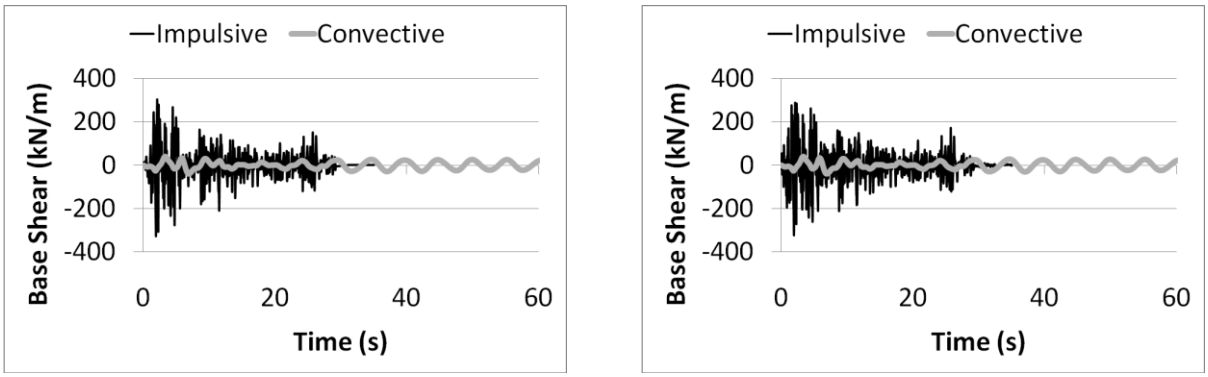


(a) (b)

Figure 5.5: Time history of base shear for tall tank model with rigid side walls: (a) Horizontal excitation (b) Horizontal and vertical excitation

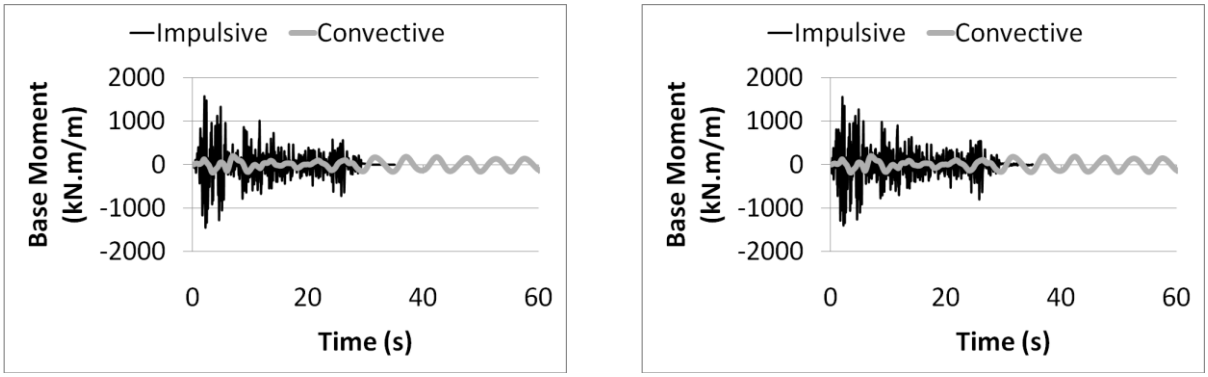


(a) (b)

Figure 5.6: Time history of base moment for tall tank model with rigid side walls: (a) Horizontal excitation (b) Horizontal and vertical excitation

Due to effect of vertical ground motion, the impulsive response decrease by 1 percent while the convective response increase by about 4 percent which shows the same trend as seen previously in shallow tank model.

The time history diagram of sloshing height at the top corner of the liquid domain at wall location is shown in Figure 5.7. Due to effect of vertical acceleration, the absolute maximum value of sloshing has increased from $\delta_{max} = 636$ mm at t=28.74 s to $\delta_{max} = 708$ mm at t=28.2 s.

Clearly, this increase due to vertical earthquake component is about 11 percent higher than its value in shallow tank model.

In addition, the ratio of maximum sloshing height to fluid height ($\eta=\delta_{max}/H_L$) is calculated for both shallow and tall tank configurations. The corresponding values are 0.095 and 0.058 under horizontal excitations for shallow and tall tank models, respectively. This indicates that the sloshing effect on liquid-tank system is more significant in shallow tank than tall tank.

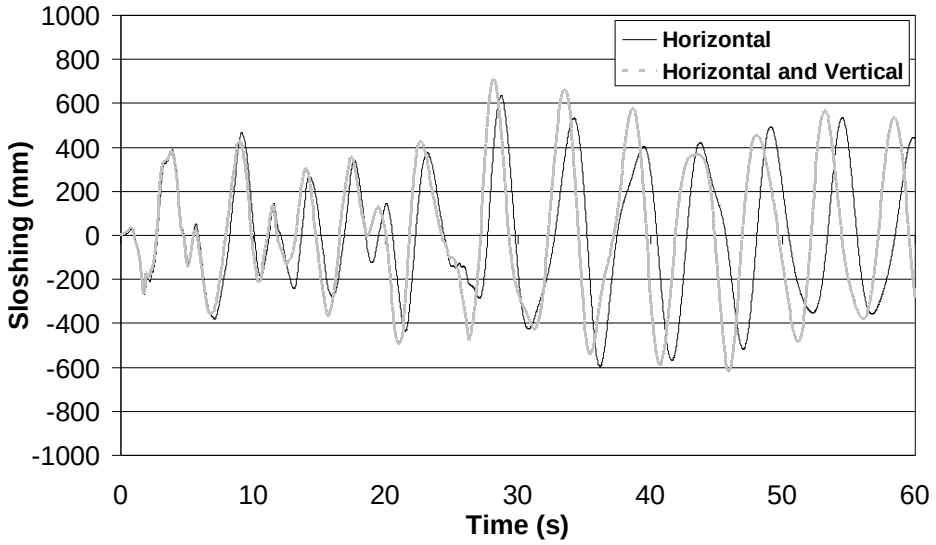


Figure 5.7: Time history of sloshing height at the top of the tank wall for rigid tall tank model

### 5.2.2 Behaviour of liquid tanks with flexible walls

#### 5.2.2.1 Response of 2D shallow tank model

As mentioned before, in order to consider the effects of flexibility of tank wall on both dynamic pressure distribution and dynamic response of tank structure, an additional FE flexible wall boundary condition is investigated in this study. The dynamic responses of shallow tank structure in terms of base shear and base moment are presented in Figures 5.8 and 5.9.

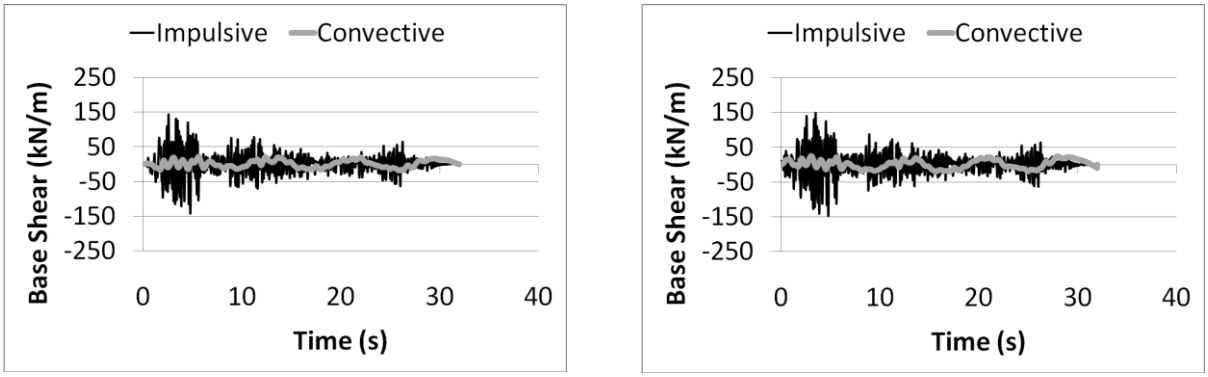


(a) (b)

Figure 5.8: Time history of base shear for shallow tank model with flexible side walls: (a) Horizontal (b) Horizontal and vertical

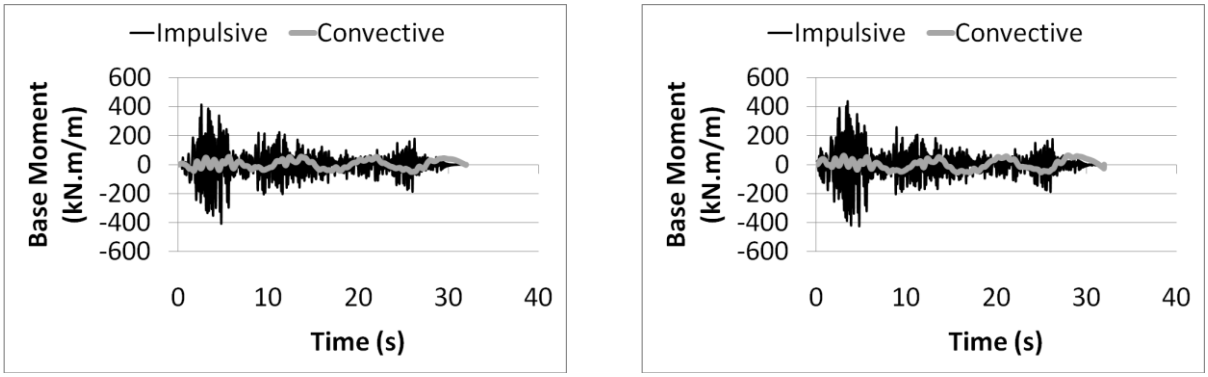


(a) (b)

Figure 5.9: Time history of base moment for shallow tank model with flexible side walls: (a) Horizontal (b) Horizontal and vertical

Under horizontal excitation, the absolute maximum values of the resulting base shear and base moment are 142 kN/m and 415 kNm/m as impulsive terms and 22 kN/m and 55 kNm/m as convective terms, respectively. In comparison with rigid boundary condition results, the maximum values associated with impulsive base shear and base moments are significantly increased by about 60 and 99 percents due to flexibility of side walls, respectively. However, the

effect of wall flexibility on convective response is much less significant than its effect on impulsive responses as presented in Table 5.2.

Similar to the rigid tank, the vertical component of earthquake affects the convective term more than that of impulsive. The convective base shear and base moment maximum values have increased by 9 and 13 percent, respectively. The increase for impulsive terms is about 5 percent. Since the total response is governed by impulsive component, it can be concluded that effect of vertical acceleration is insignificant on the total response of liquid tank system.

The pressure distribution along the tank height is shown in Figure 5.10. In fact, hydrodynamic pressure tends to be amplified due to fluid-structure interaction effect in a flexible container and its distribution differs from that in the corresponding rigid container. In shallow tank model, the bottom pressure value of the flexible tank is about three times higher than the corresponding value of the rigid tank. This trend has also been reported by Haroun and Housner (1981). However, the effect of wall flexibility will lead to a slight reduction about 2 percent in surface convective pressure values as shown in this diagram.

Although most current codes and standards assume that the value of convective pressure at the bottom of tank is zero, the obtained results show different trend for both rigid and flexible models.

As presented in Table 5.2, due to effect of vertical acceleration, the absolute maximum values of sloshing has increased from $\delta_{max} = 488$ mm at t=34 s to $\delta_{max} = 490$ mm at t=33 s. These values show that the flexibility of tank wall has led to a reduction about 7 and 11 percents in sloshing heights in comparison with those values obtained for rigid tank model.

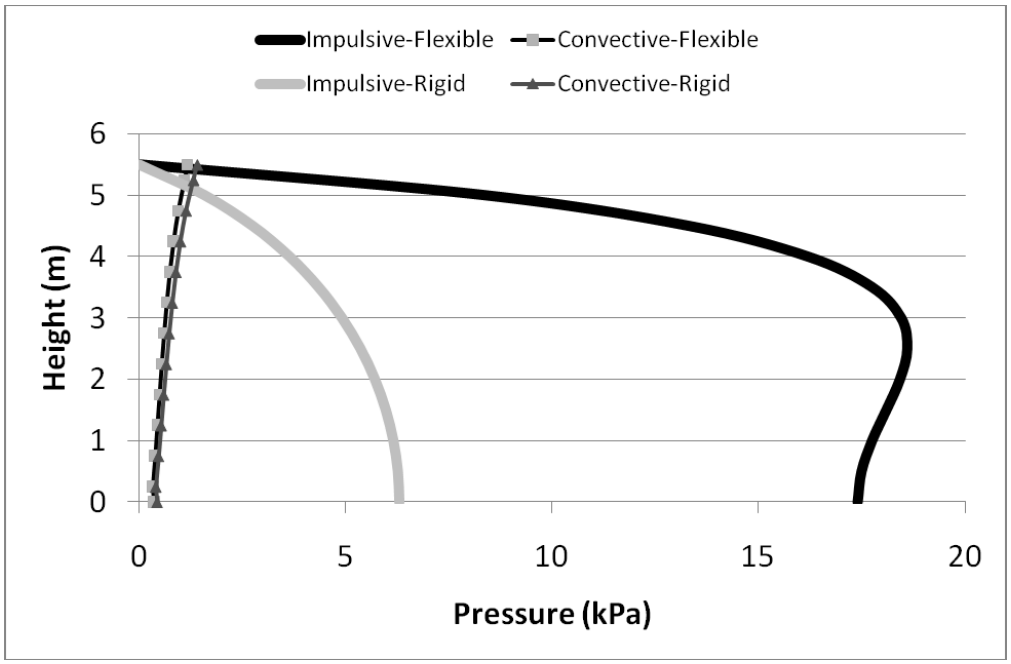


Figure 5.10: Impulsive and convective pressure distribution along height of shallow tank wall for both rigid and flexible wall conditions under horizontal excitation

#### 5.2.2.2 Response of 2D tall tank model

Figures 5.11 and 5.12 show the structural responses in terms of base shear and base moment time history for flexible tall tank model. In comparison with the rigid boundary condition, the maximum absolute values of impulsive base shear and base moment due to horizontal earthquake component are increased by about 79 and 130 percents to the values of 588 kN/m and 3330 kNm/m, respectively. It is found that the effect of flexibility on impulsive terms is more significant in tall tank model than shallow tank model as indicated in Table 5.2. In addition, due to the wall flexibility the convective base shear and base moment responses have increased by 10 and 13 percents. Similar to shallow tank model, flexibility of tank wall has major effect on impulsive term rather than convective term.

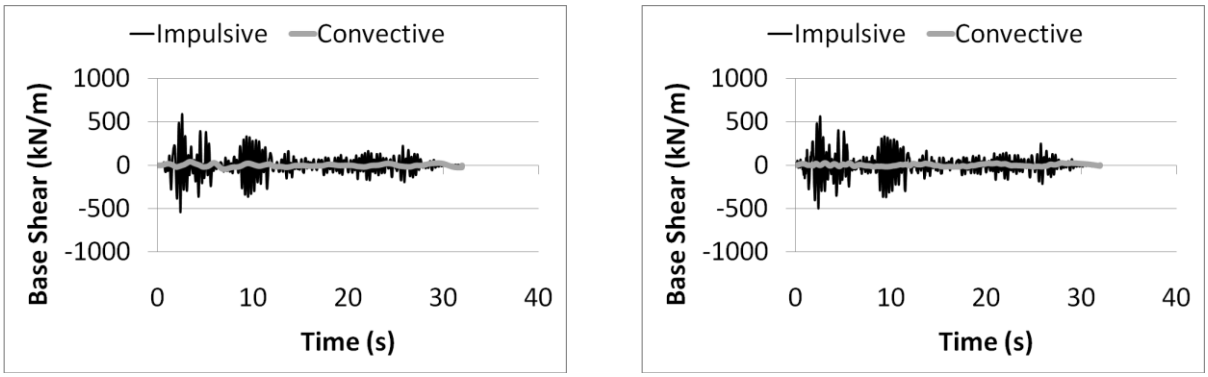


(a) (b)

Figure 5.11: Time history of base shear for shallow tank model with flexible side walls: (a) Horizontal (b) Horizontal and vertical

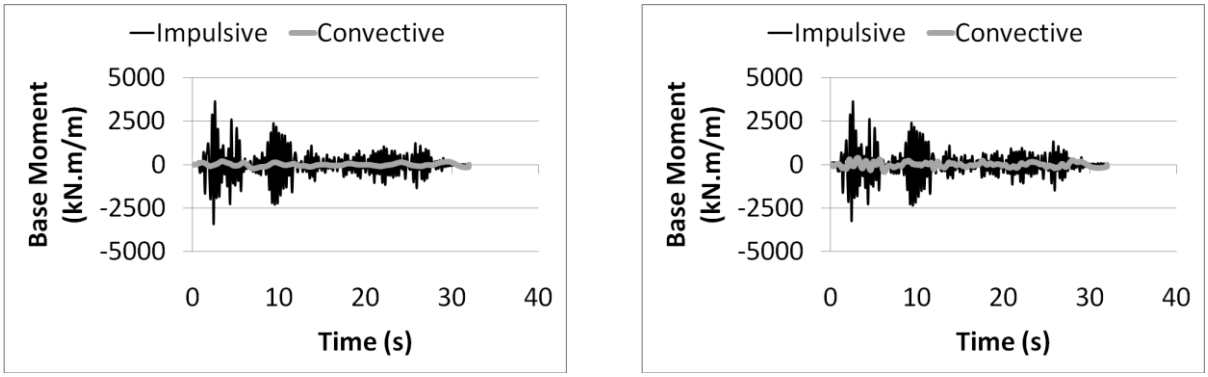


(a) (b)

Figure 5.12: Time history of base shear for shallow tank model with flexible side walls: (a) Horizontal (b) Horizontal and vertical

Accounting for the vertical acceleration effects, the convective base shear and base moment show an average increase of about 10 percent. In this case, the impulsive base shear decreases by 4 percent while impulsive base moment almost remains unchanged.

As seen in time-history response diagrams, the convective term may lead to an increase or decrease in structural responses. This phenomenon can be explained as the phase difference between impulsive and convective responses which depends on various parameters such as tank configuration, earthquake frequency and fluid-structure boundary conditions.

The pressure distribution curves for tall tank model presented in Figure 5.13 show that hydrodynamic pressure is significantly amplified in the middle of the flexible side wall due to wall flexibility. The same trend was seen for shallow tank model.

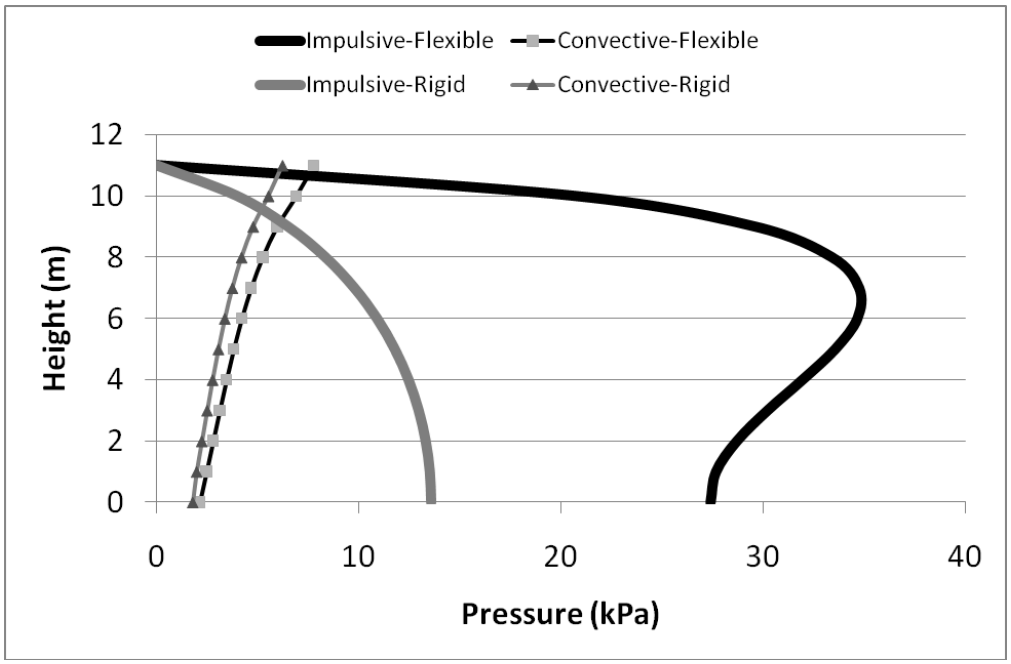


Figure 5.13: Impulsive and convective pressure distribution along height of flexible side wall of tall tank model for both rigid and flexible wall conditions

The maximum sloshing heights due to horizontal and combined horizontal and vertical excitation are $\delta_{max} = 623$ mm at t=28.8 s and $\delta_{max} = 706$ mm at t=28.2 s, respectively. The vertical component of earthquake results in an increase in sloshing height of about 13 percent. The increase in sloshing heights due to the effect of vertical acceleration is higher in tall tank model than shallow tank model and should not be neglected. In addition, the wall flexibility does not have a noticeable effect on sloshing heights as a similar trend was also observed for the shallow tank.

### 5.2.3 Liquid tank response using cracked section properties

As mentioned before, an additional flexible boundary condition is used to investigate the effects of variation of flexibility over the tank heights on impulsive and convective behaviour of tank-fluid system. Instead of considering an uncracked section, a cracked section with a reduced moment of inertia which varies from a maximum value at the bottom section of wall to zero at the top of the wall (i.e. uncracked) is adopted in the numerical model. Two reduction factors of 30 and 50 percents are used (Figure 5.14). These factors are chosen in accordance with CSA Standard A23.3 (2004) to take into account the influence of the presence of cracked regions along the length of the wall members.

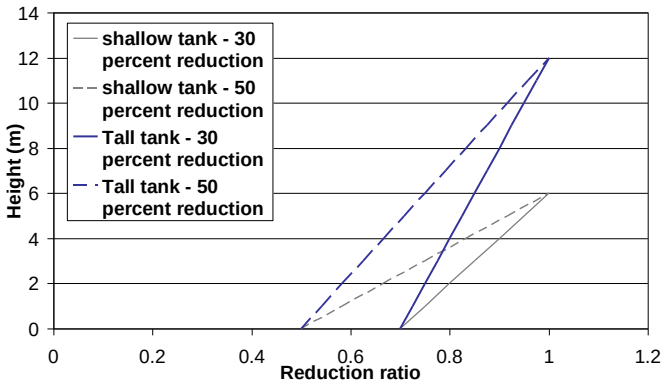


Fig. 5.14: Linear distribution of moment of inertia over wall height for flexible cracked wall boundary condition

As a quantitative comparison, the amount of response variation in liquid tank model with cracked section over the uncracked section is shown in Table 5.3 for both shallow and tall tank models, respectively.

Table 5.3: Variation of response due to cracked section in comparison with uncracked section

| | | | Impulsive response | | Convective response | |
|---|---|---|---|---|---|---|
| | | | H | H+V | H | H+V |
| Shallow | Flexible cracked (30 percent) | Base Shear (kN/m) | 148 (4%)* | 151 (2%) | 22.2 (1%) | 24 (0%) |
| | | Base Moment (kNm/m) | 448 (8%) | 463 (6%) | 56 (2%) | 62 (0%) |
| | | Sloshing (mm) | - | - | 488 (0%) | 495 (1%) |
| | Flexible cracked (50 percent) | Base Shear (kN/m) | 162 (14%) | 481 (10%) | 22.5 (2%) | 24 (0%) |
| | | Base Moment (kNm/m) | 486 (17%) | 481 (10%) | 57 (3%) | 62 (0%) |
| | | Sloshing (mm) | - | - | 489 (0%) | 492 (0%) |
| Tall | Flexible cracked (30 percent) | Base Shear (kN/m) | 617 (5%) | 586 (4%) | 45 (4%) | 48 (2%) |
| | | Base Moment (kNm/m) | 3884 (7%) | 3844 (6%) | 235 (3%) | 262 (3%) |
| | | Sloshing (mm) | - | - | 692 (0%) | 794 (1%) |
| | Flexible cracked (50 percent) | Base Shear (kN/m) | 653 (11%) | (608) 8% | 43 0% | 48 (2%) |
| | | Base Moment (kNm/m) | 4283 (18%) | 4170 (15%) | 230 (1%) | (257) 1% |
| | | Sloshing (mm) | - | - | 691 (0%) | (802) 2% |

*The values in the bracket indicate percentage increase over 2D rigid model

Clearly, the behaviour of tank with cracked section properties result in minor changes in convective terms which indicates that the convective behaviour is almost independent of the flexibility characteristics of the side walls. However, as the moment of inertia of the side wall decrease, the impulsive structural responses increase up to a maximum of 18 percent as seen in tall tank model.

### 5.3 Effect of three-dimensional geometry on dynamic behaviour of liquid tanks

To investigate the effect of three-dimensional geometry on dynamic behaviour of liquid tanks, both two and three-dimensional flexible tank responses have been obtained. As mentioned before, the cross-section parallel to short side wall is adopted for 2D FE models including both impulsive and convective responses. It should be noticed that both longitudinal and transversal components of earthquake perpendicular to longer and shorter tank walls are applied simultaneously in 3D analysis and are referred to as horizontal excitation.

Since the sloshing height variation is a matter of concern in design of rectangular tanks, its value is measured at three different locations (points A, B and C in Figure 4.6) of 3D model and then compared to 2D model. In Figure 4.6, points A, B and C are located at the fluid surface at the middle of longer and shorter walls and at the corner of the tank wall, respectively.

Finally, seismic analyses are performed using both horizontal and vertical components of ground acceleration and the results are compared with other relevant methods available in literature.

#### 5.3.1 Comparison between 2D and 3D seismic response of liquid tanks

##### 5.3.1.1 Response of 3D shallow tank model

The transient base shear and base moment for flexible shallow tank model due to horizontal and vertical excitations acting per unit width of the side wall are calculated by proposed method. A comparison between 2D and 3D modelling of impulsive transient base shear is presented in Figure 5.15.

The absolute maximum values of 3D impulsive response of base shear and base moment due to the horizontal excitations are 191 kN/m and 479 kNm/m which are 34 and 15 percent higher than the corresponding values in 2D model, respectively. These values are measured at the

middle cross-section of the longer wall. It is found that the effect of 3D geometry is significant on the structural response of liquid tank models and may cause a considerable increase in time-domain peak response values as mentioned above. A summary of the results for maximum 3D responses are provided in Table 5.4.

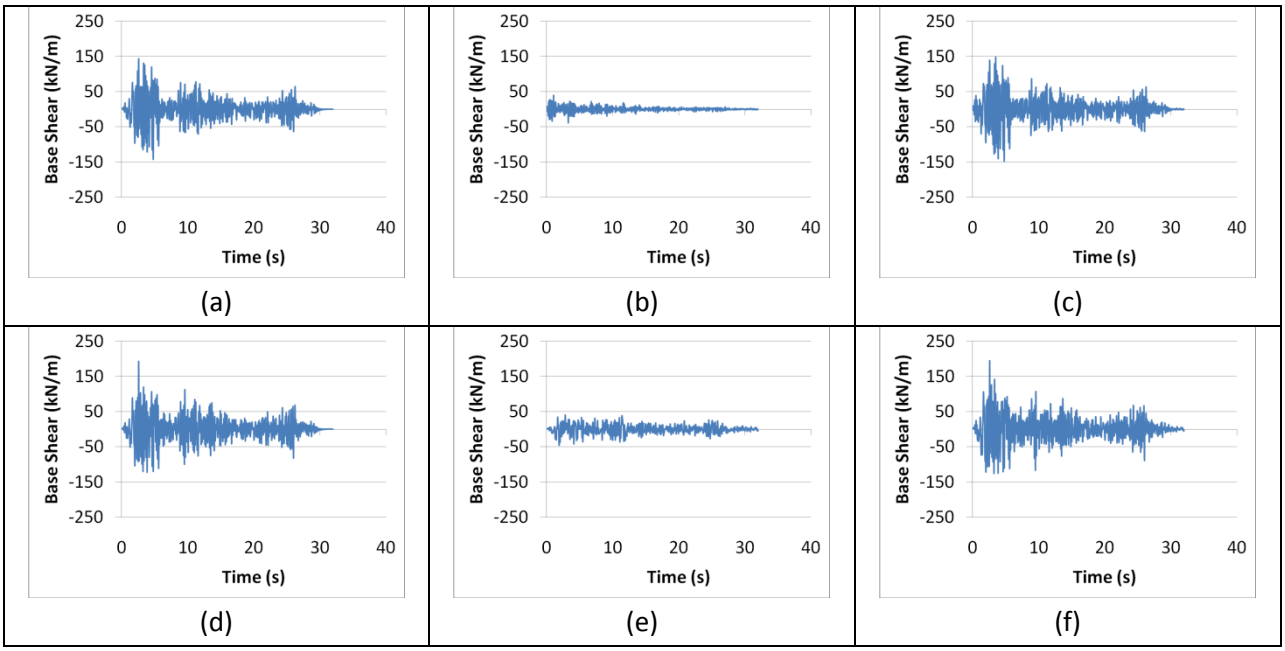


Figure 5.15: Time history of base shear response due to impulsive behaviour of shallow tank model: (a) Horizontal excitation (2D model) (b) Vertical excitation (2D model) (c) Horizontal and vertical excitation (2D model) (d) Horizontal excitation (3D model) (e) Vertical excitation (3D model) (f) Horizontal and vertical excitation (3D model)

In addition to the structural response, the fluid dynamic behaviour is thoroughly investigated. The time history diagrams of surface sloshing height are shown in Figures 5.16(a) and 5.16(b) for 2D and 3D shallow tank models, respectively. As previously mentioned, these values are measured at points A, B and C for 3D model. In 2D model, this value is measured at the top corner of fluid domain which corresponds to point A in 3D configuration.

Table 5.4: Summary of dynamic responses of 3D shallow tank and tall tank models

| | | Impulsive response | | | Convective response | | |
|---|---|---|---|---|---|---|---|
| | | H | H+V | (H+V)/H | H | H+V | (H+V)/H |
| 3D Shallow tank model | Base Shear (kN/m) | 191 (34%)* | 193 (30%) | 1.01 | 36 (64%) | 40 (67%) | 1.11 |
| | Base Moment (kNm/m) | 479 (15%) | 478 (9%) | 1.00 | 59 (7%) | 64 (3%) | 1.08 |
| | Sloshing (mm) | - | - | - | 734 (50%) | 838 (71%) | 1.14 |
| 3D Tall tank model | Base Shear (kN/m) | 846 (44%) | 839 (49%) | 0.99 | 50 (16%) | 60 (28%) | 1.2 |
| | Base Moment (kNm/m) | 4261 (17%) | 4251 (17%) | 0.99 | 211 (-8%) | 231 (-9%) | 1.09 |
| | Sloshing (mm) | - | - | | 920 (48%) | 1134 (62%) | 1.23 |

*The values in the bracket indicate percentage increase over 2D model

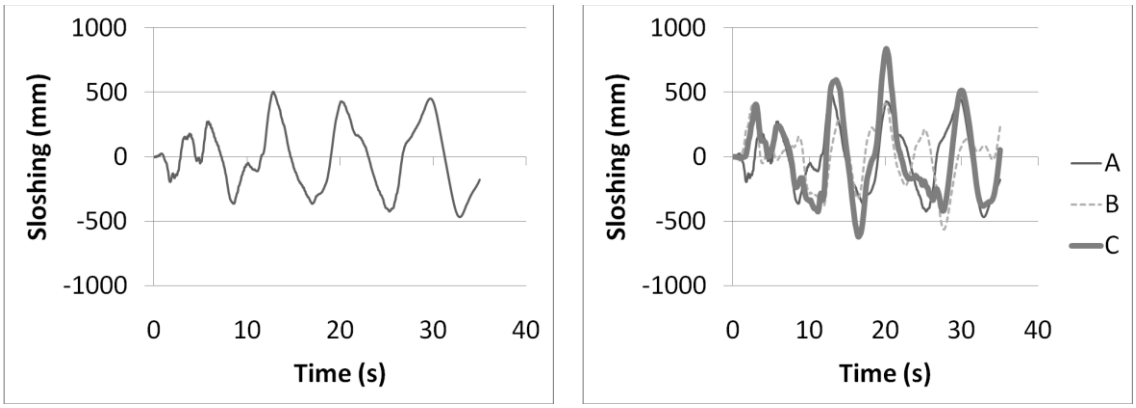


Figure 5.16: Time history of sloshing height of shallow tank model due to all components of earthquake: (a) 2D model (b) 3D model

The sloshing time-history heights measured at point A for both 2D and 3D models are similar and the maximum value is about $\delta_{max} = 488$ mm. However, in 3D model, the maximum sloshing

height of 734mm has occurred at point C which represents an increase about 50 percent over the 2D model.

This phenomenon is mainly because of the interaction of generated waves at the corner of 3D tank model due to both components of longitudinal and transversal ground motion and should be considered in design of rectangular liquid tanks.

As presented in Table 5.4, the effect of vertical acceleration is more significant on the 3D seismic behaviour of fluid domain. The 3D effect results in an increase of about 14 percent in sloshing height whereas, the sloshing height remains unchanged after applying vertical motions in 2D model.

Unlike the convective behaviour, the impulsive behaviour is less sensitive to vertical motions as seen for both 2D and 3D tank models. Since the impulsive response values are much higher than those of convective, it can be concluded that vertical excitation has insignificant effect on overall seismic behaviour of the shallow tank.

The dynamic pressure distributions along the wall height measured at the middle section of the longer wall are shown in Figure 5.17 for both 2D and 3D models. It is found that the variation of dynamic pressure due to vertical acceleration is linear for both impulsive and convective components. Although the dynamic pressure value measured at the bottom of tank is about 13 percent lower in two-dimensional model under horizontal motion, the same values are obtain under the vertical ground motion component.

The vertical excitation has insignificant effect on the magnitude and the distribution of pressure when all earthquake components are applied simultaneously.

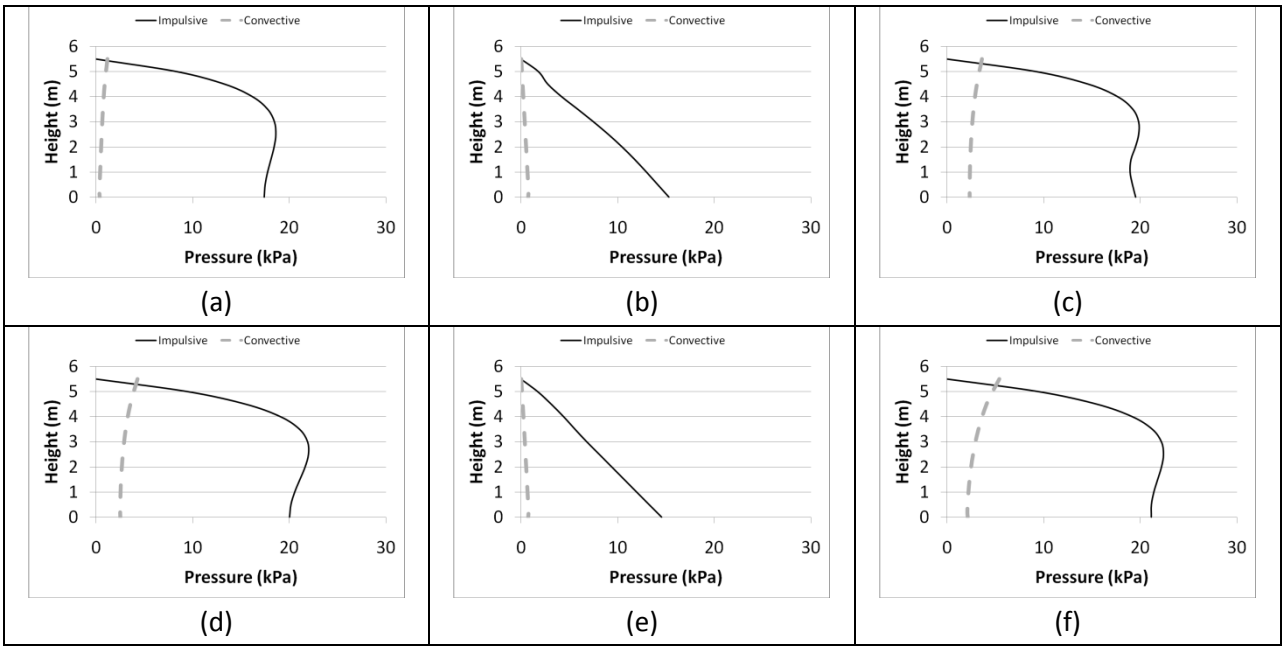


Figure 5.17: Pressure distribution along height of shallow tank model measured at the middle section of longer wall: (a) Horizontal excitation (2D) (b) Vertical excitation (2D) (c) Horizontal and vertical excitation (2D) (d) Horizontal excitation (3D) (e) Vertical excitation (3D) (f) Horizontal and vertical excitation (3D)

#### 5.3.1.2 Response of 3D tall tank model

Figure 5.18 presents the diagrams of impulsive structural response in terms of base moment time history for tall tank model in both 2D and 3D spaces. The absolute maximum values of the resulting base shear and base moment of the impulsive component due to the horizontal excitations are 846kN/m and 4261kNm/m in 3D space which are 44 and 17 percent higher than corresponding values in 2D model, respectively.

As previously seen in shallow tank model, the effect of 3D geometry has significantly amplified the structural responses. As shown in Table 5.4, it is clear that the effect of 3D geometry is more important on impulsive behaviour of tall tank model in comparison with

shallow tank model. Unlike the shallow tank, convective behaviour may decrease due to 3D geometry as seen for calculated base moments.

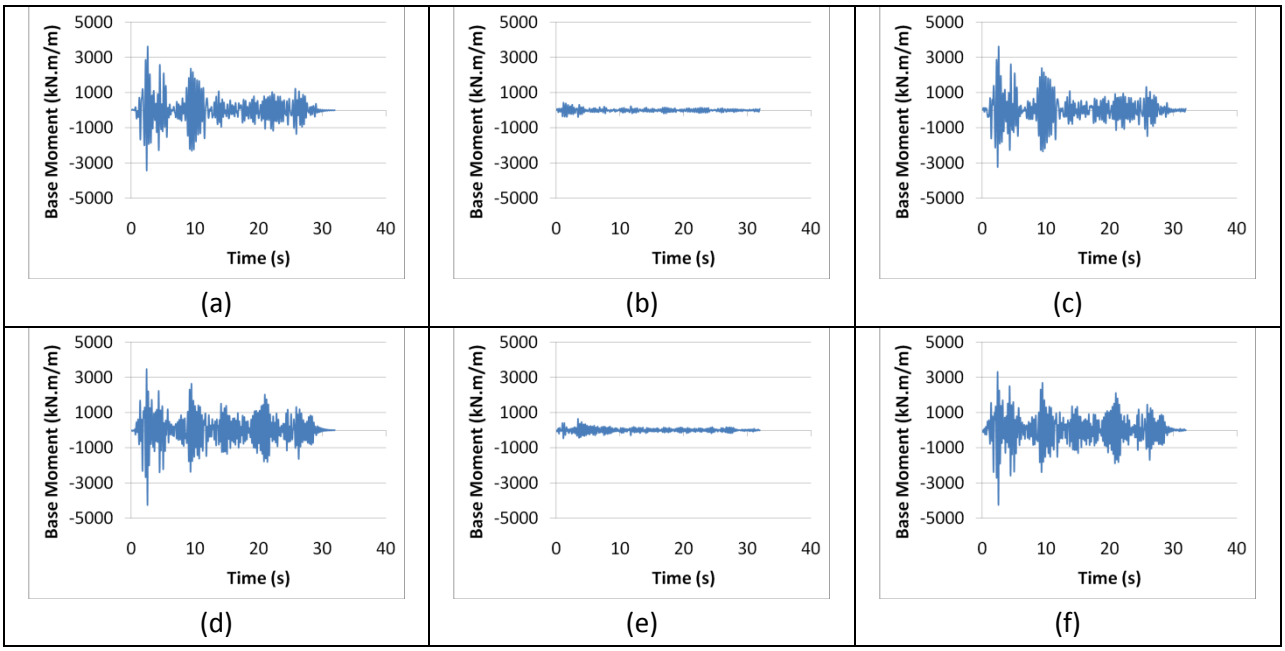


Figure 5.18: Time history of base moment response due to impulsive behaviour of tall tank model: (a) Horizontal excitation (2D model) (b) Vertical excitation (2D model) (c) Horizontal and vertical excitation (2D model) (d) Horizontal excitation (3D model) (e) Vertical excitation (3D model) (f) Horizontal and vertical excitation (3D model)

Under applying all components of ground motion including vertical acceleration, the impulsive responses slightly decrease up to 4 percent while the convective responses increase up to 20 percent in some cases as shown in Table 5.4. This trend is similar for both 2D and 3D models. This indicates that the impulsive term is not sensitive to vertical excitations in both shallow and tall tank which is valid for both 2D and 3D models. The time history diagrams of sloshing height due to all components of earthquake are shown in Figures 5.19(a) and 5.19(b) for 2D and 3D models, respectively. Similar to shallow tank model, the maximum sloshing height

has occurred at point C in 3D model which is almost 20 percent higher than its value measured at point A. Applying vertical acceleration in addition to horizontal acceleration has increased peak sloshing height from $\delta_{max} = 622$ mm to $\delta_{max} = 704$ mm in 2D model. Similarly, its effect has caused a significant increase in peak sloshing height from $\delta_{max} = 920$ mm in 2D model to $\delta_{max} = 1134$ mm in 3D model.

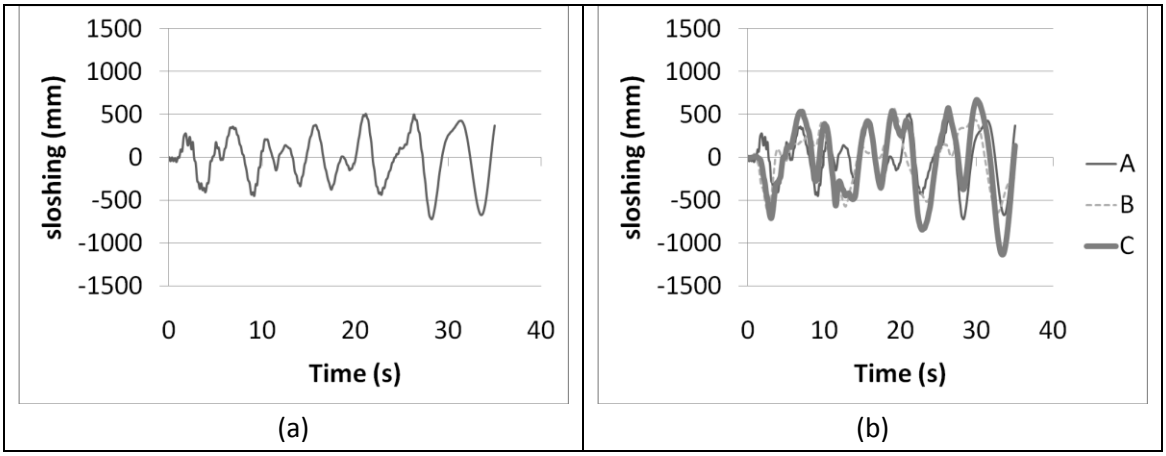


Figure 5.19: Time history of sloshing height of tall tank model due to all components of earthquake: (a) 2D model (b) 3D model

A detailed comparison between peak impulsive pressure distributions over the height of the tank wall measured at the middle section of longer wall is presented in Figure 5.20 for both 2D and 3D models.

Similar to shallow tank model, higher values are obtained accounting for the effect of 3D geometry. For example, the maximum pressure value in 3D model is about 40 percent higher than the corresponding value in 2D model under horizontal excitation. Due to single vertical component, the same linear pressure distribution is obtained similar to shallow tank model and

its peak value at the tank bottom is almost equal to peak vertical acceleration multiplied by the liquid height. This linear variation is valid for both 2D and 3D tank models. Also, the dynamic pressure distribution along the side walls under combined horizontal and vertical ground motions indicates that the effect of vertical ground motion is negligible on the seismic behaviour of fluid-structure system.

It is concluded that dynamic pressure in 3D containers may be highly dependent on the 3D restraint conditions. It is observed that this condition can exert a significant influence on the fluid-structure interaction in liquid tanks subjected to seismic ground excitations.

It should be noted that in 3D models, impulsive hydrodynamic pressure varies not only in the vertical direction but also in horizontal direction over the wall surface. However, hydrodynamic values measured at the wall corners are much lower than those of middle section. A schematic view of impulsive pressure distribution in a 3D rectangular tank is shown in Figure 5.21. On this basis, the difference between 2D and 3D results can be justified.

It is clear that as the length to height ratio of tank increases, the dynamic characteristics of responses tend to approach those of corresponding 2D model. Kim et al. (1996) showed that acceleration and displacement responses at the top of the middle cross section of the flexible wall appear to be very sensitive to the length to height ratio when the ratio is not large. However, as this ratio exceeds 10, those responses become insensitive to the change of the ratio. This fact may justify the use of 2D model.

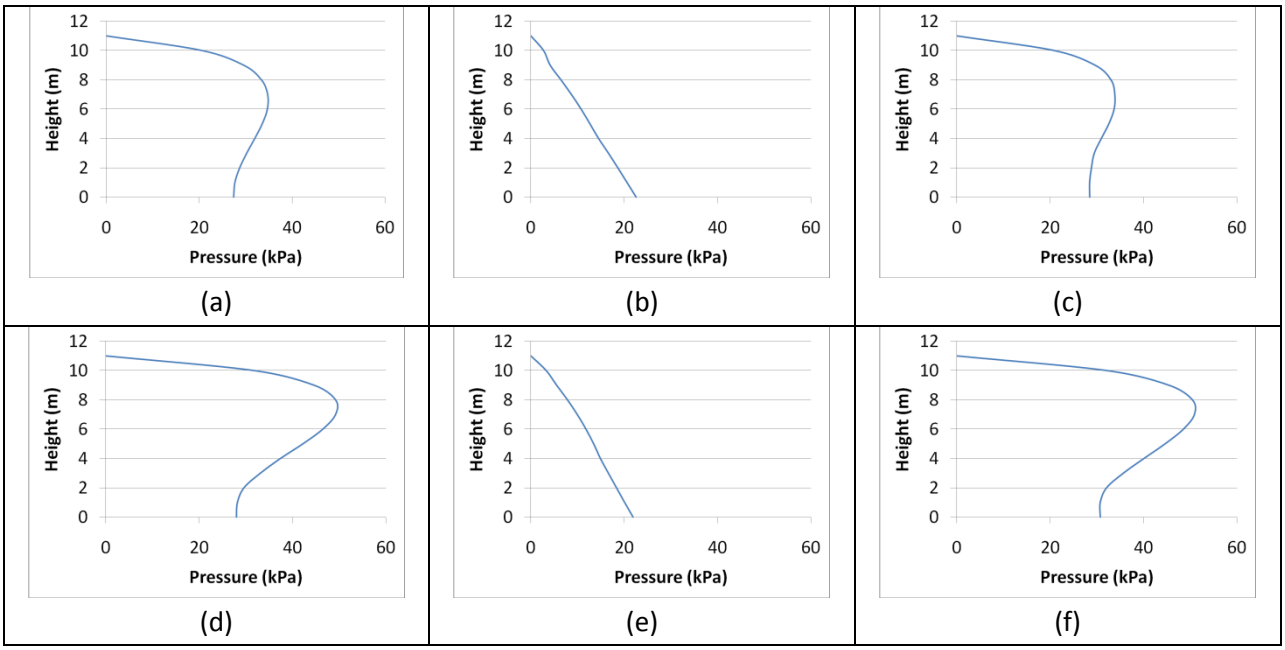


Figure 5.20: Impulsive pressure distribution along height of tall tank model measured at the middle section of longer wall: (a) Horizontal excitation (2D) (b) Vertical excitation (2D) (c) Horizontal and vertical excitation (2D) (d) Horizontal excitation (3D) (e) Vertical excitation (3D) (f) Horizontal and vertical excitation (3D)

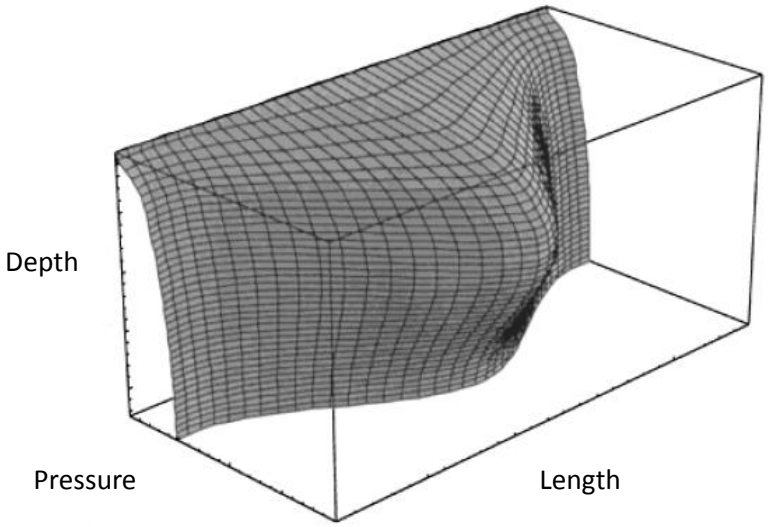


Figure 5.21: Schematic distribution of impulsive hydrodynamic pressure distribution along height of a 3D rectangular tank model

### 5.4 Results summary and comparison with other methods

The seismic impulsive and convective behaviour of liquid tank models are obtained in this study as discussed previously considering both flexible and rigid boundary conditions and fluid damping properties.

In current analytical methods and lumped mass approximations the impulsive wave absorbance boundary condition and fluid viscosity are ignored. In order to verify the proposed FE method as well as to consider the effect of fluid damping properties, two different conditions with zero and non-zero fluid damping ratios are used for 2D rigid tank models and the results are compared with analytical solutions. These results are presented in terms of impulsive hydrodynamic pressure over the tank height.

The analytical impulsive pressure distribution for the rigid wall subjected to an earthquake can be obtained using the potential function method presented in Chapter 3. This equation has been derived by Haroun and Housner (1981) as following:

$$P = \sum_{n=1}^{\infty} \frac{2.(-1)^n.\rho_l}{\lambda_{i,n}^2.H_l} \tanh(\lambda_{i,n} L_x).\cos(\lambda_{i,n} y).\ddot{u}_g(t) \qquad (5.3)$$

In which $\lambda_{i,n} = \frac{(2n-1)\pi}{2H_l}$ and $\ddot{u}_g$ is the horizontal ground acceleration.

The impulsive hydrodynamic pressure distributions over the rigid tank wall calculated by both equation 5.3 and finite element method with two different damping conditions are shown in Figure 5.22 for both shallow and tall tanks. It is obvious that the FE pressure distribution is in full agreement with analytical results when the fluid damping is ignored. For a 5 percent damping ratio, the impulsive pressure has decreased by almost 50 percent for both shallow and tall tank models. This indicates that the fluid damping is an important parameter in considering

the seismic behaviour of liquid containers. This fact is not directly considered in current codes and standards which are based on lumped mass models.

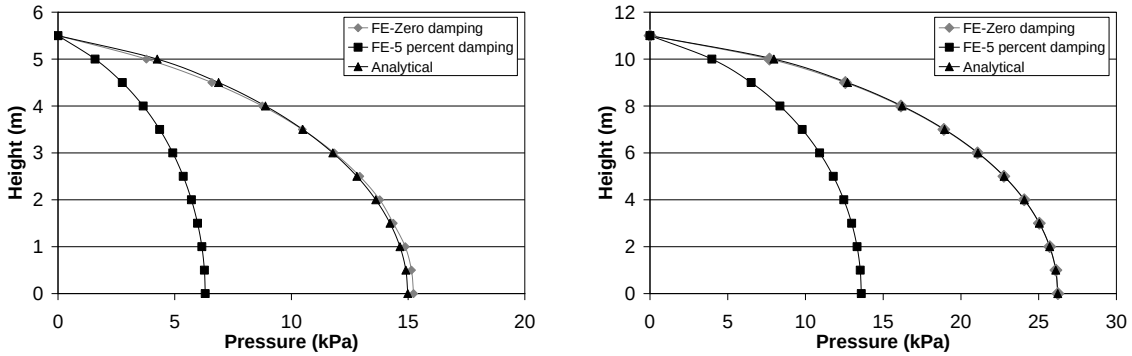


Figure 5.22: Impulsive hydrodynamic pressure distribution over rigid wall tank: (a) Shallow tank (b) Tall tank

As previously mentioned, a summary of FE results for 2D rigid and flexible models is presented in Table 5.2 for both shallow and tall tank models. The base shear and base moment responses are very similar to those reported by Kianoush et al. (2006) for shallow tank model under scaled components of El-Centro earthquake with peak acceleration of 0.4g. It should be noted that the tank analyzed by Kianoush et al. (2006) was slightly different in dimensions from that used in the current study.

The same tall tank model was investigated by Kim et al. (1996) using a BEM-FEM under horizontal excitation of El-Centro record with peak acceleration of 0.32g. The reported 2D base shear response is almost the same as the corresponding value in current study but a significant difference about 50 percent is seen between three-dimensional responses.

The 2D impulsive responses are also comparable to those obtained by Chen and Kianoush (2005) using a sequential method under horizontal component of El-Centro earthquake with peak

ground acceleration of 0.32g for both shallow and tall tank models. In their sequential method, the flexibility of wall was taken into account. However, only the impulsive behaviour of tank was considered and the convective component was ignored. In their study, the maximum impulsive base shear and base moments are 78.7 kN/m and 241.8 kNm/m for shallow tank model while the maximum impulsive base shear is 338.1 kNm/m for tall tank model. These values are much lower than the proposed FE results. However, it is clear that for a peak ground acceleration of 0.4g used in this study slightly higher values are expected using the sequential method.

In addition, the dynamic responses are calculated by Housner's method in which the mapped spectral response acceleration $S_s$ and $S_1$ for Imperial Valley location are chosen as 1.5g and 0.6g, respectively. It should be noticed that in this approximation the flexibility of wall and fluid damping are ignored. This method is commonly used in current design standards such as ACI 350.3-06. A summary of calculated structural responses is shown in Table 5.5.

Table 5.5: 2D structural responses based on Housner's method used in ACI 350.3-06 for rigid wall boundary condition

| | Spectral response acceleration (g) | | Base shear (kN/m) | | | | Base moment (kNm/m) | | | |
|---|---|---|---|---|---|---|---|---|---|---|
| | | | ACI | | FE | | ACI | | FE | |
| | $S_s$ | $S_1$ | $V_i$ | $V_c$ | $V_i$ | $V_c$ | $M_i$ | $M_c$ | $M_i$ | $M_c$ |
| Shallow tank | 1.5 | 0.6 | 171 | 20 | 89 | 25 | 463 | 56 | 209 | 67 |
| Tall tank | 1.5 | 0.6 | 625 | 43 | 328 | 39 | 4063 | 281 | 1575 | 202 |

According to Housner's method, for shallow tank model, the impulsive base shear and base moments are 171 kN/m and 463 kNm/m under horizontal excitations while for tall tank model, the impulsive base shear and base moments are 625 kN/m and 4063 kNm/m, respectively. These

values are about 100 percent higher than those obtained using FE method for rigid tank models. However, the FE convective response is in satisfactory agreement with Housner's model in terms of base shear and sloshing height for rigid wall boundary condition. For instance, the convective base shear calculated by Housner's method for tall tank model under horizontal ground motion is 43 kN/m which is only 10 percent higher than the value obtained using FE method. For this case, the sloshing height is 710 mm based on Housner's model which is about 12 percent higher than the value calculated by the FE method.

Instead of using design response spectrum, the El-Centro response spectrum in longitudinal direction as shown in Figure 5.23 can be used for the purpose of spectrum analysis. The values of base shear and base moment can be easily calculated for two-dimensional model due to horizontal excitation accounting for wall flexibility. The impulsive base shear and base moments of shallow tank model are 159 kN/m and 346 kNm/m under horizontal excitations while the impulsive base shear and base moments of tall tank model are 816 kN/m and 3423 kNm/m, respectively. A comparison between peak structural responses obtained by spectrum analysis and time-history FE method is shown in Figure 5.24.

It is clear that calculated peak structural responses in 3D models are higher than those values calculated by spectrum analysis and 2D models for all cases. As a result, 3D geometry plays an important role in dynamic behaviour of rectangular liquid tanks and magnifies the structural responses. It should be noticed that the spectrum analysis method which is commonly used in design codes is based on a two-dimensional tank model and it does not consider the effect of 3D geometry. This effect needs further consideration in design codes and standards.

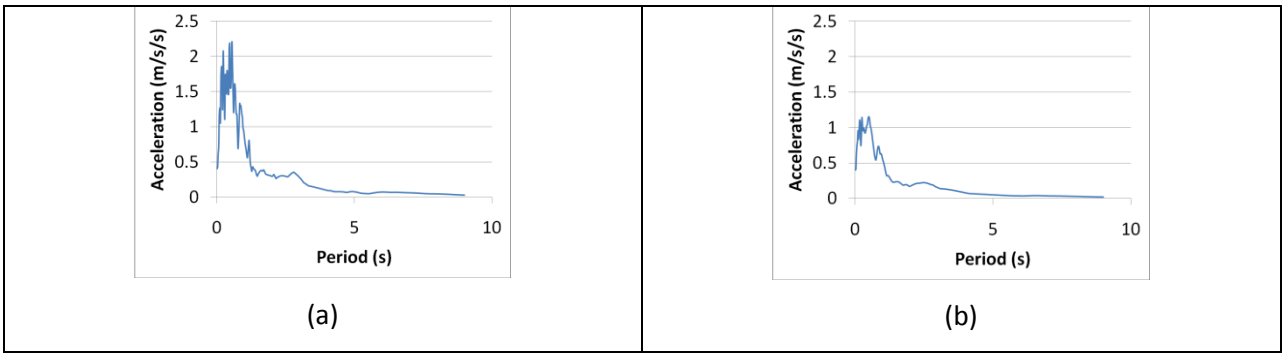


Figure 5.23: Response spectrum of 1940 El-Centro earthquake in longitudinal direction: (a) 0.5 percent damping (convective) (b) 5 percent damping (impulsive)

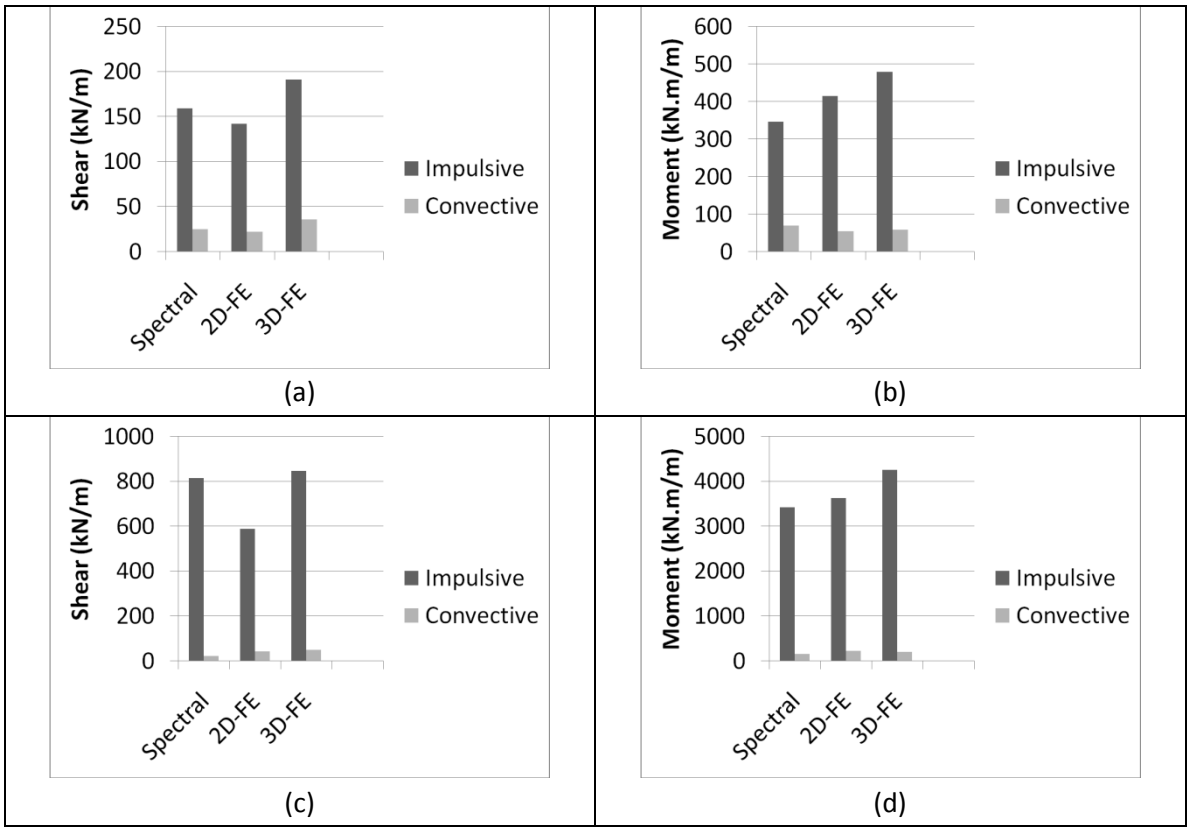


Figure 5.24: impulsive and convective structural responses: (a) Base shear (shallow tank) (b) Base moment (shallow tank) (c) Base shear (tall tank) (d) Base moment (tall tank)

Finally, the FE analysis results by the present method are compared with experimental results of shaking-table tests of a 3D rectangular tank model made of acrylic plates done by Koh et al. (1998) to verify the accuracy of 3D modeling of sloshing behaviour.

This model is designed according to the following material properties and geometric specifications as follows:

$$\rho_w = 1200kg/m^3 \quad \rho_l = 1000kg/m^3 \quad E_c = 2.9GPa \quad \nu = 0.35$$
$$L_x = 1.1m \quad L_z = 0.57m \quad H_w = 0.9m \quad H_l = 0.7m \quad t_w = 0.035m$$

In their study, from the preliminary test performed with an empty tank model, the viscous damping ratio was found to be approximately 5%. Six pressure gauges, twelve accelerometers and two water level gauges were placed to measure the dynamic responses of the tanks.

The calculated sloshing height at the top of the middle cross-section of the long side wall using proposed FE along with the experimental results are presented in Figure 5.25. It is clear that the numerical results are in satisfactory agreement with experimental results.

However, a significant difference can be noticed during the last part of time-history results. This anomaly may be justified as a result of increase in energy dissipation during the experiment leading to a variation in the fluid damping characteristic.

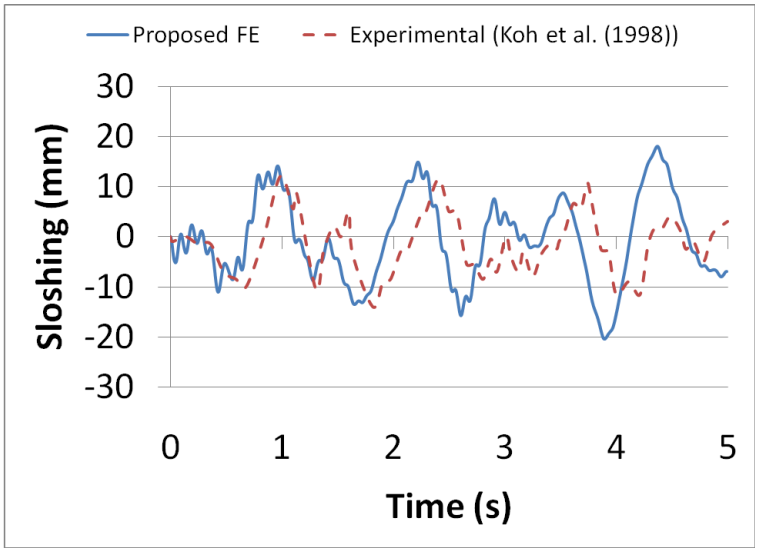


Figure 5.25: Proposed FE sloshing height at the top of the middle cross-section of the long side wall of the tank model used in shaking table tests done by Koh et al. (1998)

### 5.5 Summary

In this Chapter, dynamic behaviour of partially filled rectangular fluid container under horizontal and vertical ground excitations is investigated using FEM in both 2D and 3D spaces. The liquid sloshing is modeled using an appropriate boundary condition and the damping effects due to impulsive and convective components of the stored liquid are modeled using the Rayleigh method. Two different configurations including shallow and tall tank models are considered to investigate the effect of geometry on the response of the liquid-structure system. In this chapter, the effect of wall flexibility on the overall dynamic response of system is investigated by comparing the results between 2D rigid and flexible models. In the second part, a comparison between 2D and 3D flexible tank model responses is made to study the effect of three-dimensional geometry on the dynamic behaviour of liquid tanks. In addition, the effect of vertical ground motion on the seismic responses of liquid tank models is discussed.

The results show that the maximum impulsive base shear and base moment obtained from time history analysis of the considered system are increased due to flexibility of side walls which is a result of dynamic pressure amplification in the middle of the wall. However, the convective response is almost independent of variations of flexibility of the side walls and seems to be related to geometric configurations of tank, earthquake characteristics and liquid properties. Due to wall flexibility, a slight variation is observed in convective pressure values in comparison with impulsive pressure values. Although the current practice assumes that the numerical value of convective pressure at the bottom of tank reaches zero, the proposed FE method shows different results.

Furthermore, the peak responses of impulsive and convective components do not occur at the same phase and time. As a result, convective terms may lead to increase or decrease in the maximum absolute values of the structural responses in terms of base shear and base moment. Also, applying the vertical excitations will lead to an increase in the convective response of the system. However, it does not affect the impulsive behaviour significantly. This increase is more noticeable in tall tank model. This point is valid for both 2D and 3D tank models.

Although the 2D finite element convective responses are in satisfactory agreement with corresponding responses obtained by Housner's method for a rigid tank model, the seismic impulsive response of liquid tanks according to Housner's method which is used currently in current codes and standards in terms of shear and moment forces seems too conservative.

In addition, the results show that the maximum structural base shear and base moment obtained from time history analyses are amplified due to 3D geometry effect. The same trend is seen for the convective responses. Due to effect of 3D geometry, the maximum sloshing height is

highly amplified at the corner of liquid domain. This is mainly because of the interaction of waves generated by two longitudinal and transversal components of earthquake in this location.

Peak structural responses in 3D models are higher than those values calculated by spectrum analysis and 2D models for all cases. This point needs more consideration in current liquid tank design codes and standards which are commonly based on 2D models. The 3D effect has been considered in building codes such as ASCE 7-05 code for minimum design loads for buildings and other structures. Accordingly, the building structures are analyzed in 3D space using equivalent lateral force analysis procedure in which 100 percent of the forces for horizontal direction plus 30 percent of the forces for the transversal direction are considered for design purpose. Similarly, as seen in Table 5.3, the results of this study show a significant increase in dynamic responses due to transversal component of earthquake and 3D geometry effect. In design of liquid containing structures, a similar treatment to that of buildings is needed for the 3D effect.

It is clear that the dynamic behaviour of liquid concrete tanks depends on a wide range of parameters such as seismic properties of earthquake, tank dimensions and fluid-structure interaction which should be considered in future researches. This study shows that the proposed FE method can be used in the time history analysis of rectangular liquid tanks. One of the major advantages of this method is in accounting for wall flexibility, three-dimensional geometry effects, damping properties of liquid domain and calculating impulsive and convective terms, separately. Also, this includes applying different damping ratios to different impulsive and convective components and considering wall flexibility, which has a major role in seismic response. However, this method is not able to accurately simulate the nonlinear behaviour of sloshing in liquid tanks.

The present study is done based on both 2D and 3D analysis of rectangular tanks in time-domain. Although the liquid tank design procedure are based on simplified frequency-based methods, the FE time-history results which are more realistic can be used to verify these methods in future works.

# Chapter 6

# Seismic behaviour of liquid tanks under different ground motions incorporating soil-structure interaction

## 6.1 Introduction

In this chapter, a three-dimensional soil-structure-liquid interaction is numerically simulated using finite element method in order to analyze the seismic behaviour of partially filled concrete rectangular tanks subjected to different ground motions. The effect of earthquake frequency content on the seismic behaviour of fluid-rectangular tank system is investigated using four different seismic motions including Northridge, El-Centro, San-Fernando and San-Francisco earthquake records. These records are scaled in such a way that all horizontal peak ground accelerations reach 0.4g.

Considering the previous works, it is clear that very limited research has been done on the soil-structure-fluid interaction (SSI) effect on seismic behaviour of concrete rectangular tanks in time domain. Here, a simple model with viscous boundary is used to include deformable foundation effects as a linear elastic medium. It should be noted that the simulation of real behaviour of soil foundation is beyond the scope of this study and needs more complicated numerical approaches. The proposed method is capable of considering both impulsive and convective responses of liquid-tank system. Six different soil types defined in the well-known seismic codes were considered. The sloshing behaviour is simulated using linear free surface boundary condition. Two different finite element models corresponding with flexible shallow

and tall tank configurations are studied under the effects of longitudinal, transversal and vertical ground motions. By means of changing the soil properties, some comparisons are made on base shear, base moment and sloshing responses under different ground motions.

### 6.2 Time history analysis

Two rectangular concrete liquid container models presented in section 4.6 are used basically for the example analyses in three-dimensional space. The longitudinal, transversal and vertical components recorded for 1994 Northridge, 1940 El-Centro, 1971 San-Fernando and 1957 San-Francisco earthquakes are used as excitations of the tank–liquid system. The components are scaled in such a way that the peak ground acceleration in the longitudinal direction reach 0.4g, as shown in Figure 6.1.

A good indicator of the frequency content of the ground motion is the ratio of peak ground acceleration (PGA) which is expressed in units of g to peak ground velocity (PGV) expressed in units of m/s. Earthquake records may be classified according to the frequency content ratio into three categories, high PGA/PGV ratio when PGA/PGV>1.2, intermediate PGA/PGV ratio when 1.2>PGA/PGV>0.8 and low PGA/PGV ratio when PGA/PGV<0.8. The Northridge record has low frequency content, the El-Centro and San-Fernando earthquakes have intermediate frequency contents and the San-Francisco record has the high frequency content.

It should be noted that both longitudinal and transversal components of earthquake perpendicular to longer and shorter tank wall (X and Y directions), respectively are applied simultaneously in three-dimensional modeling and are referred to as horizontal excitation.

Since the sloshing height variation is a matter of concern in design of rectangular tanks, its value is measured at three different locations (points A, B and C shown in Figure 4.6) of three-

dimensional model. Points A, B and C are located at the fluid surface at the middle of longer length, middle of shorter length and the corner of tank wall, respectively

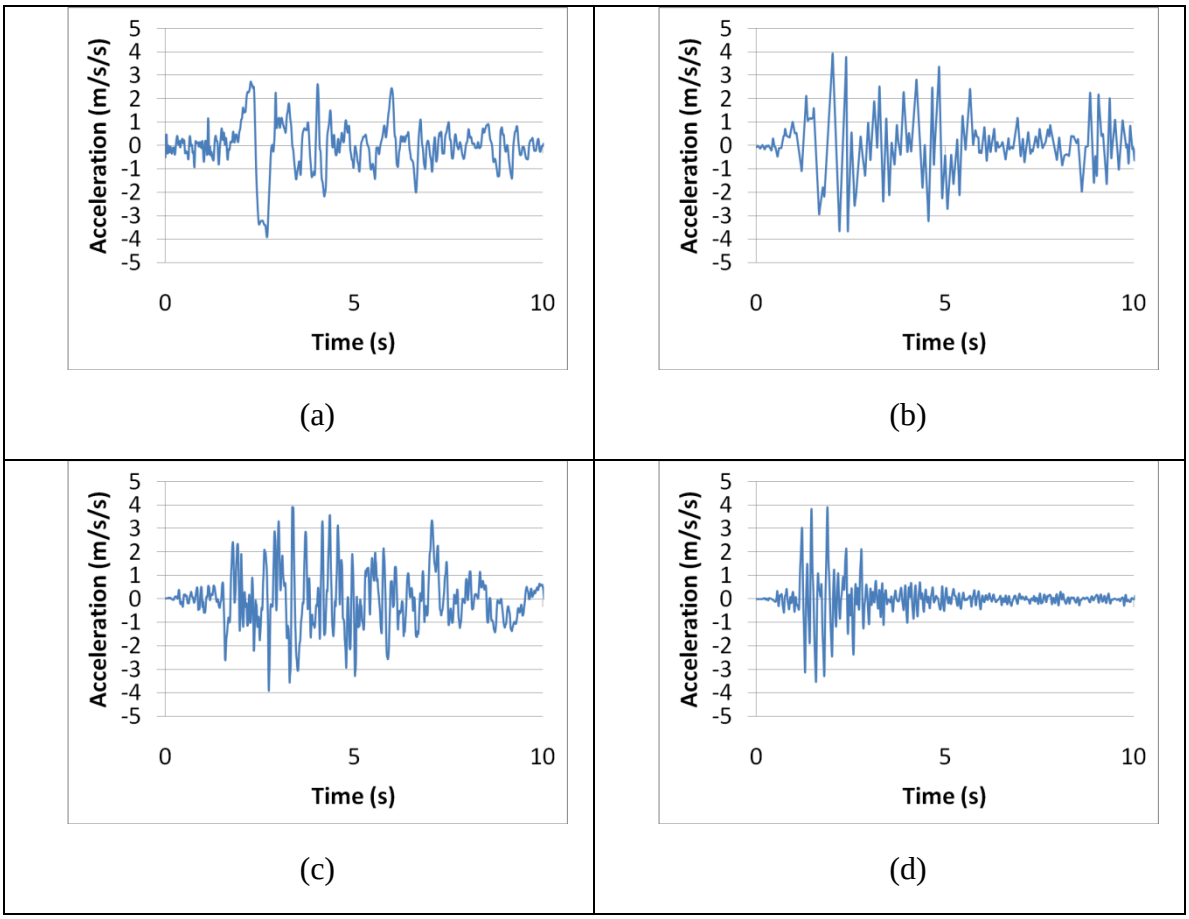


Figure 6.1: Scaled longitudinal components of earthquake records: (a) 1994 Northridge (b) 1940 El-Centro (c) 1971 San-Fernando (d) 1957 San-Francisco

In addition, using the earthquake response spectra in longitudinal direction (Figure 6.2), the values of base shear and base moment can be easily calculated for unit length of wall. A comparison between spectrum analysis results with those calculated in accordance with ACI 350.3-06(2006) and FE time-history will be discussed later.

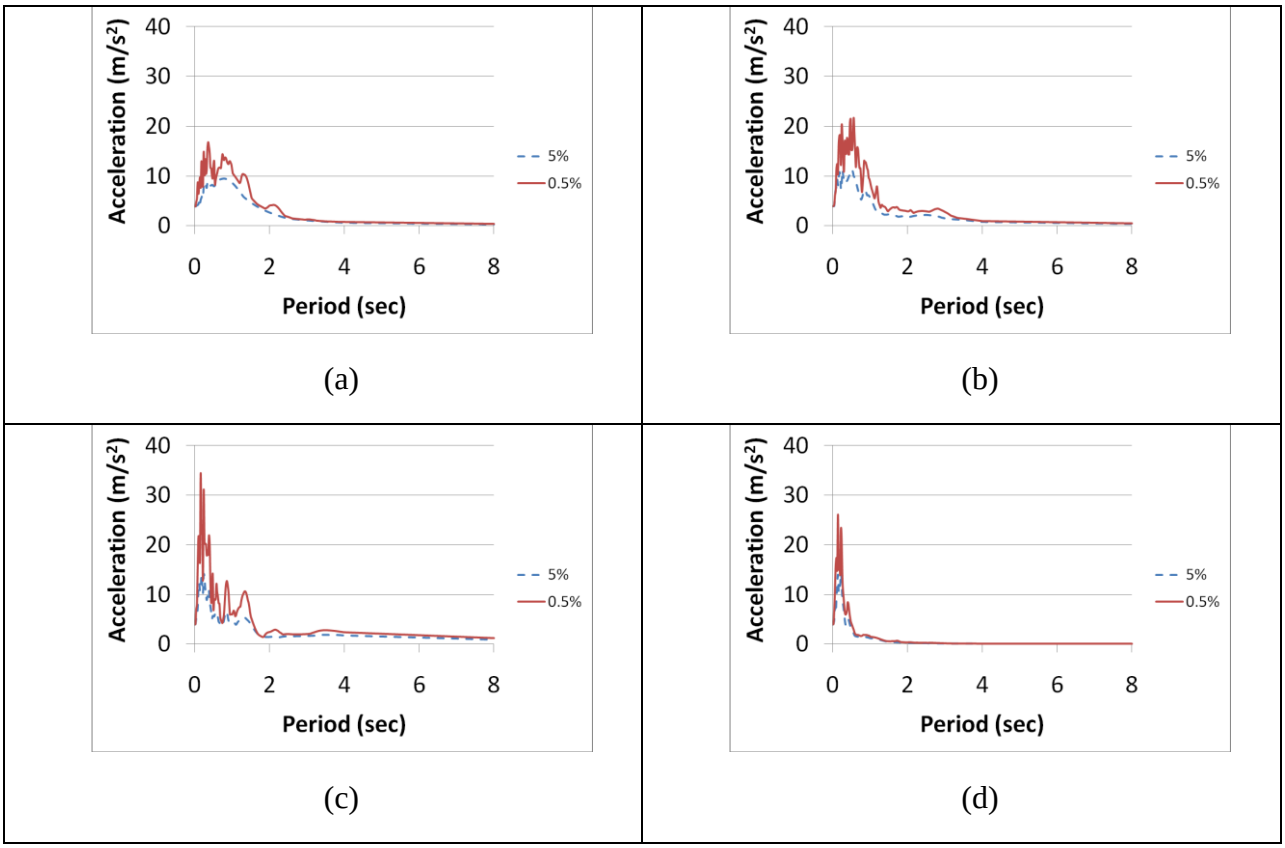


Figure 6.2: Response spectra of earthquakes in longitudinal direction for 0.5 and 5 percent damping ratios: (a) Northridge (b) El-Centro (c) San-Fernando (d) San-Francisco

The results of this study are presented in two parts. In the first part, the effect of earthquake frequency-content on the seismic behaviour of liquid tanks supported on a rigid foundation is described.

In the second part, the combined effect of SSI and earthquake frequency content on the dynamic behaviour of liquid tanks is described.

### 6.3 Effect of earthquake frequency on the dynamic behaviour of liquid tanks

#### 6.3.1 Seismic behaviour of shallow tank model with rigid base

The transient base shear and base moment for flexible shallow tank model due to horizontal and vertical excitations are calculated by proposed method. Four different earthquake records are applied to investigate the effect of frequency content on the response of tank-liquid system. The base shear response of the tank measured at the middle cross-section of the longer wall due to longitudinal ground motion is presented in Figure 6.3. It should be noted that these values correspond with the average forces acting on unit length of tank wall.

The absolute maximum values of resulting base shear and base moment are shown in Table 6.1. In addition, the results are presented in brackets in terms of normalized values with respect to those of El-Centro record. These results show that the responses due to high frequency content earthquake of San-Francisco are highly magnified because of the similarity between impulsive dynamic characteristics of the tank-liquid system and earthquake record.

Also, the least response values are obtained under low frequency Northridge earthquake which are almost one-third of the values due to San-Francisco earthquake. Unlike the impulsive behaviour, the convective response values are amplified due to intermediate frequency content earthquake of El-Centro as shown in Table 6.1. It should be noticed that when the impulsive response reaches its peak, the convective response is at the beginning stage and has not yet fully developed. As a result, the convective component does not have a major effect on the total structural response in time-domain analysis.

It is found that the effect of earthquake frequency content is significant on the structural response of liquid tank models and may cause a considerable increase in time-domain peak response values.

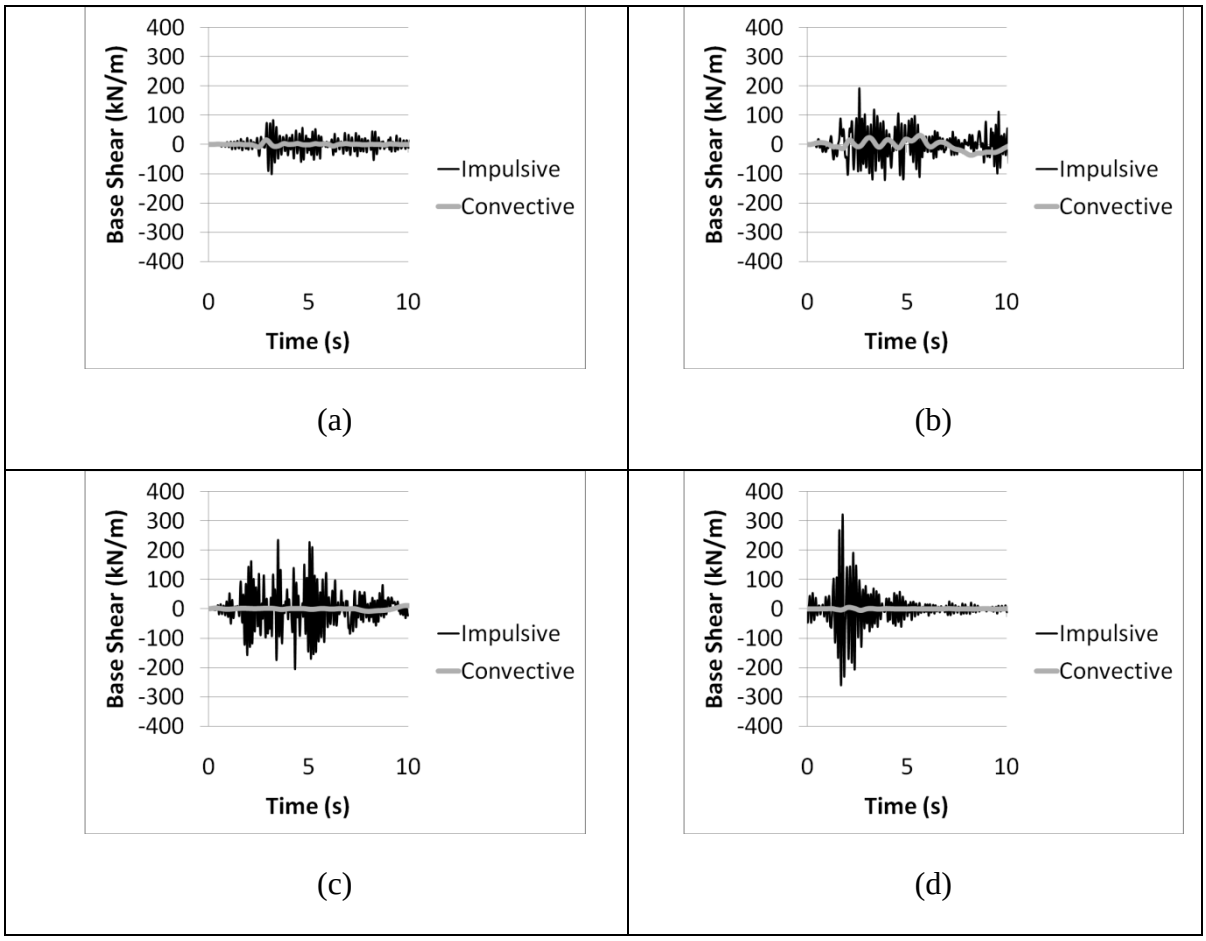


Figure 6.3: Time history of base shear response of shallow tank model under longitudinal excitation: (a) Northridge (b) El-Centro (c) San-Fernando (d) San-Francisco

Considering the combined effect of vertical and horizontal ground motions, the impulsive response almost remains unchanged for all earthquakes. The convective part increases due to both Northridge and El-Centro vertical components but remains unchanged under applying vertical components of San-Fernando and San-Francisco ground motions. A summary of the results are provided in Table 6.1.

In addition to the structural response, the fluid dynamic behaviour is thoroughly investigated. The time history diagrams of surface sloshing height are shown in Figure 6.4.

As previously mentioned, these values are measured at points A, B and C. The maximum sloshing heights which occur at point C have values of $\delta_{max} = 325$ mm, 838 mm, 311 mm and 138 mm under Northridge, El-Centro, San-Fernando and San-Francisco earthquakes, respectively. As presented in Table 6.1, the vertical acceleration has the most significant effect on sloshing behaviour of fluid domain under El-Centro earthquake and causes an increase of about 14 percent in sloshing height whereas, the sloshing height remains unchanged after applying vertical motions of Northridge and San-Fernando earthquakes.

Table 6.1: Summary of maximum dynamic responses of shallow tank model

| | | Impulsive response | | | Convective response | | |
|---|---|---|---|---|---|---|---|
| | | H | H+V | (H+V)/H | H | H+V | (H+V)/H |
| Northridge | Base Shear (kN/m) | 102 (0.53) | 104 (0.54) | 1.02 | 16 (0.44) | 17 (0.42) | 1.10 |
| | Base Moment (kN.m/m) | 273 (0.57) | 284 (0.59) | 1.04 | 36 (0.61) | 37 (0.58) | 1.03 |
| | Sloshing (mm) | - | - | - | 326 (0.44) | 325 (0.39) | 1.00 |
| El-Centro | Base Shear (kN/m) | 191 (1.00)* | 193 (1.00) | 1.01 | 36 (1.00) | 40 (1.00) | 1.11 |
| | Base Moment (kN.m/m) | 479 (1.00) | 478 (1.00) | 1.00 | 59 (1.00) | 64 (1.00) | 1.08 |
| | Sloshing (mm) | - | - | - | 734 (1.00) | 838 (1.00) | 1.14 |
| San-Fernando | Base Shear (kN/m) | 236 (1.24) | 236 (1.22) | 1.00 | 12 (0.33) | 12 (0.30) | 1.00 |
| | Base Moment (kN.m/m) | 657 (1.37) | 645 (1.35) | 0.98 | 30 (0.51) | 30 (0.47) | 1.00 |
| | Sloshing (mm) | - | - | - | 311 (0.42) | 311 (0.37) | 1.00 |
| San-Francisco | Base Shear (kN/m) | 323 (1.69) | 337 (1.75) | 1.04 | 5 (0.14) | 5 (0.13) | 1.00 |
| | Base Moment (kN.m/m) | 821 (1.71) | 860 (1.80) | 1.05 | 13 (0.22) | 13 (0.20) | 1.00 |
| | Sloshing (mm) | - | - | - | 128 (0.17) | 138 (0.16) | 1.08 |

*The values in the bracket are normalized responses with respect to El-Centro results

Unlike the convective behaviour, the impulsive behaviour is less sensitive to vertical motions as seen for all earthquake records. Since the impulsive response values are so much higher than those of convective, it can be concluded that the effect of vertical excitation is insignificant on overall seismic behaviour of shallow tank model. On the other hand the variation in maximum responses range between -2% to 5% for impulsive behaviour and 0% to 14% for convective behaviour.

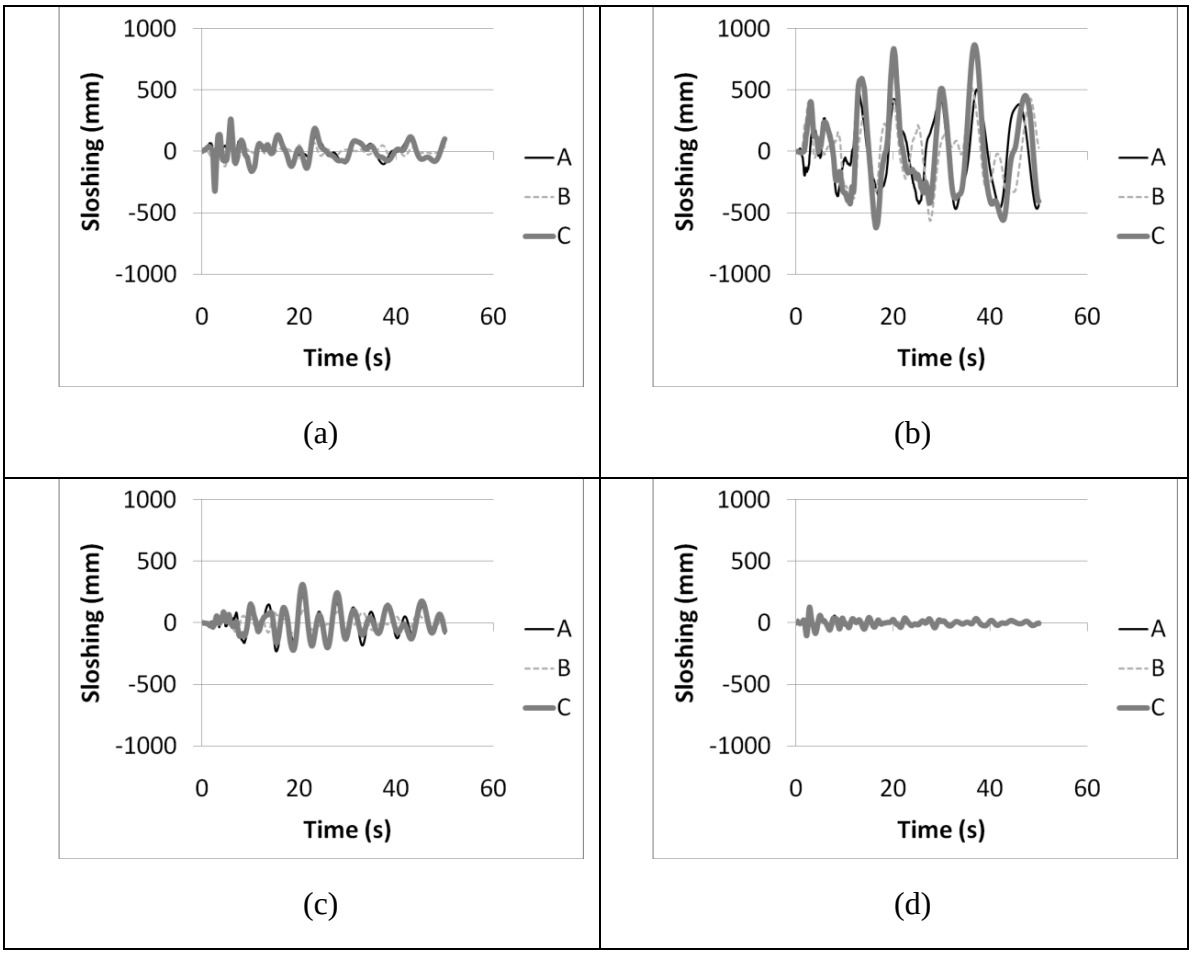


Figure 6.4: Time history of sloshing height due to all components of earthquake for shallow tank model: (a) Northridge (b) El-Centro (c) San-Fernando (d) San-Francisco

### 6.3.2 Seismic behaviour of tall tank model with rigid base

Figure 6.5 presents the diagrams of impulsive and convective structural response in terms of base moment time history for tall tank model in 3D space. The absolute maximum values of the resulting base shear and base moment of the impulsive and convective component are shown in Table 6.2. As previously seen in shallow tank model, the effect of frequency content is significant on the structural response of the tank. In this case, the highest impulsive response values are obtained under the El-Centro earthquake.

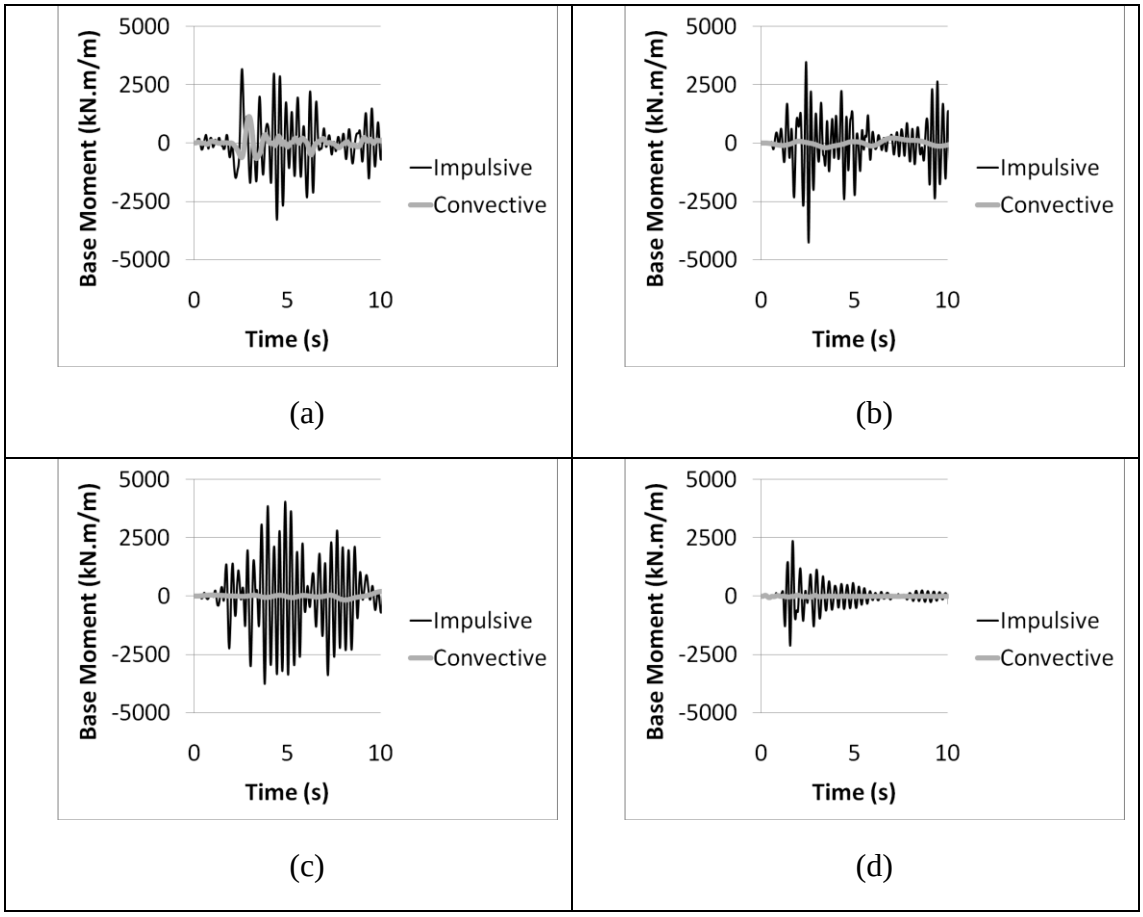


Figure 6.5: Time history of base moment response of tall tank model under longitudinal excitation: (a) Northridge (b) El-Centro (c) San-Fernando (d) San-Francisco

Unlike the impulsive behaviour, applying Northridge ground motion results in the highest convective responses. Under applying the three components of ground motion, the structure response of the tank is affected by the frequency of the earthquake. In comparison with El-Centro record, the Northridge vertical component leads to decrease in peak values of base shear and moment, while the San-Francisco earthquake result in an increase in these value as shown in Table 6.2.

Table 6.2: Summary of maximum dynamic responses of tall tank model

| | | Impulsive response | | | Convective response | | |
|---|---|---|---|---|---|---|---|
| | | H | H+V | (H+V)/H | H | H+V | (H+V)/H |
| Northridge | Base Shear (kN/m) | 700 (0.83) | 655 (0.78) | 0.94 | 279 (5.58) | 266 (4.43) | 0.95 |
| | Base Moment (kN.m/m) | 3295 (0.77) | 2994 (0.70) | 0.91 | 1131 (5.36) | 1087 (4.71) | 0.96 |
| | Sloshing (mm) | - | - | - | 1968 (2.14) | 1957 (1.73) | 0.99 |
| El-Centro | Base Shear (kN/m) | 846 (1.00) | 839 (1.00) | 0.99 | 50 (1.00) | 60 (1.00) | 1.2 |
| | Base Moment (kN.m/m) | 4261 (1.00) | 4251 (1.00) | 0.99 | 211 (1.00) | 231 (1.00) | 1.09 |
| | Sloshing (mm) | - | - | - | 920 (1.00) | 1134 (1.00) | 1.23 |
| San-Fernando | Base Shear (kN/m) | 814 (0.96) | 908 (1.08) | 1.11 | 48 (0.96) | 49 (0.82) | 1.02 |
| | Base Moment (kN.m/m) | 4059 (0.95) | 4119 (0.97) | 0.98 | 245 (1.16) | 244 (1.06) | 1.00 |
| | Sloshing (mm) | - | - | - | 973 (1.06) | 965 (0.85) | 0.99 |
| San-Francisco | Base Shear (kN/m) | 429 (0.51) | 483 (0.58) | 1.13 | 10 (0.2) | 11 (0.18) | 1.10 |
| | Base Moment (kN.m/m) | 2369 (0.56) | 2606 (0.61) | 1.10 | 56 (0.26) | 60 (0.26) | 1.08 |
| | Sloshing (mm) | - | - | - | 211 (0.23) | 254 (0.22) | 1.20 |

*The values in the bracket are normalized responses with respect to El-Centro results

The numerical results indicate that the variation of the maximum response due to the vertical ground motion range between -9% to 13% for impulsive behaviour and -5% to 23% for convective behaviour.

In comparison with the shallow tank, the tall tank is more sensitive to vertical component of ground motion and its response varies from one earthquake to another.

The impulsive pressure distribution along tank wall measured at the middle section of longer wall is presented in Figure 6.6 for all records under longitudinal ground motions. The highest values are obtained due to El-Centro earthquake as compared to other earthquake records. This is consistent with other structural response values as presented in Table 6.2.

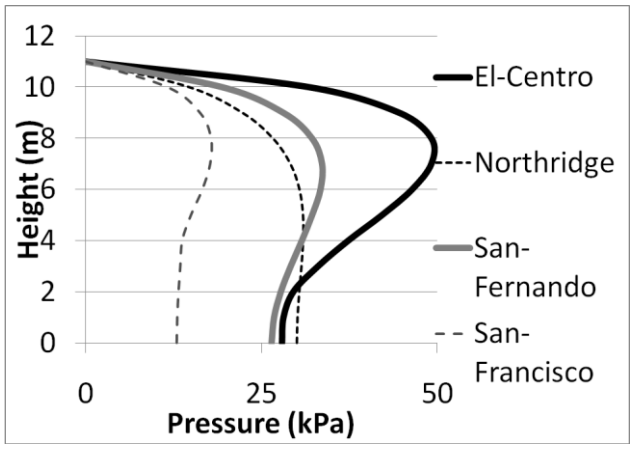


Figure 6.6: Impulsive Pressure distribution along height of three-dimensional tall tank model measured at the middle section of longer wall under longitudinal excitations for different earthquake records

The time history diagrams of sloshing height due to all components of earthquake are shown in Figure 6.7 for all records. Similar to shallow tank, the maximum sloshing height occurs at point C which is almost 20 percent higher than its value measured at point A. Applying vertical

acceleration may lead to an increase or decrease in sloshing height, or in some cases may not affect the sloshing height as seen for Northridge and San-Fernando earthquakes. This variation is affected by the characteristics of the ground motion and tank configuration

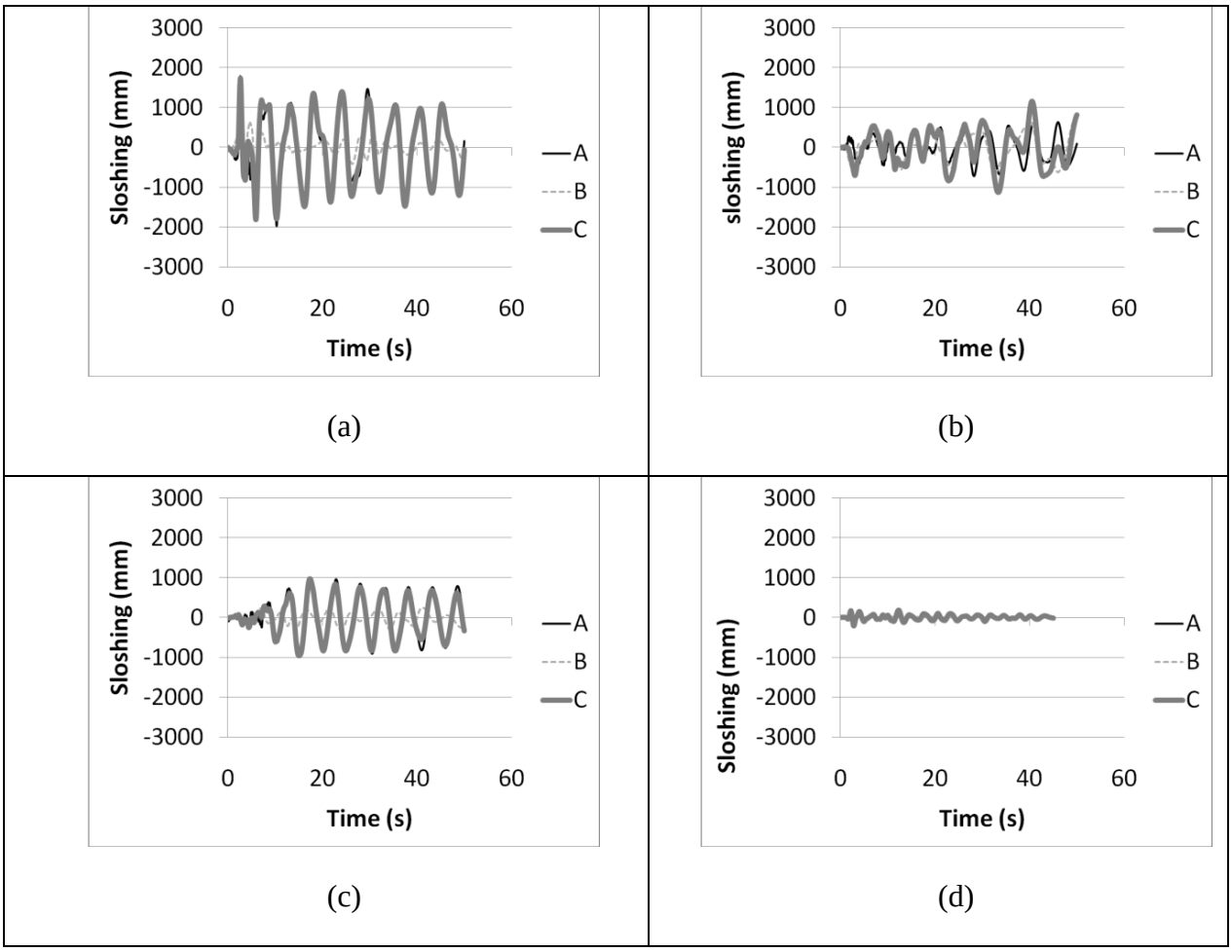


Figure 6.7: Time history of sloshing height due to all components of earthquake for tall tank model: (a) Northridge (b) El-Centro (c) San-Fernando (d) San-Francisco

### 6.4 Effect of soil-structure interaction on the dynamic behaviour of liquid tanks

#### 6.4.1 Response of shallow tank with flexible foundation

As mentioned before, in order to consider the effects of deformability of tank foundation on impulsive and convective responses of tank structure, additional FE models with flexible foundation boundary condition are investigated in this study.

The width and height of the foundation model are chosen as six and two times the value of $L_x$ for both shallow and tall tank configurations to be sufficiently large to include the effect of soil interaction. The finite element (FE) model configuration is shown in Figure 6.8. The far-field boundary condition is applied using a spring-dashpot system as prescribed in chapter 4.

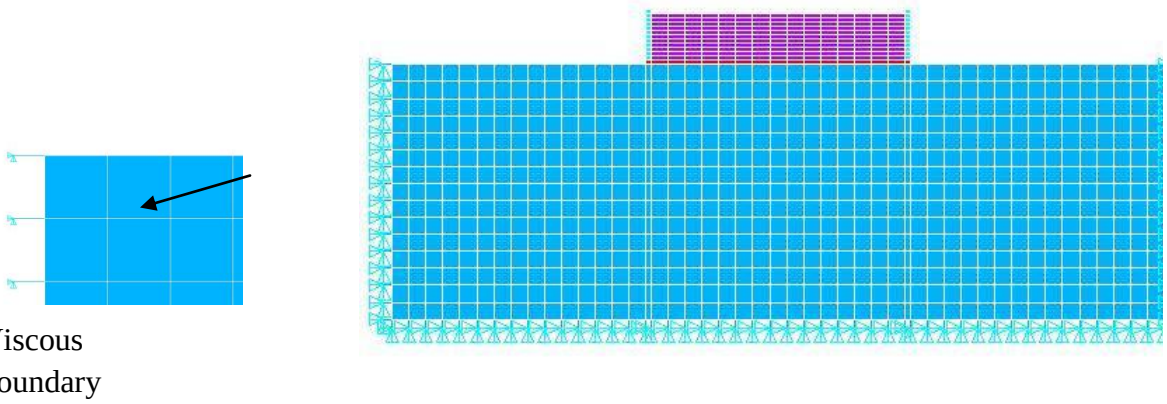


Figure 6.8: Finite element model of fluid-tank-foundation system considered in this study

The soil medium is modeled using solid elements which have 3 transitional DOFs at each node. To evaluate the dynamic response of liquid tank supported on flexible foundation, six soil types recommended in the literature and design codes are considered. The soil properties are shown in table 6.3.

Table 6.3: Properties of the soil types considered in this study

| Soil types | E ($kN/m^2$) | G ($kN/m^2$) | $\gamma$ ($kg/m^3$) | $\nu$ | $v_s$ (m/s) | $v_p$ (m/s) |
|---|---|---|---|---|---|---|
| $S_1$ | 7000000 | 2692310 | 2000 | 0.30 | 1149.10 | 2149.89 |
| $S_2$ | 2000000 | 769230 | 2000 | 0.30 | 614.25 | 1149.16 |
| $S_3$ | 500000 | 192310 | 1900 | 0.35 | 309.22 | 643.68 |
| $S_4$ | 150000 | 57690 | 1900 | 0.35 | 169.36 | 352.56 |
| $S_5$ | 75000 | 26790 | 1800 | 0.40 | 120.82 | 295.95 |
| $S_6$ | 35000 | 12500 | 1800 | 0.40 | 82.54 | 202.18 |

In this table, $S_1$, $S_2$, $S_3$, $S_4$, $S_5$ and $S_6$ soil types represent hard rock, rock, very dense soil and soft rock, stiff soil, soft clay soil and soils vulnerable to potential failure or collapse under seismic loading, such as liquefiable soils and quick and highly sensitive clays, respectively.

The variation of the dynamic response of shallow tank model in terms of peak impulsive base shear for different soil types is presented in Figure 6.9 under different ground motions.

It is clear that the effect of soil structure interaction (SSI) on the structural responses of liquid tanks is highly dependent on the earthquake frequency content. SSI has led to an increase of about 47, 64 and 52 percent in peak base shear response in comparison with rigid foundation condition under Northridge, El-Centro and San-Fernando records, respectively. These response amplifications have occurred in S6, S5 and S4 soil types which represent very soft soil, soft clay soil and stiff soil, respectively. However, a decrease of about 13 percent is seen for base shear peak value due to San-Francisco earthquake in S6 soil type.

On the other hand, the response amplification has occurred in different soil types as the input earthquake changes.

For moderate frequency-content records, the highest increase is seen in S4 and S5 soil types while under low frequency-content record, the highest values are obtained for S6 soil type which represents a very soft soil. Under high frequency-content record of San-Francisco, the peak

structural responses decrease as the soil stiffness decreases. On the other hand, the lowest peak values are obtained for S6 soil type.

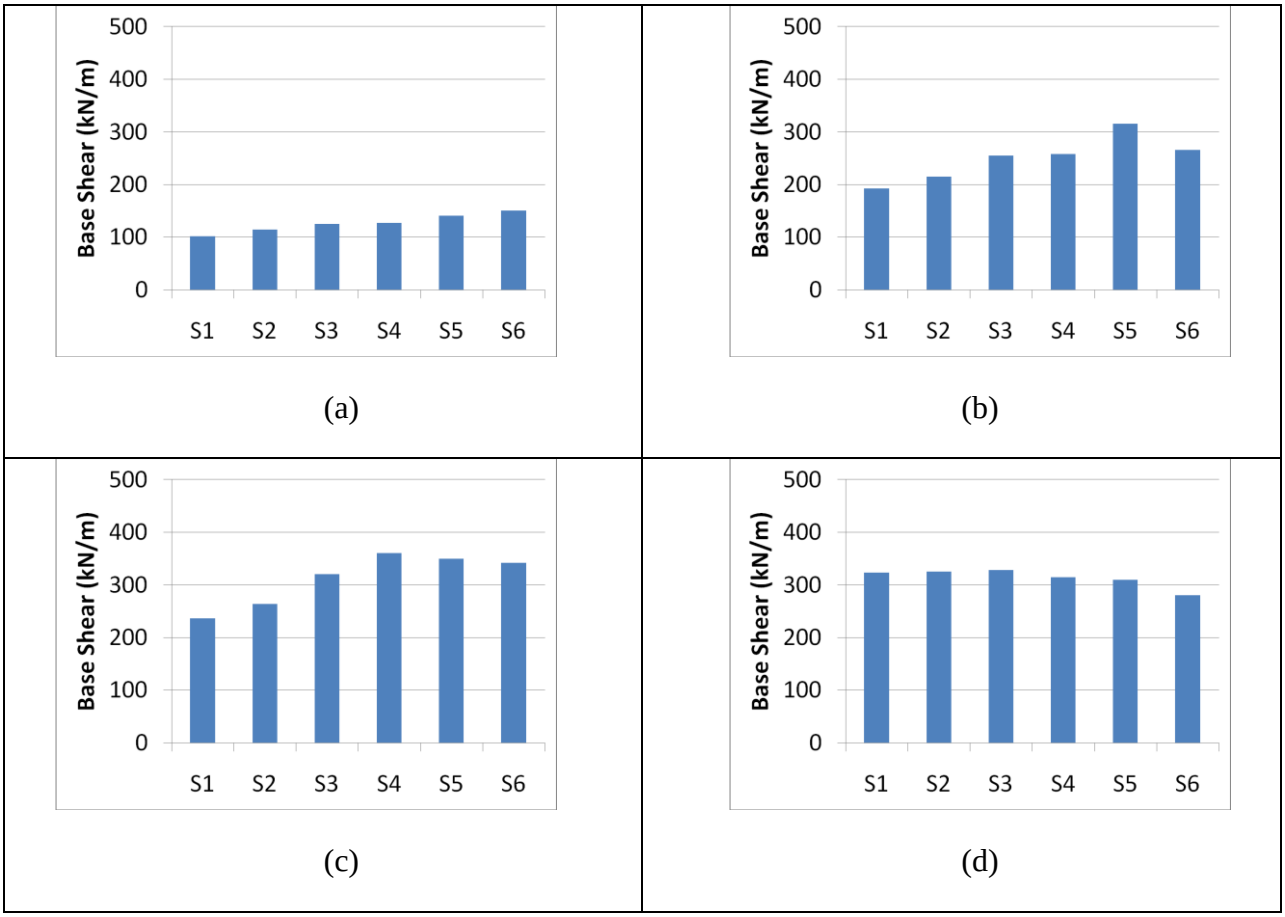


Figure 6.9: Comparisons of peak base shear responses of shallow tank model for different soil types: (a) Northridge (b) El-Centro (c) San-Fernando (d) San-Francisco

For all cases, it is found that the soil type has an insignificant effect on the convective behaviour of liquid tank. A comparison among maximum sloshing height measured at the right top corner of the liquid domain for different soil types and earthquake records is shown in Figure 6.10 under horizontal excitation. It can be concluded that the foundation deformability does not affect the sloshing height of the liquid tank.

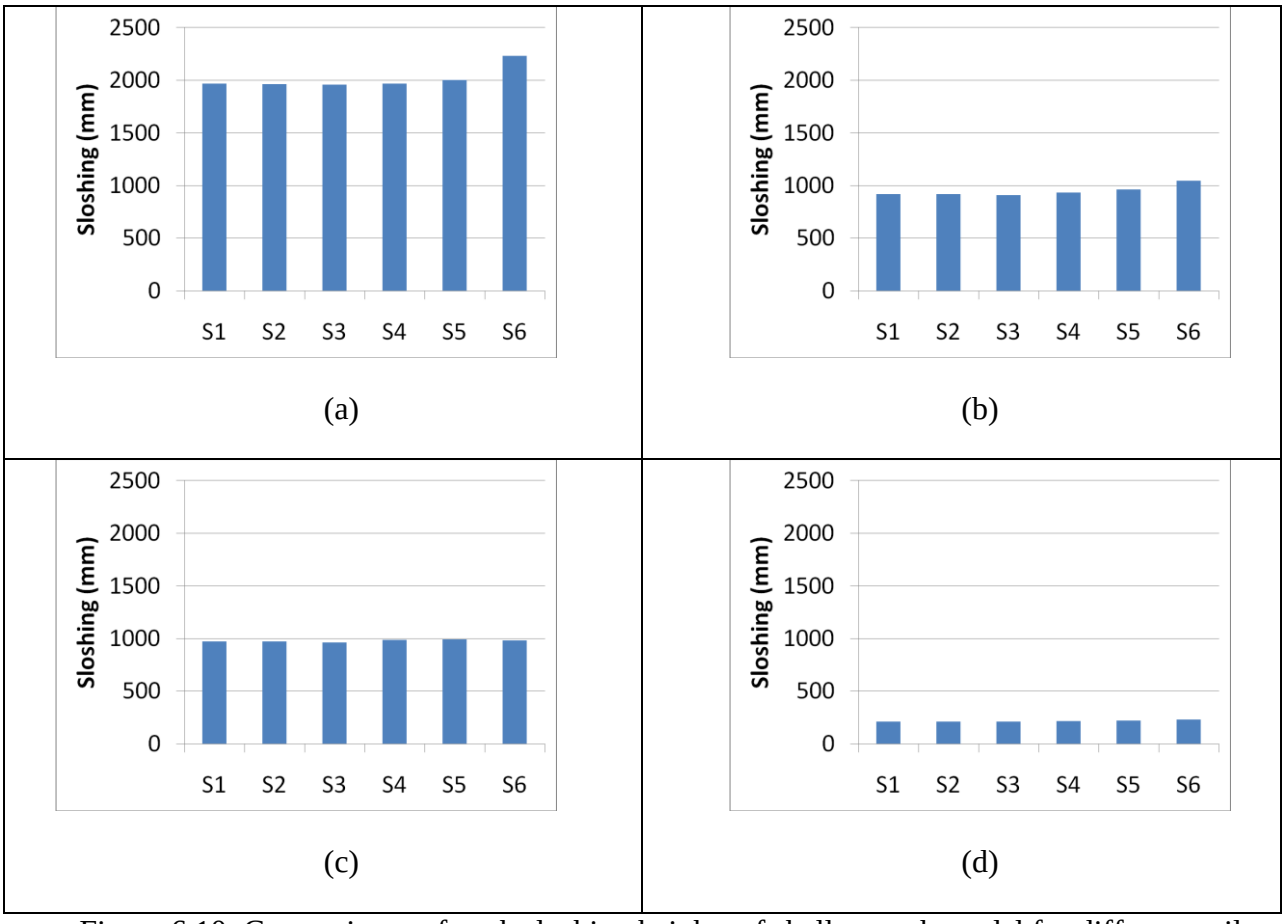


Figure 6.10: Comparisons of peak sloshing heights of shallow tank model for different soil types: (a) Northridge (b) El-Centro (c) San-Fernando (d) San-Francisco

### 6.4.2 Response of tall tank with flexible foundation

Figure 6.11 shows the effect of different soil type under different ground motions on the base moment responses of tall tank model. Except for Northridge earthquake, a significant reduction in structural response is seen for tanks supported on S6 soil type. These reduction values are about 11, 26, 28 and 47 percents for Northridge, El-Centro, San-Fernando and San-Francisco records compared to rigid base, respectively. However, an amplification of structural response

occurs in S4 soil type under Northridge earthquakes in comparison with rigid foundation condition as shown in Figure 6.11(a).

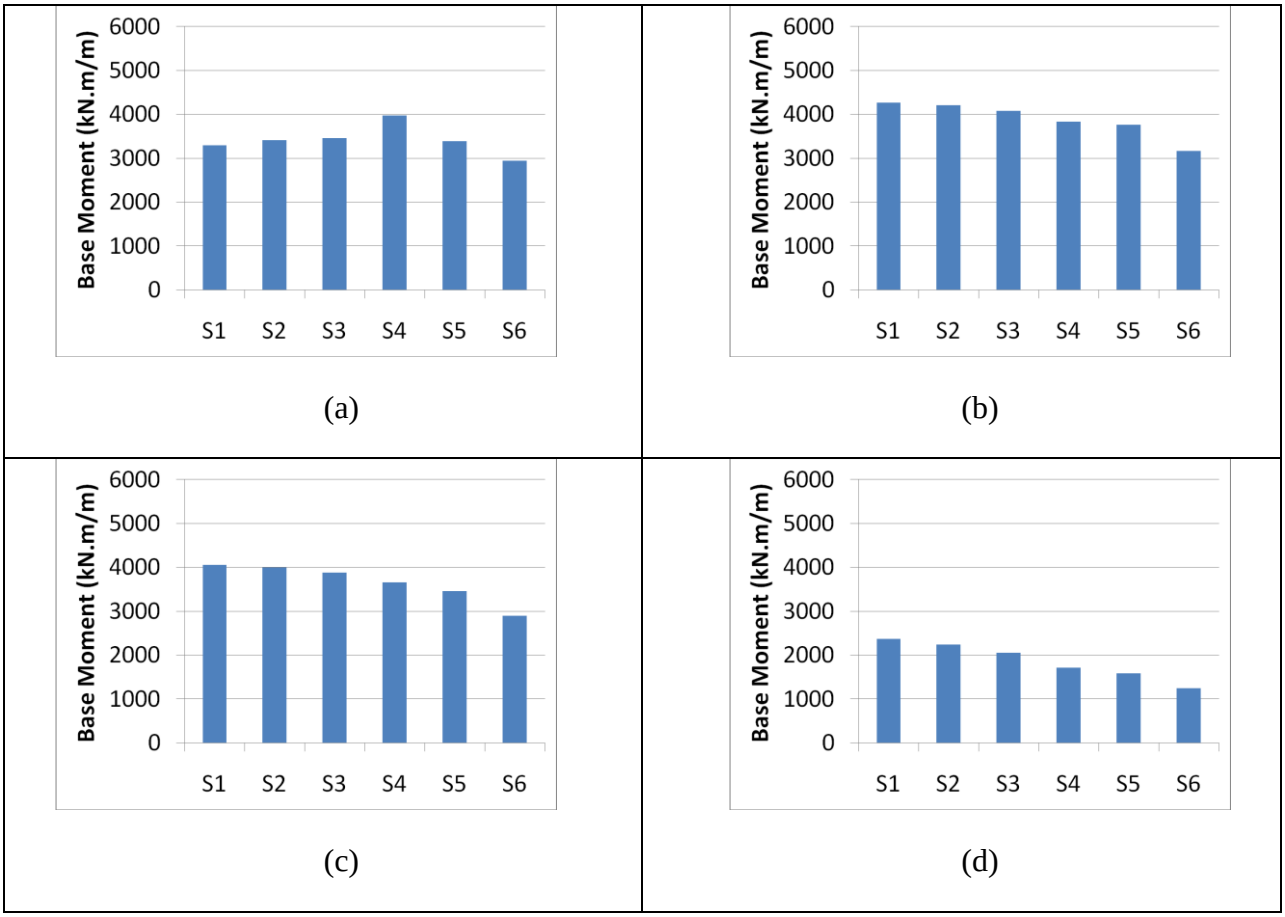


Figure 6.11: Comparisons of peak base moment responses of tall tank model for different soil types: (a) Northridge (b) El-Centro (c) San-Fernando (d) San-Francisco

In this case, the structural responses under moderate and high frequency-content earthquakes of El-Centro, San-Fernando and San-Francisco decrease as the foundation soil becomes softer.

It is clear that the response amplification or reduction pattern due to deformable foundation is highly dependent on the nature of earthquake.

To clarify the changes of structural response due to soil stiffness variation, the deviations of the base shear forces in time due to El-Centro earthquake are illustrated and compared among S1, S5 and S6 soil types for tall tank model in Figure 6.12. These time deviations have different characteristics and describe different behaviour of the tanks. For example, the fundamental periods of base shear responses are obtained as 0.328 s, 0.561 s and 0.853 s for S1, S5 and S6 soil types, respectively which shows that soil structure interaction has lead to period elongation in the structural responses. This phenomenon has also been reported by Larkin (2008).

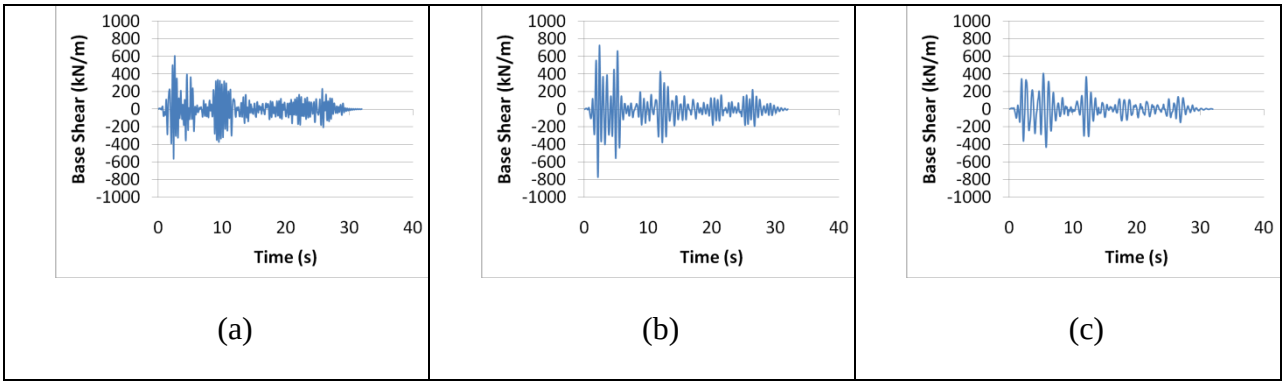


Figure 6.12: Time history of impulsive base shear for tall tank model with flexible foundation under horizontal excitation of El-Centro earthquake: (a) S1 soil type (b) S5 soil type (c) S6 soil type

In addition, the power spectral density (PSD) functions for four ground motions are shown in Figure 6.13. The center of the mass of PSD functions are located at 2.04Hz, 3.20Hz, 3.99Hz and 6.21Hz for Northridge, El-Centro, San-Fernando and San-Francisco records, respectively. These values correspond with natural periods of 0.49s, 0.31s, 0.25s and 0.16s, respectively. According to PSD concept, the significant amount of energy of the ground motion is concentrated at the center of the mass of PSD function. As a result, the maximum response of the structure is

expected under the ground motion record which has the nearest center of mass location to the fundamental natural period or frequency of the structure.

The modal analysis results of tank-liquid-foundation system are shown in Table 6.3 for both shallow and tall tank models. It is clear that the SSI significantly affect the impulsive fundamental periods. However, convective fundamental periods are almost independent of the flexibility of the foundation. This justifies the insensitivity of the sloshing height to the variation of foundation properties.

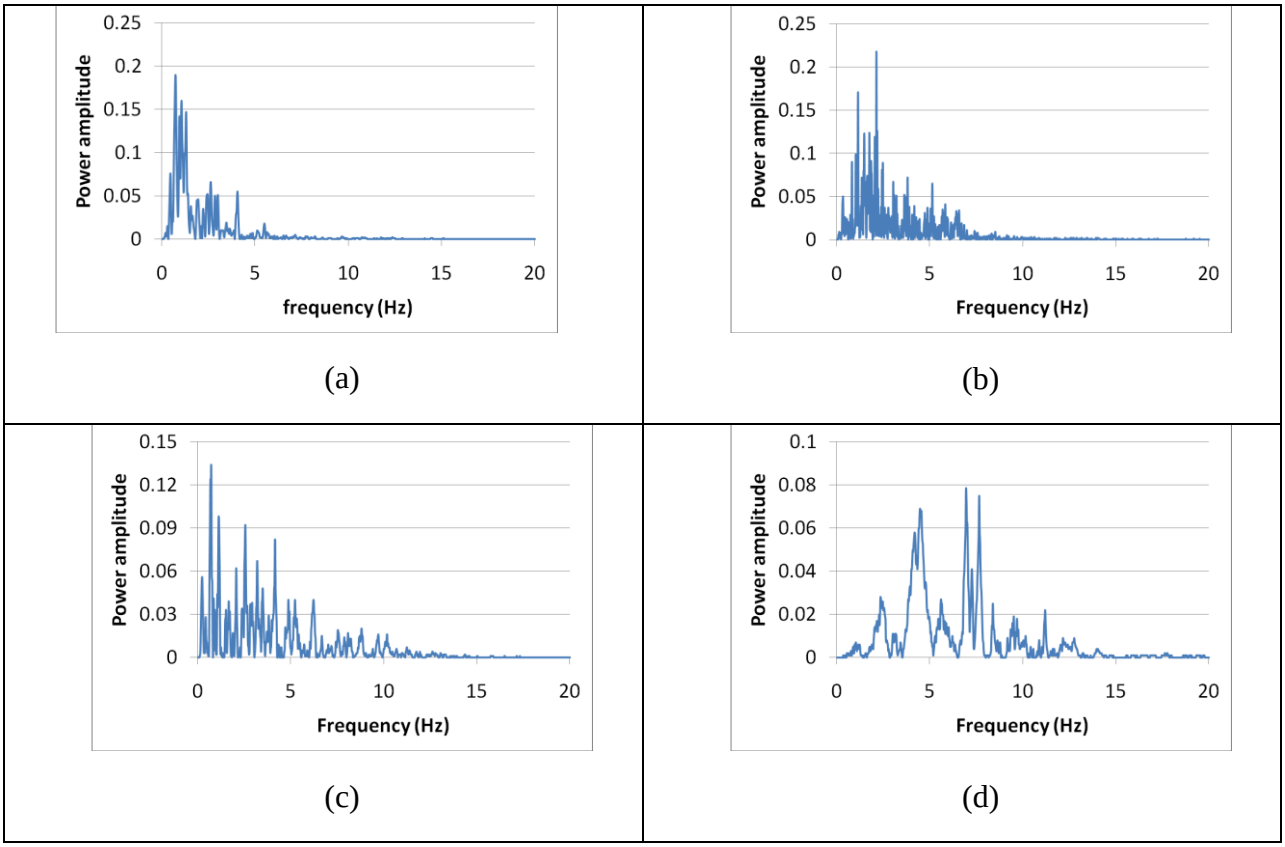


Figure 6.13: PSD function of: (a) Northridge (b) El-Centro (c) San-Fernando (d) San-Francisco

Table 6.3: Modal analysis results of soil-structure-liquid system

| | Impulsive fundamental period (sec) | | | | | | Convective fundamental period (sec) | | | | | |
|---|---|---|---|---|---|---|---|---|---|---|---|---|
| | $S_1$ | $S_2$ | $S_3$ | $S_4$ | $S_5$ | $S_6$ | $S_1$ | $S_2$ | $S_3$ | $S_4$ | $S_5$ | $S_6$ |
| Shallow tank | 0.15 | 0.14 | 0.16 | 0.22 | 0.29 | 0.41 | 8.58 | 8.58 | 8.58 | 8.57 | 8.55 | 8.49 |
| Tall tank | 0.33 | 0.34 | 0.38 | 0.52 | 0.63 | 0.87 | 5.13 | 5.13 | 5.13 | 5.13 | 5.12 | 5.09 |

Findings of this study show that the impulsive behaviour of liquid tank model does not follow a unique pattern when effect of soil-structure interaction and earthquake frequency content are combined. However, it is found that the convective behaviour is insensitive to soil properties as seen for both shallow and tall tank models.

### 6.5 Comparison with other methods

The seismic impulsive and convective responses of liquid tank models are obtained in this study as discussed previously considering four earthquake records with different frequency contents and accounting for foundation deformability, wall flexibility and fluid damping properties.

A verification of FE model was presented in previous research done by the authors (Ghaemmaghami and Kianoush (2009)). The FE pressure distribution is found to be in full agreement with analytical results when the fluid damping is ignored.

In the field of seismic behaviour of structural buildings, many studies have investigated the effect of vibration frequency on dynamic responses. Some of the major findings are reported by Jennings and Kuroiwa (1968), Foutch and Housner (1975), Mcverry (1979) and Chopra (1995).

It is clear that peak responses of the structure occur when the fundamental frequency of the vibration reaches near the corresponding natural frequencies of the structure.

Using actual earthquake response spectra, the impulsive base shear and base moments of shallow and tall tank models with rigid base are calculated and compared with those values obtained by FEM. The numerical procedure used for spectrum analysis is adopted from ACI 350.3-06. The comparisons between FE and spectral results for various ground motions are shown in Figures 6.14 and 6.15 for shallow and tall tank models, respectively.

Although the higher values are obtained using proposed FE method, the same trend due to earthquake frequency content is seen. For example, the amplification of structural responses under San-Francisco and El-Centro records is predicted in spectrum analysis for shallow and tall tank models, respectively as previously seen in FE results.

However, for both cases the FE method results in higher impulsive responses. In the most critical case, FE base shear and base moments are about 30 and 50 percent higher than spectral values for shallow tank model. These increases of base shear and base moments are about 10 and 20 percent for tall tank model, respectively.

The higher convective responses are obtained using spectral analysis for shallow tank model. For example, the deviation between FE and spectral values is up to 400 percent in calculated convective structural responses under El-Centro earthquake.

It is clear that the effect of earthquake frequency content is predicted as the same way in both methods. However, significant difference between calculated response values using FEM and spectrum analysis is seen.

Considering the SSI effect, different conclusions are reported in literature. Veletsos and Tang (1990) and Veletsos et al. (1992) showed that soil-structure interaction may reduce significantly

the critical responses of shallow tanks, but may increase those of tall, stiff tanks that have high fundamental natural frequencies. Also, it was shown that soil-structure interaction has a negligible effect on the convective components.

Moreover, Haroun and Abou-Izzeddine (1992) showed that interaction of the tank and foundation soil magnifies the tank response, and that the magnification is a factor of both shear-wave velocity of the soil as well as the geometric properties of the tank. Livaoglu (2008) concluded that the displacements and base shear forces generally decreased, with decreasing soil stiffness. However, the sloshing responses were not practically affected by soil-structure interaction in frequency domain which is similar to current FE results.

Also, Cho et al. (2004) obtained the same results as Livaoglu (2008) showed that structural responses are reduced as soil stiffness decreases. The liquid sloshing height and motion were not changed.

All of the above studies show that the convective term of dynamic response of liquid tank is insensitive to soil properties. The same results are obtained using FEM in this study. However, for both tank configurations, the soil-structure interaction effect is highly dependent on the earthquake frequency content and may amplify or reduce the structural responses.

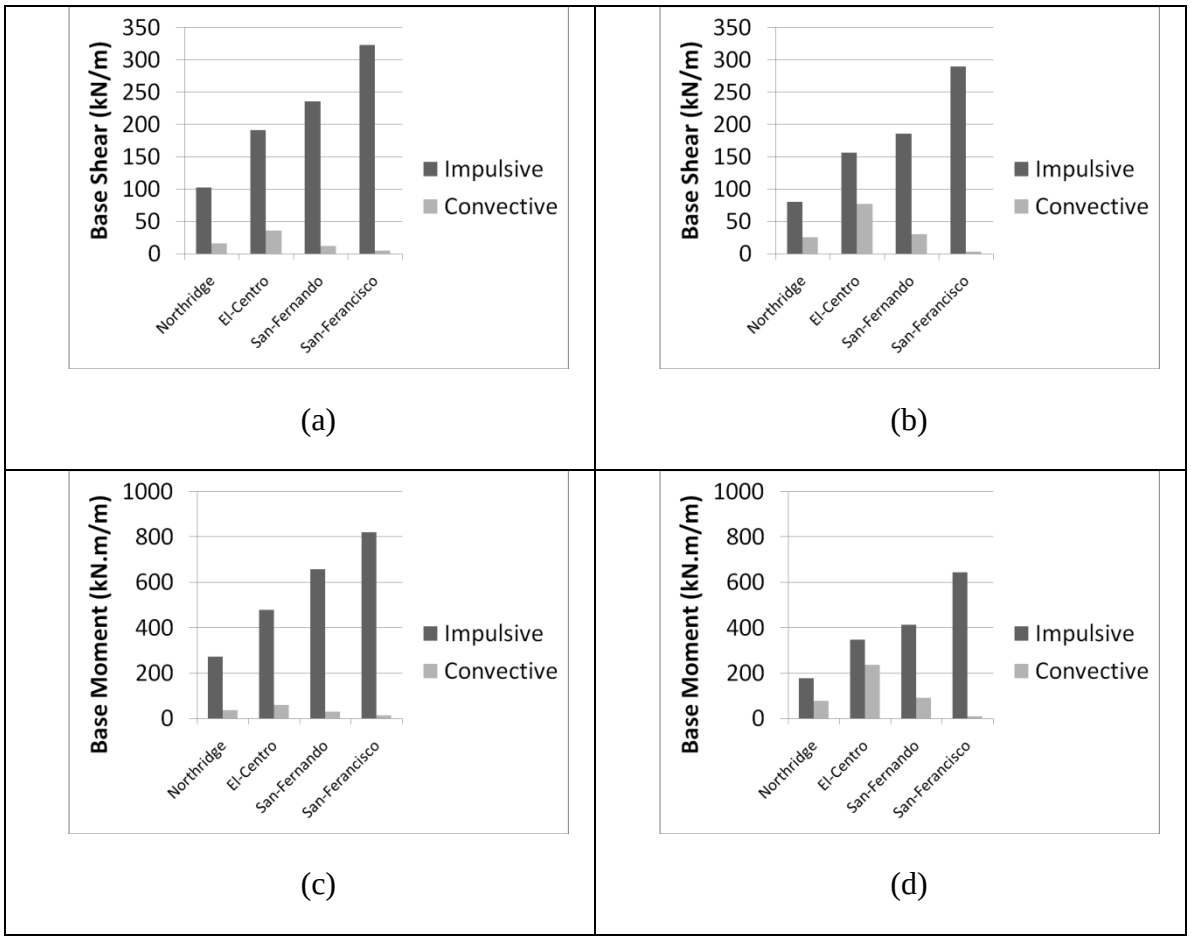


Figure 6.14: impulsive and convective structural responses of shallow tank model: (a) FE peak base shear (b) Spectrum base shear (c) FE peak base moment (d) Spectrum base moment

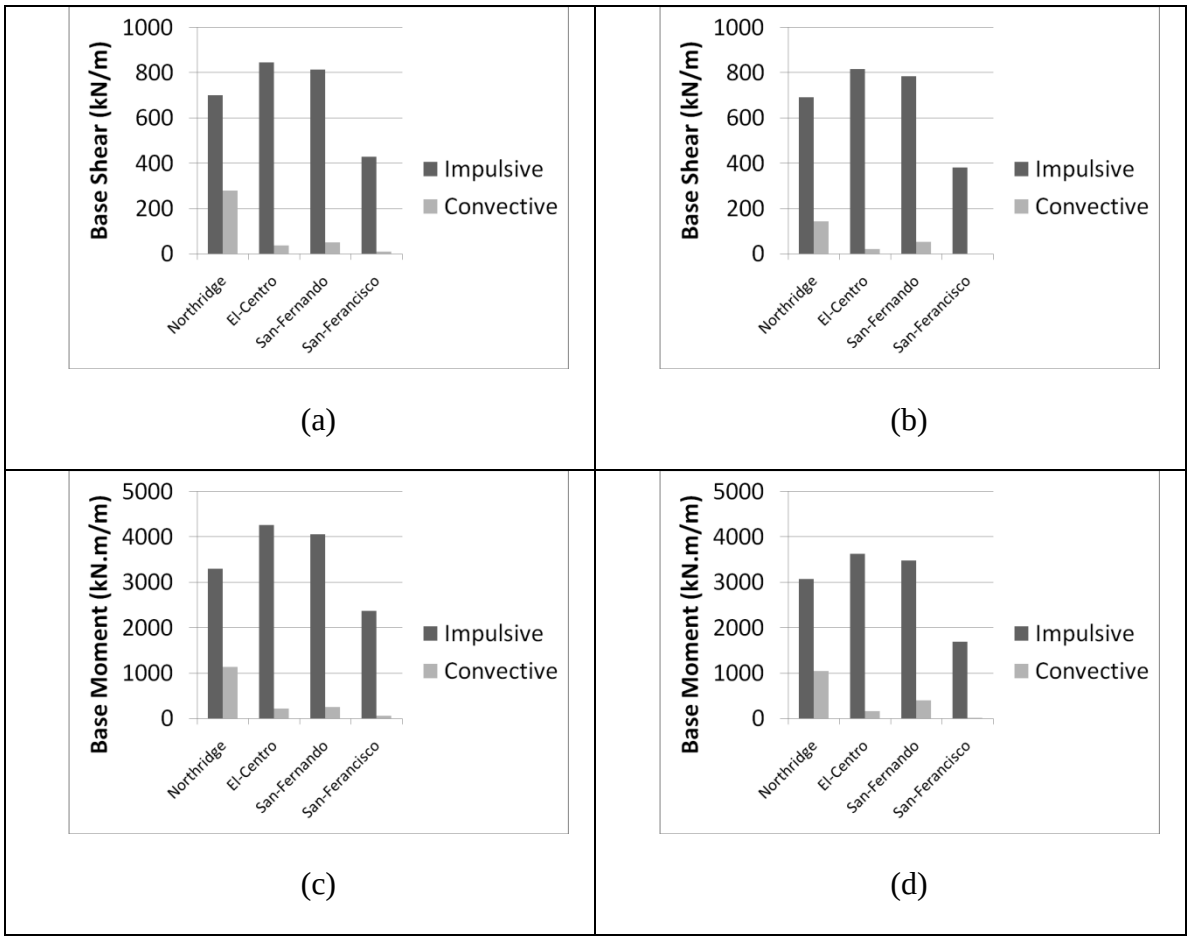


Figure 6.15: impulsive and convective structural responses of tall tank model: (a) FE peak base shear (b) Spectrum base shear (c) FE peak base moment (d) Spectrum base moment

## 6.6 Summary

In this chapter, dynamic behaviour of partially filled rectangular fluid container under different ground excitations was investigated in 3D space. The soil foundation is modeled as an elastic homogeneous medium with viscous boundary condition applied on the truncated zone to simulate the wave energy absorption. Two different configurations including shallow and tall tank models are considered to investigate the effect of geometry on the response of the liquid-

structure system in time-domain. Effect of wall flexibility on the dynamic response of system is taken into account. Four different ground motions with the same peak ground acceleration are applied to investigate the effect of earthquake frequency content on the seismic behaviour of liquid-tank system.

Effect of foundation deformability on the overall dynamic response of system is investigated by comparing the results among six different soil types.

The results are presented in terms of the maximum structural base shear and base moment obtained from time history analysis of the considered system as well as pressure distribution and surface sloshing heights for different seismic excitations. It is obvious that the records with frequency characteristics close to those of liquid tanks highly magnify the responses of the system. Assuming a rigid foundation, the high-frequency earthquakes result in the highest impulsive responses in shallow tank model, whereas the intermediate-frequency earthquakes highly amplify the tall tank model responses. Due to the significant difference between impulsive and convective fundamental frequencies, a different trend is seen for the convective responses under same earthquakes. It should be noticed that because of the high magnitude of impulsive responses and a significant time lag between peak impulsive and convective responses, the overall seismic behaviour of tank is governed by impulsive component.

Also, it is seen that applying the vertical excitation combined with horizontal excitations will result in different variations in the convective response of the system which depends on the characteristics of the earthquake and configurations of the tank. However, it does not affect the impulsive behaviour significantly as seen for all records.

In this study the FE results are compared with those obtained by spectrum analysis based on actual earthquake response spectra. Although the spectrum values are generally lower than FE results, the same trend due to earthquake frequency content is seen for both methods.

Considering the effect of SSI, the results show that the maximum impulsive base shear and base moment obtained from time history analysis of the considered system may increase or decrease as the soil stiffness changes which is a result of dynamic pressure variation in the middle of the wall due to the rocking motion of the foundation. This phenomenon is highly dependent on earthquake frequency-content and tank configuration.

A unique trend is seen under low frequency-content earthquake for both shallow and tall tank configurations. In this case, the structural responses increase as the soil stiffness increases.

In addition, the convective response is almost independent of variations of flexibility of the foundation and seems to be related to geometric configurations of tank, earthquake characteristics and liquid properties.

It should be noted that dynamic behaviour of soil foundation is governed by more complex phenomena than those discussed in this study. Limitations of the proposed FE model for soil-structure interaction should be considered in interpretation of the results.

The present study is done based on 3D analysis of rectangular tanks in time-domain using four different earthquake records and six different soil types. Although the liquid tank design procedure are based on simplified frequency-based methods, the current FE time-history results which are more realistic can be used to verify these methods in future works.

# Chapter 7

# Analysis of rectangular tank models equipped with external dampers

## 7.1 Introduction

In this chapter, the performance of external dampers including slat screens and baffles in increasing the intrinsic damping of partially filled liquid tanks is discussed. The liquid in containers displays a free-surface fluctuation when the container is subjected to an external excitation like earthquake and this liquid sloshing may be a cause of the unexpected instability and failure of structural system. As either the excitation amplitude increases or the excitation frequency approaches the natural sloshing frequency, the damage caused by liquid sloshing may become a serious concern. This hazardous situation is involved in a wide field of engineering applications, such as above-ground liquid storage tanks under earthquake waves, fuel storage tanks of aerospace vehicles and cargo tanks of liquefied natural gas (LNG) carriers in service. Thus, the sloshing suppression has become an inevitable research subject in the community associated with the fluid sloshing during several decades.

Usually, the sloshing effect is suppressed in a passive manner by introducing additional sub-structures such as baffles and slat screens into the containers. The shape and design concept of the sloshing damper varies depending on the sloshing motion, the nature of external excitation and the tank configuration. The basic concept of passive sloshing damper is to dissipate the sloshing motion energy by breaking a main sloshing flow into several weaker sub-streams.

In this study, several numerical models with different slat screen and baffle configurations are used to investigate the effect of parameters such as location and solidity ratio on the sloshing behaviour of tank model. In addition, these models are subjected to different earthquakes to

account for the effect of earthquake frequency on sloshing behaviour as previously mentioned in Chapter 6.

The results of this study can also be used in future studies on designing tuned liquid dampers (TLD) applicable in tall buildings. In common liquid tanks, the amount of viscous force is not usually enough to achieve the required inherent damping for an efficient TLD system. In such cases, external devices such as slat screens can be installed inside the tank to increase the damping ratio and reduce the sloshing height.

Finally, the results of the parametric study are presented followed by a summary of the main conclusions obtained from the study.

### 7.2 Numerical modelling of slat screen

In this study, a FE model is used to simulate the performance of rigid slat screens in liquid tanks. For this purpose, vertical slat screens are numerically modeled by introducing additional rigid planes to FE model. A schematic view of the numerical model is presented in Figure 7.1 in which the origin of coordinate system is located at the center of fluid surface. The liquid domain is modelled using 800 linear fluid elements which are able to simulate dynamic liquid pressure and free surface motions. Each element has three translational and one pressure DOF per node. Translational degrees of freedom in the direction perpendicular to screen planes are coupled with fluid elements in contact areas to account for the interaction between liquid and screen.

By changing the vertical width of slat screens, various solidity ratios are easily obtained as shown in Figure 7.1.

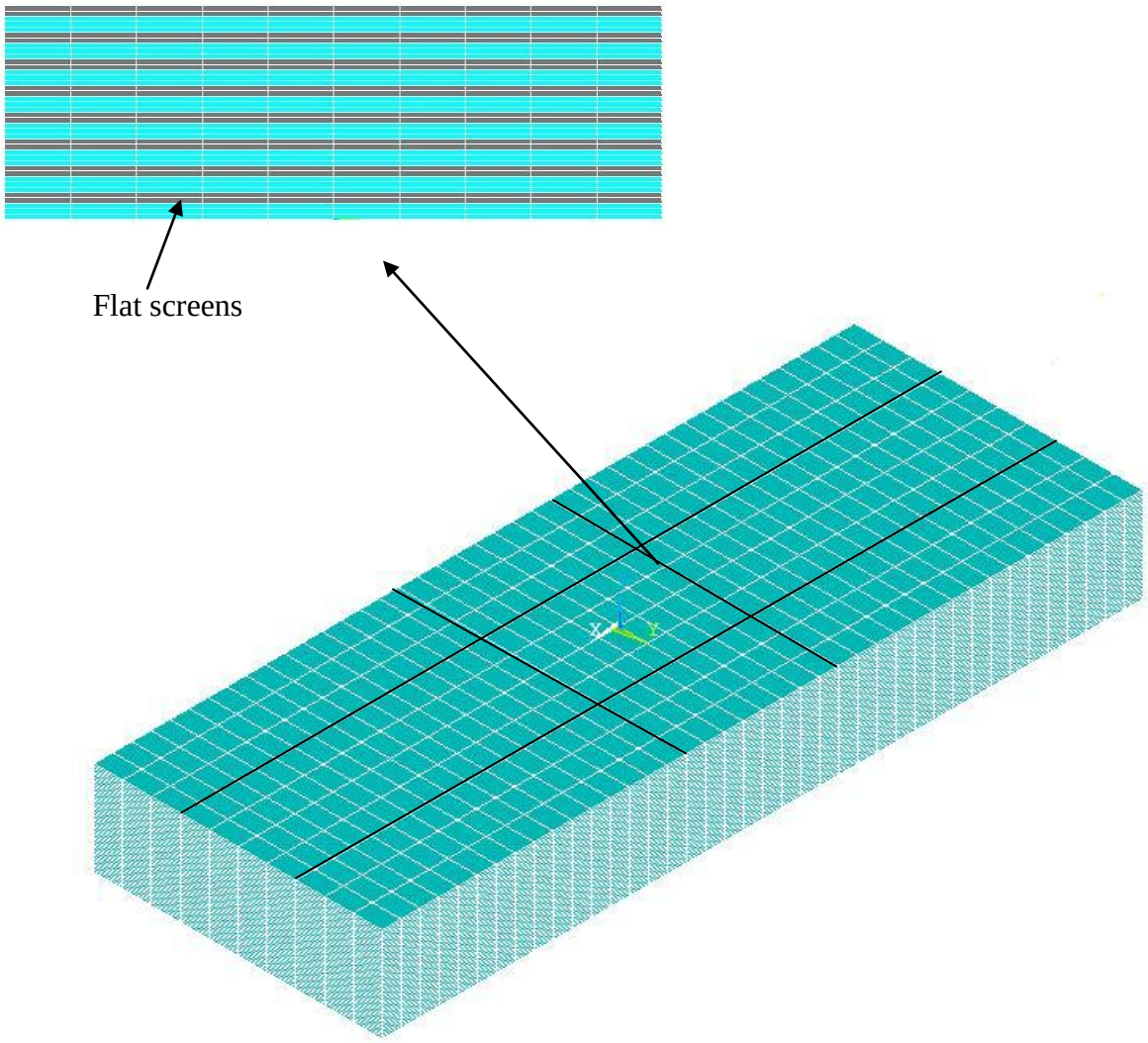


Figure 7.1: FE model of slat screens

Before starting the numerical analyses, a comparison between proposed FE model results and those obtained using experimental tests reported by Tait et al. (2005) is made to verify the proposed method. The significance of their experimental study is that the liquid tank behaviour equipped with slat screens is evaluated over a wide range of normalized excitation values. This is applicable in buildings subjected to ground accelerations.

A rectangular tank with the following dimensions was considered for the experimental test:

*L=966mm b=366mm h=119mm*

Where *L* is the tank length, *b* is the tank width and *h* is the water depth. The flat screens were located at -0.1L and 0.1L from the center of the tank as shown in Figure 7.2. Each screen had a solidity ratio S=0.42. The tank was mounted on shaking table and subjected to a horizontal sinusoidal excitation.

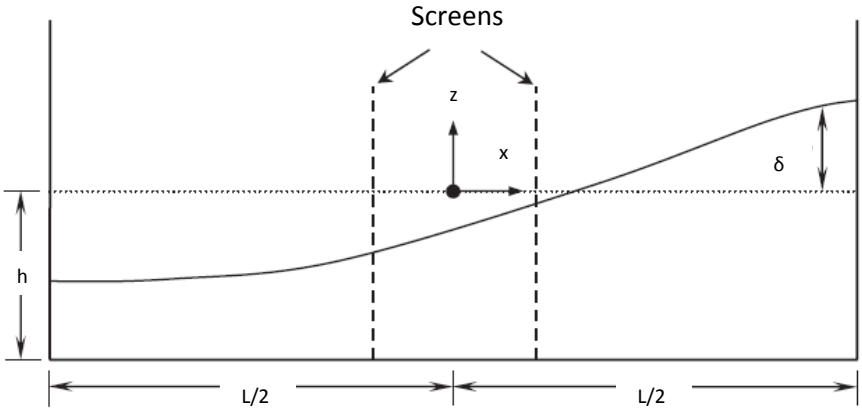


Figure 7.2: Coordinate system for tank model equipped with slat screens (Tait et al. (2005)

The response sloshing heights for the free surface motion, calculated from the finite element method, are compared with experimental results from shaking table test. The ratio of the

frequency of base harmonic displacement to the frequency of fluid sloshing is chosen as 1.01. The free surface variation near the end wall at the middle of tank width is plotted in Figures 7.3 for A/L value of 0.005 in which A is the amplitude of the harmonic displacement of the tank base for both FE and experimental results. The sloshing height and time values are normalized with respect to the liquid height and period of base vibration.

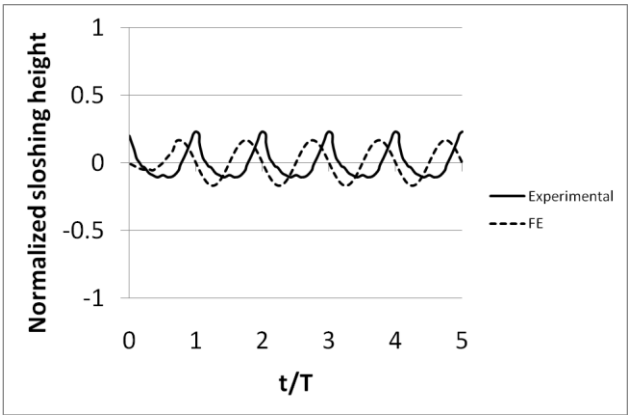


(a)

Figure 7.3: Comparison of experimental results obtained by Tait et al. (2005) with calculated normalized FE sloshing for *A/L* values of 0.005

Satisfactory agreement for the maximum sloshing amplitude is found to occur between the FE model and the experimental data.

For this study, a liquid tank model with the following dimensions which are applicable in a tall building is chosen to numerically investigate the efficiency of flat screens in reducing sloshing heights under different ground motions:

$L_x = 3m \quad L_y = 6m \quad H_l = 3m \quad \rho_l = 1000kg/m^3$

In this case, the ratio of $H_L/L_x$ is equal to 1 and the linearized boundary condition is applicable to calculate the sloshing height.

To investigate the effects of slat screen location and solidity ratio on the sloshing response, four different configurations of slat screens as shown in Table 7.1 are considered in this study. For each configuration, three different solidity ratios of 0.25, 0.33 and 0.50 are applied in FE analyses.

Table 7.1: Configurations of slat screens used in numerical analyses

| Configuration No. | Screen Location |
|---|---|
| 1 | X=0<br>Y=0 |
| 2 | X=-1, X=1<br>Y=-1, Y=1 |
| 3 | X=-2, X=2<br>Y=-3, Y=3 |
| 4 | X=-1, X=1<br>Y=-1, Y=1<br>X=-2, X=2<br>Y=-3, Y=3 |

### 7.3 Response of liquid tank model equipped with slat screen

Having validated the numerical modeling of sloshing behaviour in Chapter 5, the investigation is carried out by conduction a parametric study to assess the effects of varying locations and solidity ratio of the slat screens and earthquake frequency content on the response of the system. Three different earthquake records of Northridge, El-Centro and San-Francisco with low, moderate and high frequency contents are selected for analysis purpose. All the records are scaled in such a way that the horizontal peak acceleration is equal to 0.4g as previously

shown in Chapter 6. It should be noticed that all three components of earthquake record are applied simultaneously in these analyses.

Time-history diagrams of calculated sloshing height at the top corner of liquid model (x=3, y=6 and z=0) are shown in Figure 7.4 for El-Centro earthquake records. The sloshing values are normalized with respect to the maximum sloshing height of the tank without screen.

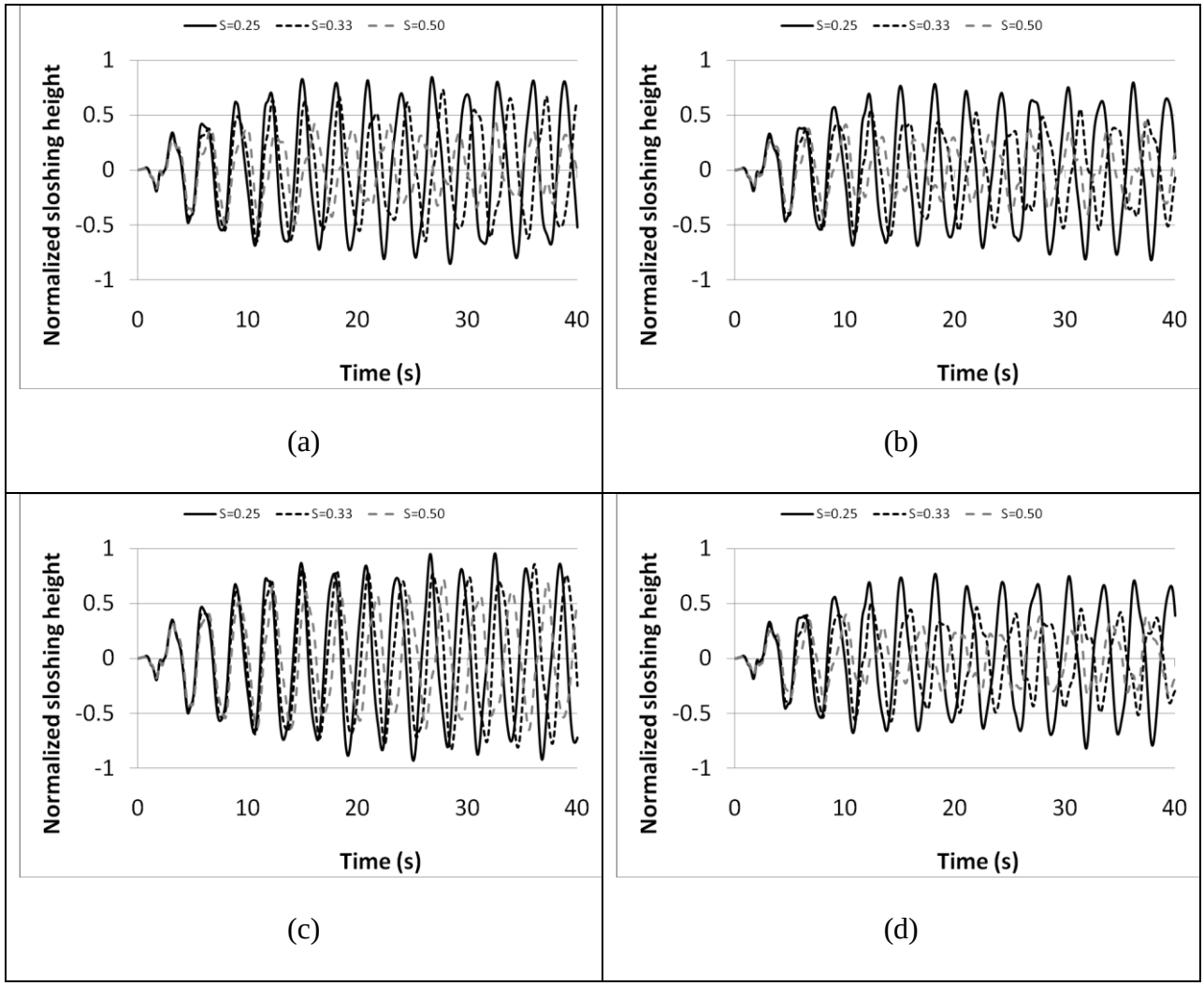


Figure 7.4: Comparison of normalized sloshing heights for different configurations under El-Centro earthquake: (a) C1 (b) C2 (c) C3 (d) C4

It is clear that the amount of reduction of peak sloshing due to installed screens in comparison with the peak sloshing value of liquid tank model without screen can be interpreted as the efficiency of the screen configuration.

These amounts are calculated for each tank configurations subjected to different earthquakes. A comparison among obtained results is shown in Figure 7.5.

The results show that the highest reductions occur when the liquid tank is equipped with screen configuration No.4 where 4 screens are placed near center and 4 screens are places near side walls. However, the difference between sloshing reduction values for configuration No.4 and No.2 where only four screens are installed near the center of the tank is insignificant. For example, this difference is about 2 percent in case of El-Centro record which indicates that most losses have occurred due to screens placed near the center of the tank. Placing the screens near the side walls does not affect the sloshing significantly.

In addition, the numerical results indicate that the reduction of the sloshing response due to slat screens is highly depending on the nature of earthquake. For example, the highest decrease in peak sloshing height is obtained for El-Centro earthquake which has moderate frequency content. In this study, the lowest screen efficiency in reducing the sloshing height is obtained under low frequency-content record of Northridge. In this case, the highest reduction value is only about 5 percent which shows that the flat screens are quite ineffective.

As a result, the efficiency of this system is highly dependent on the nature of earthquake and liquid tank configurations. This point needs more investigation in future studies.

As previously mentioned, the screen configurations, in terms of solidity ratio and locations, are varied in these analyses. The change of screen configurations leads to a change in the inherent damping which affects the calculated sloshing height

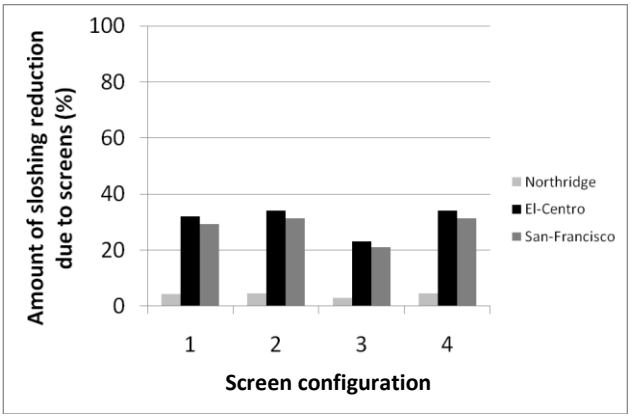


(a)

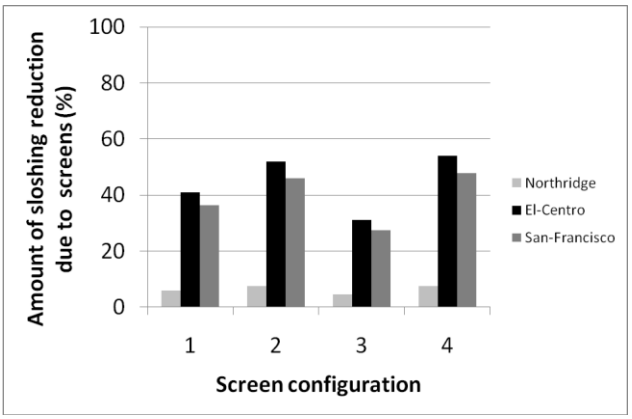


(b)

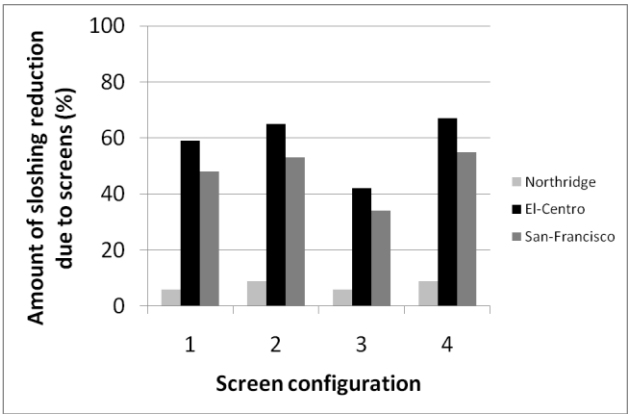


(c)

Figure 7.5: Amount of sloshing reduction for different tank configurations and earthquake records: (a) S=0.25 (b) S=0.33 (c) S=0.50

To estimate the amount of intrinsic damping due to placing slat screens in liquid tank model, several analyses are carried out by varying the fluid damping ratios in a liquid tank model without screens. By calculating the peak sloshing height for each case subjected to a particular earthquake, the amount of sloshing reduction can be found as a function of damping ratio. A sample diagram is shown in Figure 7.6 which presents the variation of sloshing reduction versus damping ratio calculated under different ground motions.

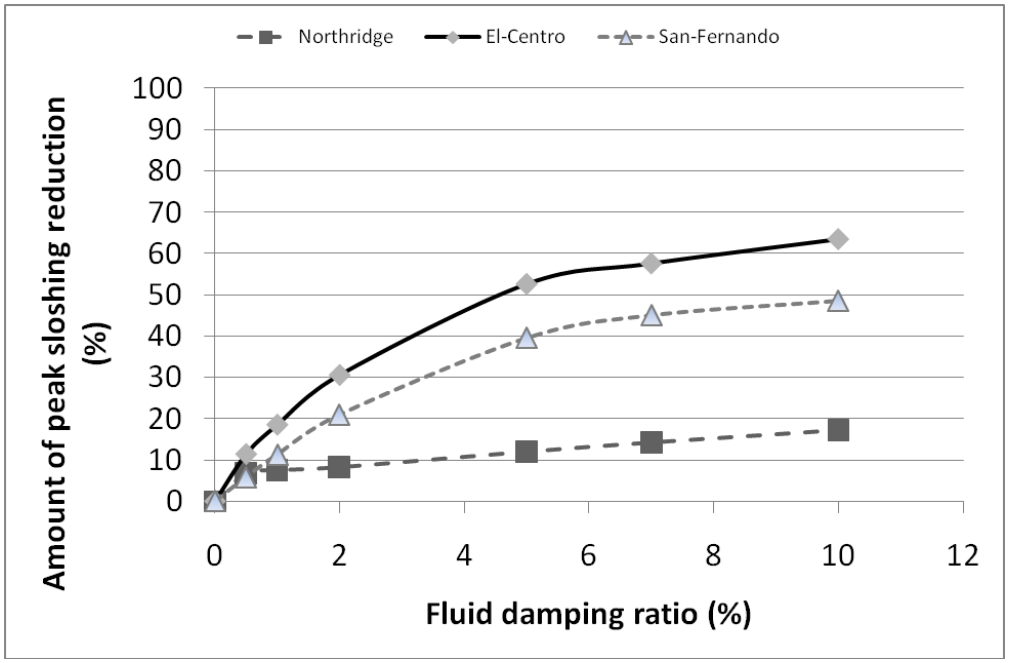


Figure 7.6: Variation of peak sloshing reduction versus fluid damping ratio under different ground motions

By comparing the presented results in Figures 7.5 and 7.6, the equivalent damping ratio for each screen configuration can be assessed. For example, a peak sloshing reduction about 67 percent due to screen configuration No.4 and a solidity ratio of 0.50 under El-Centro earthquake is equivalent to a damping ratio of about 10 percent.

However, for the same screen configuration and solidity ratio the amount of peak sloshing reduction is about 9 percent for Northridge earthquake which is corresponding to an equivalent damping ratio of about 2 percent.

In addition, for the same screen configuration, equivalent damping ratio is estimated higher than 10 percent for San-Fernando earthquake. These examples indicate that the amount of additional damping ratio due to flat screen is highly dependent on not only the location and solidity ratio of screens but also the nature of earthquake.

It should be noted that a partially filled water tank can be used as a vibration absorber or tuned liquid damper (TLD) to reduce the dynamic motion of a structure when it has the optimum inherent damping value. This value depends on the ratio of the effective mass of fluid to the generalized mass of the structure.

Expressions to determine the optimum damping of a linear tuned mass damper (TMD) as a function of mass ratio have been derived by Warburton (1982). Because of the similarity between TLD and TMD, such an expression can be adopted for TLDs.

Accordingly, the optimum inherent damping values, corresponding to typical mass ratio values, range between approximately 5% and 15%.

In this study, a FE model is proposed as described above to numerically estimate the efficiency of the screen dampers. It should be noted that the results of this study are valid when applying the linearized boundary condition is applicable. Otherwise, more complicated and accurate methods should be used to predict the nonlinear behaviour of sloshing.

### 7.4 Numerical modelling of horizontal baffles

Figure 7.7 shows a rectangular tank with a pair of baffles in which liquid is filled up to the height $H_L$ from the tank bottom in the stationary condition. In this study, the baffles are assumed to be rigid. This assumption was verified by the works done by Cho and Song (2001) and Cho et al. (2002).

A Cartesian coordinate system is originated at the center of undisturbed free surface. Since the baffle thickness is neglected, a rigid plane is defined in numerical models representing the effect of baffles on the sloshing behaviour of liquid. Similar to flat screen simulation, the rigid plane is coupled to the liquid elements in such a way that liquid velocity perpendicular to this plane is set to zero.

In order to investigate the effect of baffle configuration on reduction of sloshing height, different patterns are studied as shown in Table 7.2. Three different earthquake records, previously applied in flat screen modelling, are used as input ground motions to investigate the effect of earthquake nature on the behaviour of baffled tanks.

The same dimensions of rectangular tank model as previously mentioned in section 7.2 are used in numerical modelling. The vertical section of the corresponding FE model is shown in Figure 7.8 in which the mesh partition consists of 600 fluid elements.

Table 7.2: Configurations of horizontal baffles used in numerical analyses

| Configuration No. | $d_B/L_X$ | $H_B/H_L$ |
|---|---|---|
| 1 | 0.75 | 0.5 |
| 2 | 0.66 | 0.5 |
| 3 | 0.50 | 0.5 |
| 4 | 0.75 | 0.75 |
| 5 | 0.66 | 0.75 |
| 6 | 0.50 | 0.75 |

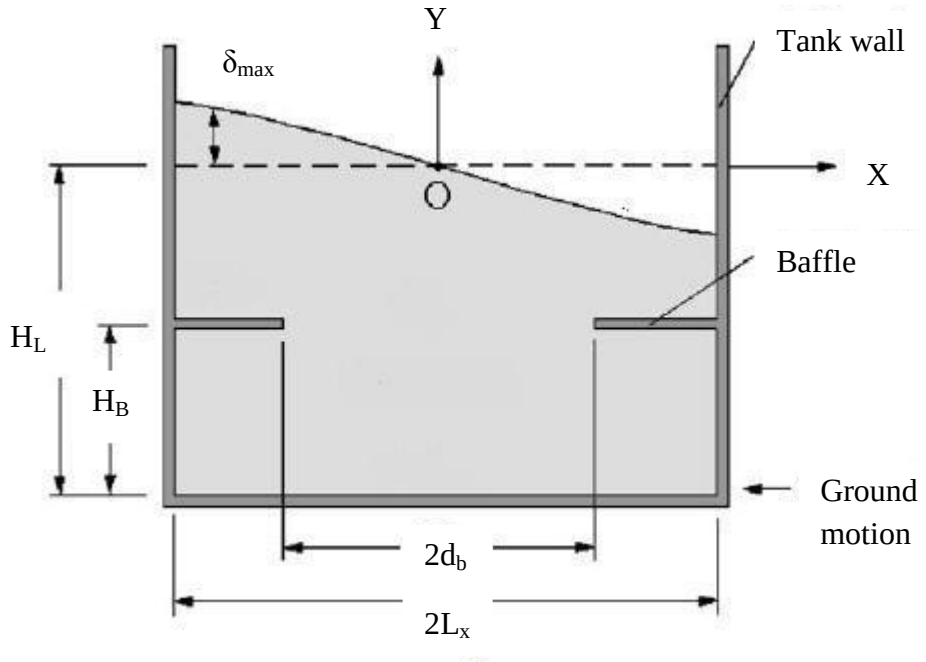


Figure 7.7: Schematic view of a rectangular baffled tank

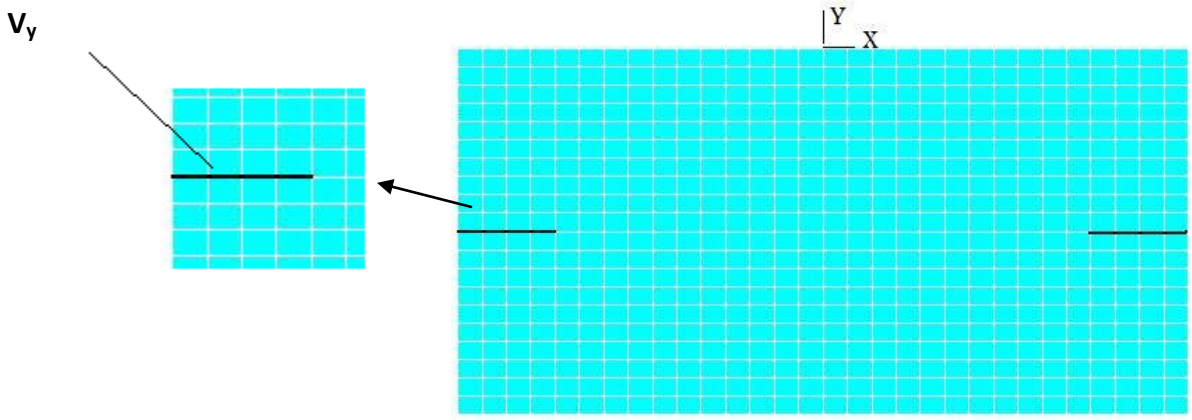


Figure 7.8: FE model of Horizontal baffles

Referring to Figure 7.7, baffles are installed with uniform vertical spacing with respect to the liquid fill height, and the occurrence of zero-thickness baffle is numerically implemented by introducing a rigid plane which is coupled to fluid elements in Y-direction.

The effect of the relative opening width of baffle ,$d_B/L_{X,}$ on the sloshing response of free-surface elevation under different ground motion is presented in Figures 7.9 and 7.10 for $H_B/H_L$=0.5 and 0.75, respectively. The time-history results due to each ground motion are normalized with respect to the maximum sloshing height calculated for liquid tank model without baffles. In addition, the values of maximum sloshing height reduction are presented in Table 7.3 which can be interpreted as the efficiency of baffles.

Form the analysis of no-baffle tank models, the maximum sloshing heights are calculated as 550, 986 and 50mm under Northridge, El-Centro and San-Fernando earthquake records. With introducing the baffles, sloshing heights are reduced due to occurrence of vortex around the baffles. This phenomenon will result in energy suppression and subsequently reduction of liquid sloshing height. A sample illustration of liquid flow pattern affected by horizontal baffles is shown in Figure 7.11.

As presented in Table 7.3, the efficiency of baffles is highly dependent on the nature of earthquake as previously observed for slat screens. For examples, the highest reduction values are obtained under El-Centro record for all baffle configurations, while the lowest values are obtained under Northridge earthquake record.

It is clear that as the ratio of $H_B/H_L$ increases from 0.5 to 0.75, the maximum sloshing height decreases for all cases. However, the amount of sloshing reduction due to variation of baffle elevation is more significant when the tank is subjected to Northridge ground motion.

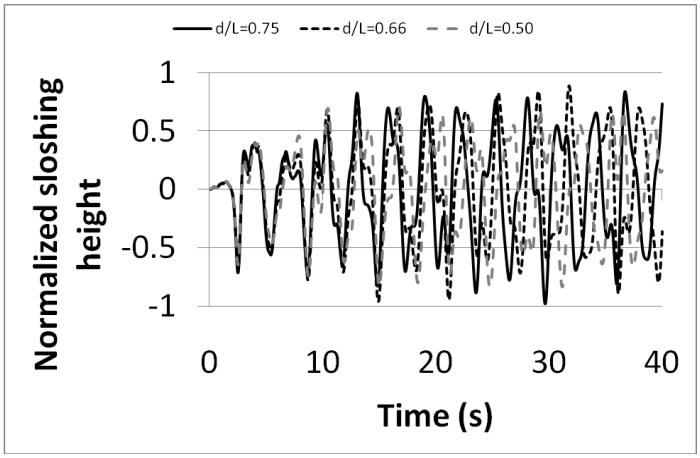


(a)

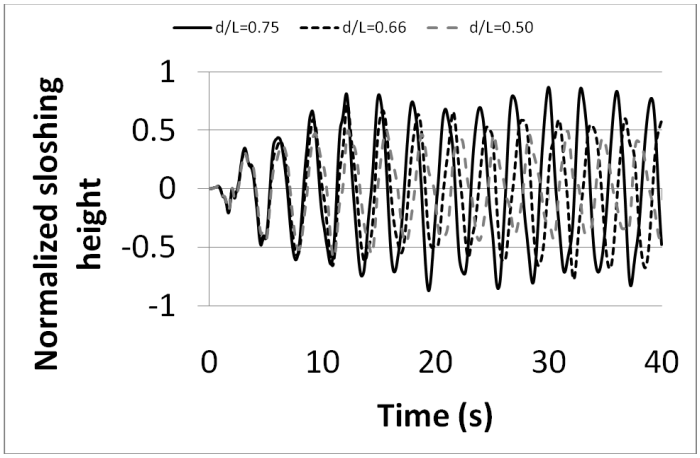


(b)

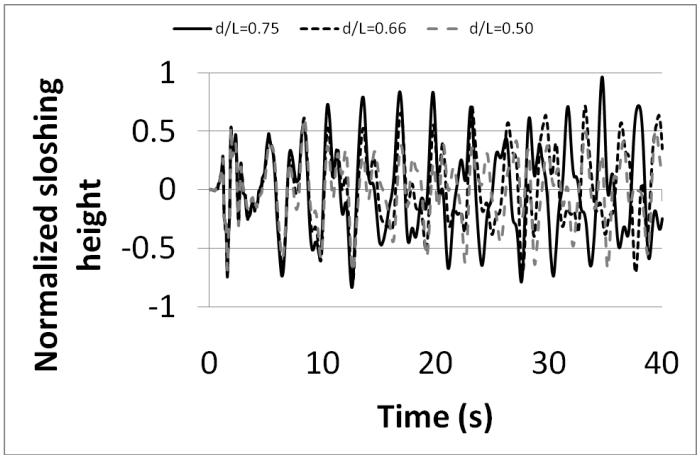


(c)

Figure 7.9: Comparison of normalized sloshing heights for $H_B/H_L$=0.5: (a) Northridge (b) El-Centro (c) San-Francisco

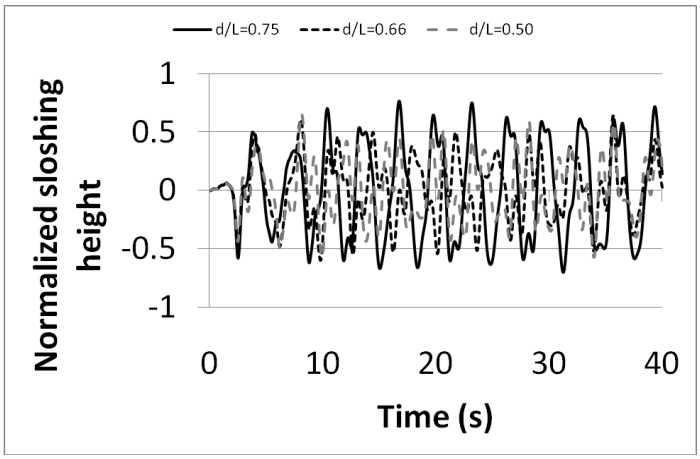


(a)

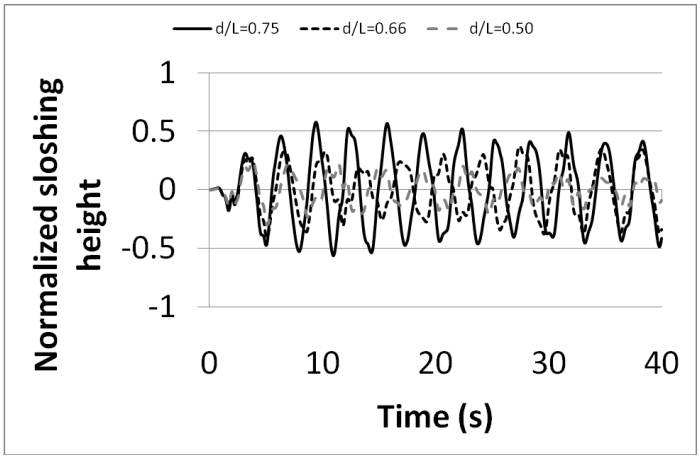


(b)

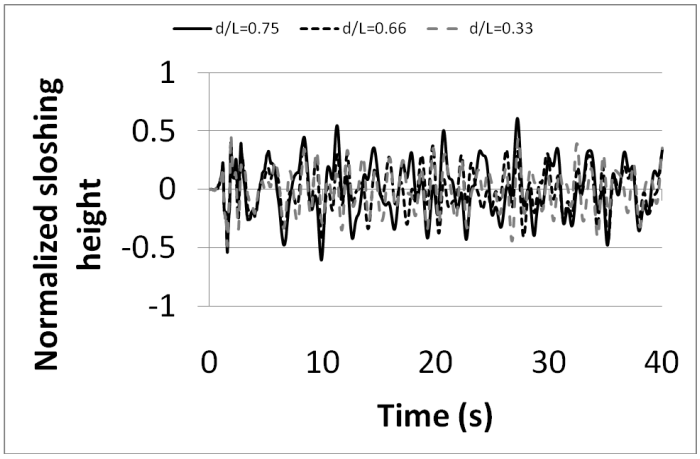


(c)

Figure 7.10: Comparison of normalized sloshing heights for $H_B/H_L$=0.75: (a) Northridge (b) El-Centro (c) San-Francisco

Table 7.3: Amount of sloshing reduction for different baffle configurations and earthquake records

| | | Maximum sloshing height reduction (%) | | |
|---|---|---|---|---|
| $d_B/L_X$ | $H_B/H_L$ | Northridge | El-Centro | San-Francisco |
| 0.75 | 0.5 | 2 | 13 | 4 |
| 0.66 | 0.5 | 4 | 22 | 19 |
| 0.50 | 0.5 | 16 | 41 | 30 |
| 0.75 | 0.75 | 25 | 42 | 39 |
| 0.66 | 0.75 | 36 | 59 | 51 |
| 0.50 | 0.75 | 40 | 70 | 52 |

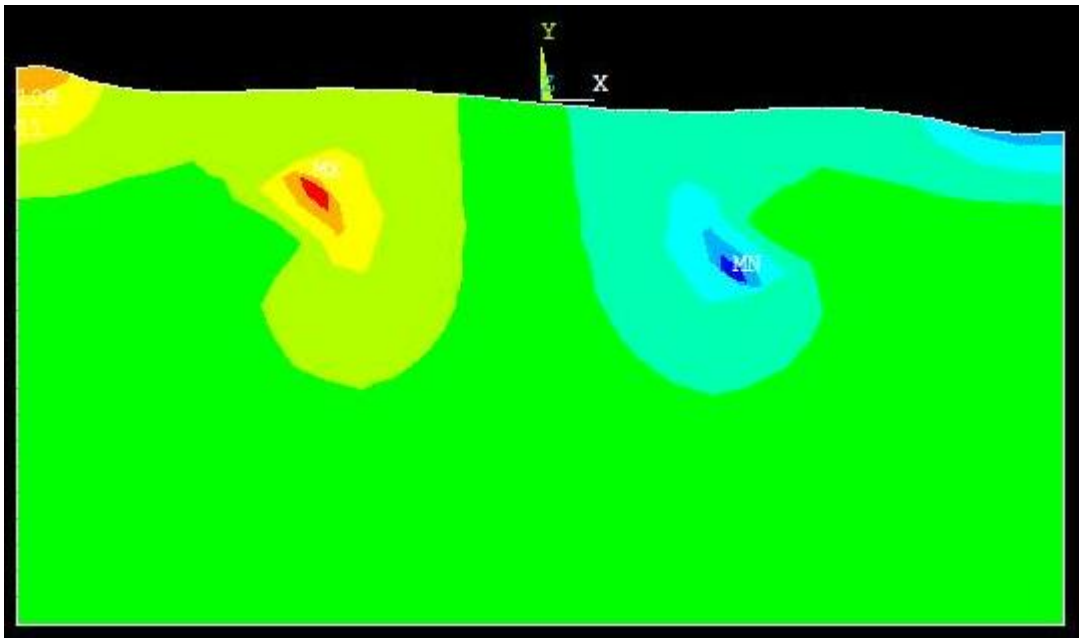


Figure 7.11: Liquid flow pattern in a baffled tank

Additional damping ratios due to installing baffles can be estimated by comparing maximum sloshing reduction values obtained by FE analysis of baffled tanks with those obtained using un-baffled tank models with varying numerical damping ratios.

As an example, by comparing the results presented in Table 7.3 with those shown in Figure 7.7 for El-Centro record, it is found that the intrinsic damping ratio of liquid has increased to about 10 percent when baffled are installed at $d_B/L_X=0.5$ and $H_B/H_L=0.75$.

It is clear that as the opening width of baffle increases, the amount of additional damping decrease. In this case, the lowest equivalent damping ratio is estimated as 0.5 percent when $d_B/L_X=0.75$ and $H_B/H_L=0.5$.

However, similar to the results obtained for flat screens, the additional damping ratio due to baffles is highly dependent on the nature of earthquake.

### 7.5 Summary

In this chapter, numerical analyses have been carried out to investigate the effectiveness of slat screens and baffles in reducing the sloshing response of liquid tank model under different ground motions. Rigid planes are introduced in liquid model to simulate the interaction between slat screens and liquid domain. Effect of flexibility is ignored in this study.

The FE model is then used to perform a parametric study by varying screen configurations, in terms of location and solidity ratio, and earthquake characteristics. It is concluded that the effectiveness of slat screens is highly dependent on the frequency content of applied ground motion. Finally, the findings of this Chapter can be used in future works on numerical modelling of liquid tanks equipped with slat screens and baffles applicable in tuned liquid dampers (TLD) for tall buildings.

# Chapter 8
# Summary, conclusions and recommendations

## 8.1 Summary

The primary goal of this study was to develop a robust and efficient finite element method for the analysis of partially filled rectangular liquid tanks subjected to seismic ground motions. The most important issues concerned in this study are assessing the effects of wall flexibility, three-dimensional geometry, earthquake frequency content and soil-structure interaction on the dynamic behaviour of liquid tanks. The current design practice is based on a major simplification and the effects of the above parameters are not usually considered in design of liquid containing structures.

Current design standards are commonly based on simplified mechanical models and a frequency based procedure is used to calculate the seismic responses. The most common approach in designing liquid tanks is based on Housner's method which is based on Laplace equation for modeling the liquid domain. In this method, the liquid mass is divided into two parts, impulsive and convective. The impulsive mass is assumed to be rigidly attached to the tank wall while the convective mass is assumed to oscillate through a spring connected to the tank wall. It should be noticed that expressions for distribution of impulsive and convective hydrodynamic pressure are available in design codes only for rigid tanks.

In most standards the effect of vertical acceleration is considered only for circular tanks, and there are no specific provisions on rectangular tanks. In addition, except for NZSEE and Euro Code guidelines, provisions for consideration of soil-structure interaction are not provided in design codes. However, the available provisions only discussed about the effect of soil flexibility on the period of tank structure.

With the development of robust numerical methods and computer software in recent decades, the modeling of such physical phenomenon can be more accurate and realistic. For example, time-history analysis of liquid tanks subjected to earthquake records can lead to a better understanding of the actual behaviour of such structures which can be included in future design codes.

In this study, a finite element method is used to solve the coupling equations governing fluid-structure-soil interaction in time domain. The advantage of this proposed method is that it can consider the effect of wall flexibility, three-dimensional geometry and viscous boundary conditions which is applied to soil media.

Also, problems associated with fluid damping characteristics and free surface are discussed. As mentioned before, the ANSYS computer program along with some additional computer subroutines are used for the purpose of liquid-tank analysis in time-domain.

In order to demonstrate the efficiency of the proposed method, a comparison between FE results and other analytical and experimental results are made to prove the validity of the numerical method.

Two different tank configurations representing shallow and tall tank model are analyzed in 2D and 3D spaces under bi-dimensional horizontal as well as vertical components of earthquake records. Both rigid and flexible wall boundary conditions are studied to investigate the effect of wall flexibility on pressure distribution and structural responses.

In addition, effect of earthquake frequency content and soil-structure interaction are studied by applying different ground motions and soil properties. Furthermore, sloshing behaviour is modeled using a linearized boundary condition. Contribution of three-dimensional geometry to development of sloshing waves is discussed in this study.

Finally, numerical modeling of slat screens and baffles as external dampers is presented in this research using a FE model. A parametric study has been done to investigate the effects of varying locations and solidarity ratio of the external dampers and earthquake frequency content on the sloshing response of the system.

### 8.2 Conclusions

Based on detailed finite element study reported in this thesis, the following conclusions are drawn:

1. The magnitude of impulsive structural responses obtained from time history analysis increases due to flexibility of side walls which is a result of dynamic pressure amplification in the middle of the wall. For example, the bottom pressure value of the flexible tank is about three times and two times higher than the corresponding values of the rigid shallow and tall tanks, respectively. On the contrary, the convective term is almost independent of the variations of flexibility of the side walls. However, the distributed convective pressure over the height of the liquid obtained from finite element analysis is different from that used in design codes. For example, the current practice assumes that the numerical value of convective pressure at the bottom of tank reaches to zero but the proposed FE method shows different results.
2. The peak values of impulsive and convective components do not occur at the same phase and time under time-history analysis. This is due to different frequency characteristics of impulsive and convective behaviour. As a result, convective terms may lead to increase or decrease the maximum absolute values of the structural responses in terms of base shear

and base moment. However, the overall response of liquid tank is governed by the impulsive term.

3. Applying the vertical excitations reveals in increase in the convective response of the system. However, it does not affect the impulsive behaviour significantly. The increase in convective response is more noticeable in tall tank model and is valid for both 2D and 3D tank models. Since the impulsive behaviour is governing the structural responses, it can be concluded that the vertical ground motion has insignificant effect on the overall dynamic behaviour of liquid tank system.
4. In comparison with FE results, the corresponding responses obtained by Housner's method which is used currently in current codes and standards in terms of impulsive shear and moment forces seems too conservative. For example, these values are about 100 percent higher than those obtained using FE method for rigid tank models.
5. The magnitude of both impulsive and convective structural base shear and base moment obtained from time history analyses are amplified due to three-dimensional geometry effect. For example, this increase reaches about 50 percent in tall tank model. Due to effect of three-dimensional geometry, the maximum sloshing height is highly amplified at the corner of liquid domain up to 70 percent. This is mainly because of the interaction of waves generated by two longitudinal and transversal components of earthquake at this location and needs to be considered in design codes.
6. The liquid tank behaviour is highly dependent on the earthquake frequency content. It is obvious that the records with frequency characteristics close to those of liquid tanks highly magnify the responses of the system. For a rigid foundation, the high-frequency earthquake results in the highest impulsive response in shallow tank model, whereas the

intermediate-frequency earthquake highly amplifies the tall tank model response. Due to the significant difference between impulsive and convective fundamental frequencies, a different trend is seen for the convective response. On the other words, for a rigid foundation, the intermediate-frequency earthquake results in the highest convective response in shallow tank model, whereas the low-frequency earthquake amplifies the tall tank convective response.

7. Considering the effect of soil-structure-interaction, the results show that the impulsive structural responses may increase or decrease as the soil stiffness changes. This is a result of dynamic pressure variation due to the rocking motion of the foundation. This phenomenon is highly dependent on earthquake frequency-content and tank configuration. However, the convective response is almost independent of variations of flexibility of the foundation and seems to be related to geometric configurations of tank, earthquake characteristics and liquid properties.
8. Slat screens and baffles are effective tools to reduce the magnitude of sloshing height in liquid tanks. However, their effectiveness is highly dependent on the frequency characteristics of applied earthquakes.

### 8.3 Recommendations for future studies

The fluid-structure-soil interaction can be investigated through peer studies as follows:

1. The interaction between flexural wall and fluid domain has not yet been quantified into a simplified and practical model. Once a reliable model is developed, fluid-structure interaction should be used in future studies to present the most accurate model for

predicting dynamic behaviour of liquid tanks. The FE results can be used as a tool to verify such models.

2. The effect of nonlinear sloshing behaviour on dynamic responses must be studied in future studies. On the other hand, a nonlinear surface boundary condition will lead to more accurate results beyond the parameters used in current study where the linearized surface boundary condition is applicable.
3. Further studies with different tank configurations and different fluid depths can be carried out to investigate the effect of size and fluid level on the seismic responses of liquid tanks.
4. The application of slat screens and baffles in designing an effective tuned liquid damper in tall buildings can be studied in future works. The numerical analysis can be carried out using the proposed finite element method.
5. The nonlinear behaviour of reinforced concrete including major cracking and crushing of concrete and yielding of steel bars can be investigated in future studies.
6. Additional tank models with top roofs can be studied to simulate the resulting pressure on tank roofs due to impact of the free surface sloshing.

## References


ACI 350.3-06, 2006. Seismic design of liquid-containing concrete structures (ACI 350.3-06) and commentary (350.3R-06). American Concrete Institute (ACI) Committee 350, Environmental Engineering Concrete Structures, Farmington Hills, Mich.

American Society of Civil Engineering (ASCE), 2005. Minimum design loads for buildings and other structures, ASCE Standard ASCE/SEI 7-05

Anrade W.P. 1999. Implementation of second order absorbing boundary condition in frequency domain computations, PhD Thesis. Texas: The University of Texas of Austin.

Anshel J.S. 1999. Kobe earthquake of January 17, 1995. Lifeline performance. 1995.ASCE Publication.

ANSYS Inc. ANSYS help manual (Version 11.1), 2004. Global headquarters, Southpointe, 275 Technology drive, Canonsburg, PA 15317

Bathe, K. J., 1996. Finite Element Procedures, Prentice-Hall, Englewood Cliffs.

Bowles, J.E., 1996. Foundation analysis and design. McGraw-Hill International Editions, 5th ed. Civil Engineering Series.

Chen, J.Z., and Kianoush, M.R. 2005. Seismic response of concrete rectangular tanks for liquid containing structures. Canadian Journal of Civil Engineering, **32**: 739–752.

Chopra, A.K. and Liaw, C.Y. 1975. Earthquake resistant design of intake-outlet towers. Journal of structural division. **101**(7): 1349-1366

Chopra, A.K. 1995. Dynamics of structures. Prentice-Hall. Upper Saddle River. N.J.

Clough, R, and Penzien, J. 1993. Dynamics of structures. 2nd Edition, New York: McGraw-Hill, Inc.

Cho, J.R. and Song, J.M. 2001. Assessments of the classical numerical models for the separate fluid-structure modal analysis. Journal of sound and vibration. **239**(5): 995-1012

Cho, J.R., Lee, H.W. and Kim, K.W. 2002. Free vibration analysis of baffled liquid-storage tanks by the structural-acoustic finite element formulation, Journal of Sound and Vibration **258** (5): 847–866.

Cho, K.H., Kim, M.K. and Lim, M.Y. 2004. Seismic responses of base-isolated liquid storage tanks considering fluid-structure-soil interaction in time domain. Soil Dynamics and Earthquake Engineering, **24**: 839-852

Cho, J.R., Lee, H.W. and Ha, S.Y. 2005. Finite element analysis of resonant sloshing response in 2-D baffled tank, Journal of Sound and Vibration **288** (5): 829–845.
CSA Standard A23.3. (2004). Design of concrete structures. Cement Association of Canada

Doganun, A. ,Durmus, A. and Ayvaz, Y. 1997. Earthquake analysis of flexible rectangular tanks using the lagrangian fluid finite element. Euro. J Mech.-A/Solids, **16**: 165-182

Dutta, S.C., and Roy, R. 2002. A critical review on idealization and modeling for interaction among soil-foundation-structure system. Computers and Structures. **80**: 1579-1594

Epstein, H.I. 1976. Seismic design of liquid-storage tanks. Journal of the Structural Division, **102**(9): 1659-1673

Edwards, N.W. 1969. A Procedure for Dynamic Analysis of Thin Walled Cylindrical Liquid Storage Tanks subjected to Lateral Ground Motions, Ph.D. Thesis, University of Michigan, Ann Arbor.

Eurocode 8. 1998. Design provisions for earthquake resistance of structures. European committee for standardization, Brussels

Fediw AA, Isyumov N, Vickery BJ. 1995. Performance of a tuned sloshing water damper. Journal of Wind Engineering and Industrial Aerodynamics. **56**: 237–47.

Foutch, D.H., Housner, G.W., and Jennings, P.C. 1975. Dynamic responses of six multistory buildings during the San Fernando earthquake. Report No. EERL 75-02, California Institute of Technology.

Fox, D. W., and Kuttler, J. R., 1983. Sloshing Frequencies, Journal of Applied Mathematics and Physics. **34**: 668-696.

Gedikli, A. and Erguven, M.E. 1999. Seismic analysis of a liquid storage tank with a baffle, Journal of Sound and Vibration. **223**(1): 141–155.

Ghaemian, M. and Ghobarah, A. 1997. Nonlinear seismic response of concrete gravity dams with dam-reservoir interaction. Journal of engineering structures. **21**(4): 306-315

Ghaemmaghami, A.R. and Kianoush, M.R. 2009. Effect of wall flexibility on dynamic response of concrete rectangular tanks under horizontal and vertical ground motions. ASCE Journal of Structural Engineering, Accepted for publication.

Hall, J.R., Kissenpfenning, J.F., and Rizzo, P.C. 1976. Discussion on the paper of soil-structure interaction analysis for seismic response. ASCE Journal of Geotechnical Engineering. **102**(6): 650

Haroun, M.A., and Housner, G.W. 1981. Earthquake response of deformable liquid storage tanks. Journal of Applied Mechanics, ASME, **48**: 411–418.

Haroun, M.A. 1983. Vibration Studies and Tests of Liquid Storage Tanks. Earthquake Engineering and Structural Dynamics, **11**: 190-206.

Haroun, M.A. 1984. Stress Analysis of Rectangular Walls under Seismically Induced Hydrodynamic Loads. Bulletin of the Seismological Society of America, **74**(3): 1031-1041.

Haroun, M.A., and Ellaithy, M.H., 1985. Seismically induced fluid forced on elevated tanks. Journal of Technical Topics in Civil Engineering, **111**, 1-15

Haroun, M.A., and Tayel, M.A. 1985. Response of tanks to vertical seismic excitations. Earthquake Engineering and Structural Dynamics, **13**: 583–595.

Haroun, M.A., and Abou-Izzeddine, W. 1992. Parametric study of seismic soil–tank interaction. I: horizontal excitation. ASCE Journal of Structural Engineering, **118**(3): 783–797.

Haroun, M.A., and Abou-Izzeddine, W. 1992. Parametric study of seismic soil–tank interaction. II: vertical excitation. ASCE Journal of Structural Engineering, **118**(3): 798-812.

Hoskins, L.M. and Jacobsen, L.S. 1934. Water pressure in tank caused by a simulated earthquake. Bulletin of the seismological society of America, **24**(1): 21-34

Housner, G.W. 1957. Dynamic pressure on accelerated fluid containers. Bulletin of the seismological society of America, **47**(1): 15-37

Housner, G.W. 1963. The dynamic behavior of water tanks. Bulletin of the Seismological Society of America, **53**(2): 381–387.

Ibrahim, R.A. 2005. Liquid sloshing dynamics. Cambridge University Press.

Jennings, P.C. and Kuroiwa, J.H. 1968. Vibration and soil-structure interaction tests of a nine-story reinforced concrete building. Bulletin of Seismological Society of America. **58**: 891-916

Karamanos S.A., Patkas, L.A., and Platyrrachos, M.A., 2006. Sloshing effects on the seismic design of horizontal-cylindrical and spherical industrial vessels, ASME J. of Pressure Vessel Technology, **128**(3), pp. 328-340.

Kianoush, M.R., and Chen, J.Z. 2006. Effect of vertical acceleration on response of concrete rectangular liquid storage tanks. Engineering Structures, **28**(5): 704–715.

Kianoush, M.R., Mirzabozorg, H. and Ghaemian, M. 2006 "Dynamic Analysis of Rectangular Liquid Containers in Three-Dimensional Space" Canadian Journal of Civil Engineering, **33**:501-507

Kim, J.K., Koh, H.M., and Kwahk, I.J. 1996. Dynamic response of rectangular flexible fluid containers. ASCE Journal of Engineering Mechanics, **122**(9): 807–817.

Koh, H.M., Kim, J.K., and Park, J.H. 1998. Fluid–structure interaction analysis of 3D rectangular tanks by a variationally coupled BEM–FEM and comparison with test results. Earthquake Engineering and Structural Dynamics, **27**: 109–124.

Livaoglu, R. 2008. Investigation of seismic behavior of fluid-rectangular tank-soil/foundation systems in frequency domain. Soil Dynamics and Earthquake Engineering, **28**(2): 132-146.

Lysmer J, and Kuhlmeyer R.L. 1969. Finite dynamic model for infinite media, ASCE. Eng Mech Div J, **95**: 859–77.

Mikishev, G.N. and Dorozhkin, N.Y. 1961. An experimental investigation of free oscillations of a liquid in containers, Izvestiya Akademii Nauk SSSR, Otdelenie Tekhnicheskikh Nauk, Mekhanika I Mashinostroenie, **4**: 48–83.

Mcverry, G.H., 1979. Frequency domain identifications of structural models from earthquake records. Report No. EERL 79-02, California Institute of Technology.

Minowa C. 1980. Dynamic analysis for rectangular water tanks. Recent Advances in Lifeline Earthquake Engineering in Japan: 135–142.

Minowa C. 1984. Experimental studies of seismic properties of various type water tanks. In: Proceedings of eighth WCEE, San Francisco: 945–52.

Mirzabozorg, H., Khaloo, A.R., and Ghaemian, M. 2003. Staggered solution scheme for three dimensional analysis of dam reservoir interaction. Dam Engineering, **14**(3): 147–179.

Modi, V.J. and Akinturk, A. 2002. An efficient liquid sloshing damper for control of wind-induced instabilities, Journal of Wind Engineering and Industrial Aerodynamics, **90**. 1907–1918.

Munshi, J.M. 2002. Design of liquid-containing concrete structures for earthquake forces, Portland Cement Association, ISBN 0-89312-219-X.

NASA special publications. 1966. The dynamic behaviour of liquid in moving containers. NASA SP-106, Washington, D.C.

New Zealand Standards Association. 2010. NZS3106: The New Zealand Code of Practice for Concrete Structures for the Storage of Liquids.

Noji T, Yoshida H, Tatsumi E, Kosaka H, Hagiuda H., 1988. Study on vibration control damper utilizing sloshing of water. Journal of Wind Engineering and Industrial Aerodynamics. **37**:557–66.

Panigrahy, P.K., Saha, U.K. and Maity, D. 2009. Experimental studies on sloshing behavior due to horizontal movement of liquids in baffled tanks. Ocean engineering. **36**:213-222

Park, J.H., Koh, H.M., and Kim, J. 1992. Liquid–structure interaction analysis by coupled boundary element – finite element method in time domain. *In* Proceedings of the 7th International Conference on Boundary Element Technology, Albuquerque, New Mexico, 1992. *Edited by* C.A. Brebbia and M.S. Ingber. Computational Mechanics Publication BE-TECH/92, Computational Mechanics Publications, Southampton, UK. Pp. 89–92.

Patkas, L.A., and Karamanos S.A., 2007., Variational solutions for externally induced sloshing in horizontal-cylindrical and spherical vessels, ASCE J. of Engineering Mechanics, **133**(6), 641-655.

Rai, D.C., 2002. Seismic retrofitting of R/C shaft support of elevated tanks. Earthquake Spectra, **(18)**: 745-760

Rashed, A.A., and Iwan W.D., 1984. Hydrodynamic pressure on short-length gravity dams. ASCE Journal of Engineering Mechanics, **110**(9): 1264-1283

Seed, H.B., and Lysmer, J., 1975. Soil-structure interaction analysis for seismic response. ASCE Journal of Geotechnical Engineering, **102**(6): 439-457

Sezen, H., and Whittaker, A.S., 2006. Seismic performance of industrial facilities affected by the 1999 Turkey earthquake. ASCE Journal of Performance of Constructed Facilities, **20**(1): 28-36

Song CH, Wolf JP. 1994. Dynamic stiffness of unbounded medium based on solvent damping extraction method. Earthquake Engineering and Structural Dynamics, **23**:1073–86.

Subhash, S., and Bhattachryya, S.K. 1996. Finite element analysis of fluid-structure interaction effect on liquid retaining structures due to sloshing. Computers and Structures, **59**(6): 1165-1171.

Sung, T.Y., 1953. Vibrations in semi-infinite solids due to periodic surface loading. ASTM STP. **156**: 35-68

Tait, M.J., El Damatty, A.A., Isyumov N. and Siddique M.R., 2005. Numerical flow models to simulate tuned liquid dampers (TLD) with slat screens. Journal of Fluids and Structures. **20**(8): 1007-1023

Tait, M.J., Isyumov, N. and El Damatty, A.A. 2007. Effectiveness of a 2D TLD and its numerical modeling. ASCE Journal of Structural Engineering, **133**(2): 251-263

Veletsos, A.S., and Tang, Y. 1986. Dynamics of vertically excited liquid storage tanks. ASCE Journal of Structural Engineering, **112**(6): 1228–1246.

Veletsos, A.S., Tang, Y. and Tang H.T. 1992. Dynamic response of flexibly supported liquid storage tanks. ASCE Journal of Structural Engineering, **118**: 264-283

Veletsos, A.S., and Yang, J.Y. 1977. Earthquake response of liquid storage tanks-advances in civil engineering through mechanics. ASCE Proceedings of the second engineering mechanics specially conference, Raleigh, NC: 1-24.

Veletsos, A.S., and Shivakumar, P. 1997. Tanks containing liquid or solids. A handbook in computer analysis and design of earthquake resistant structures. Computational mechanical publications: 725-774

Virella, J.C., Prato, C.A. and Godoy L.A. 2008. Linear and nonlinear 2D finite element analysis of sloshing modes and pressure in rectangular tanks subjected to horizontal harmonic motions. Journal of Sound and Vibration, **312**(3): 442-460

Warburton, G.B., 1982. Optimum absorber parameters for various combinations of response and excitation parameters. Earthquake Engineering and Structural Dynamics, **10**: 381–401.

Warnitchai P, Pinkaew T. 1998. Modelling of liquid sloshing in rectangular tanks with flow-dampening devices. Engineering Structures. **20**:593–600.

Westergaard, H.M. 1938. Water pressure on dams during earthquakes. Transaction, American society of civil engineers. **98**: 418-433

Wilson E.L. 2002. Three-dimensional static and dynamic analysis of structures- a physical approach with emphasis on earthquake engineering. 3rd Edition, Berkeley, California, USA: Computers and Structures, Inc.

Wolf J.P., and Song C.H. 1995. Doubly asymptotic multi-directional transmitting boundary for dynamic unbounded medium-structure-interaction analysis. Earthquake Engineering and Structural Dynamics: **24**(2): 175-188

Wolf J.P., and Song C.H. 1996. Finite element modeling of unbounded media. The 11$^{th}$ world conference on earthquake engineering, San Francisco 1996:70:1-9

Yang, J.Y. 1976. Dynamic behavior of fluid–tank systems. Ph.D. thesis, Department of Civil Engineering, Rice University, Houston, Tex.

Zienkiewicz, O. C., 1977. The Finite Element Method, McGraw-Hill Company, London.

# Appendices

## Appendix A: The Fluid subroutine reads fluid data file and generates associated matrices.

**All the procedure dealing with coupling has been brought here.**

```
c-----------------------------------------------------------------|
c       PROGRAM FLUID                                             |
|
c-----------------------------------------------------------------|
c            Amirreza Ghaemmaghami        November,2007           |
c                                                                 |
c-----------------------------------------------------------------|
c-------------------------------------------------------------fluidf
      subroutine fluidf (iaf,lnodef,lleleb,lekh,lekg,lekhg,ladresf,
     +   lcoordf,lloadf,ldummyg,ldummyh,ldispf,lvelof,laccef,
     +   lekd,ldummyc,rho,thkf,eqvelo,neqcomp,mtotf,llastf,
     +   lekb,nelerb,axgrv)
c       call fluidf (iaf,lnodef,lleleb,lekh,lekg,lekhg,ladresf,lcoordf,
c    +   lloadf,ldummyg,ldummyh,ldispf,lvelof,laccef,
c    +   lekd,ldummyc,rho,thkf,eqvelo,neqcomp,mtotf,llastf,
c    +   lekb,nelerb,axgrv)
c
      implicit double precision (a-h,o-z)
      common /cntrlf/ numnpf,numelf,nleleb,neletb,mbandf,nstof,neqf,
     +istag
      common /seismic/ am,bk,apha,bta,gama,dt,tt,ddat,dme,dmf,ic,kpd,kac
     +              ,ndata,bim
      common /bacupf/ iaccf,ivelf,idisf,nwetf
      common /gausstb/ sg(4),tg(4),wg(4),nint
      common /iolist/ ntm,ntr,nin,not,nsp,nfl,nt7,nt8,nt9,nt10,nt11(4)
     +,nfi,nfo,nfe
c
      CHARACTER*80 title
c      common iaf(150000)
      DIMENSION IAF(1)
C
C-----OPEN FILES FOR FLUID ------------------------
C
c     OPEN(60,FILE='teq.OUT',STATUS='NEW')
c     OPEN(65,FILE='force.OUT',STATUS='NEW')
c
C ## note: in combined prog. we can use the file name as *.fld
C ## where * is the input  file name
```

```
C
c
C-------------------------------------------------
c     mtotf =150000
c     call izerof (iaf,mtotf)
C
C     READ THE TITLE CARD FROM INUT FLUID FILE AND PRINT
C
      write (*,2000)
C
C     READ THE CONTROL IFORMATION
C
C      NUMNPF=number of fluid nodal points,
C      NUMELF=number of fluid elements
C      NLELEB=number of surface elements on the accelerated boundary
C      NELETB=number of surface elements on the truncated boundary
C      NELERB=number of surface elements on the reservoir bottom
C      RHO   = density of water
C      THKf   = velocity of sound in water
C      FACTOR= factor to magnify x,y and z coordinates
C
      read (nfi,2001) title
      write(nfo,2001) title
      k=0
      call findf ('FLUD',k)
      if (k .ne. 0) then
        write (ntm,1998)
        write (ntm,1998)
        stop
      else
        continue
      endif
C
      call pfreef
      call pfreei ('N',numnpf,1)
      call pfreei ('E',numelf,1)
      call pfreei ('B',nleleb,1)
      call pfreei ('T',neletb,1)
      call pfreei ('A',nelerb,1)
      call pfreei ('H',nnodedr,1)
      call pfreer ('R',rho,1)
      call pfreer ('V',thkf,1)
      call pfreer ('F',factor,1)
      call pfreei ('I',istag,1)
c     read (nfi,*) numnpf,numelf,nleleb,neletb,nelerb,nnodedr,rho,
```

```
c     +factor,thkf,istag
c
C     ECHO PRINT OF CONTROL INFORMATION
C
      icouple=1
      ieigf=0
      write (nfo,2002) numnpf,numelf,nleleb,neletb,nelerb,nnodedr,
     +rho,factor,thkf,istag
c      write (nfo,1999) istag
c
c     Reserve space in the array IAf for
c
c      nodal data=Restraints (numnp x 1) spaces
c      nodal coordinates=x,y and z coordinates (numnp x 6) spaces
c      element data=nodes
c                  =(numel x 8) spaces
c     surface element on the boundary of accelerationed=
c     4 nodes for each surface element and a code for ground acceleration
c                  =(nleleb*5) spaces
c
      lnodef=1
      llastf=lnodef+numnpf*1
      call defrf (llastf,lcoordf,numnpf*6)
      lelef=llastf
      llastf=lelef+numelf*8
      lleleb=llastf
      llastf=lleleb+nleleb*5
      if (llastf .gt. mtotf) call termif (llastf,mtotf)
c
c.....Reading of fluid input file
c
      write (*,2003)
      write (nfo,2003)
c
      call inpuf (iaf(lnodef),iaf(lcoordf),iaf(lelef),
     +iaf(lleleb),factor,nelerb)
c
c.....Assign equation numbers to pfree dof
c
      call eqnumf (iaf(lnodef))
      neqqf=neqf+1
      ladresf=llastf
      llastf=ladresf+neqqf
c
c.....bandwidth calculation and finding the diagonal address sequence
```

```
c.....of global stiffness [H] and mass [G] matrices.
c
      call bandwidthf (iaf(lnodef),iaf(lelef),iaf(ladresf),nnodedr)
c
      lekh=llastf
      lekg=lekh+nstof*2
      lekhg=lekg+nstof*2
      llastf=lekhg+nstof*2
      if (llastf .gt. mtotf) call termif (llastf,mtotf)
c
c.....Generate the fluid stiffness [H] and mass [G] matrices for each element,
c.....and assembling of element matrixces to global ones.
c
      write (*,2007)
      write (nfo,2007)
c
      call stifff (iaf(lnodef),iaf(lcoordf),iaf(lelef),iaf(ladresf),
     +iaf(lekh),iaf(lekg),iaf(lleleb),thkf,axgrv)
c
c.... reading of element on the boundary
      if (neletb.lt.1) go to 99
      lekd=llastf+1
c     leletb=lekd+nstof*2
c     ldummyc=leletb+neletb
      ldummyc=lekd+nstof*2
      llastf=ldummyc+neqqf*2
      if (llastf .gt. mtotf) call termif (llastf,mtotf)
c
c.....Input Elements no.
c
c     call findf ('EFTR',kb)
c     if (kb .ne. 0) then
c        write (nfo, *) 'ERROR IN READING OF ELEMENTS ON THE
c    + TRUNCATED BOUNDARY'
c        write (ntm,*)  'ERROR IN READING OF ELEMENTS ON THE
c    + TRUNCATED BOUNDARY'
c     stop
c     else
c     call readtb(iaf(leletb),neletb)
c     endif
c
c
c     call stifftb (iaf(lnodef),iaf(lcoordf),iaf(lelef),iaf(ladresf),
c    +iaf(lekd),iaf(leletb),thkf)
      call stifftb (iaf(lnodef),iaf(lcoordf),iaf(ladresf),
```

```
     +iaf(lekd),iaf(llelеb),thkf)
c
 99   continue
c
c.... reading of element on the tank bottom boundary
      if (nelerb.lt.1) go to 999
      lekb=llastf+1
cc      lelerb=lekb+nstof*2
c      ldummyc=leletb+neletb
c      llastf=ldummyc+neqqf*2
cc      llastf=lelerb+nelerb
      llastf=lekb+nstof*2
      if (llastf .gt. mtotf) call termif (llastf,mtotf)
c
      call findf ('EARB',kb)
      if (kb .ne. 0) then
         write (nfo, *) 'ERROR IN READING OF ELEMENTS ON THE
     + ABSORBTIVE RESERVOIR BOTTOM'
         write (ntm,*)  'ERROR IN READING OF ELEMENTS ON THE
     + ABSORBTIVE RESERVOIR BOTTOM'
      stop
      else
c      call readrb(iaf(lelerb),nelerb,qqa)
      call readrb(qqa)
      endif
c
      if(abs(qqa+1.d0).lt. 0.0001) then
      qqf=1e30
      else
      qqf=(1.d0-qqa)/((1.d0+qqa)*thkf)
      endif
cc      if(abs(qqa+1.d0).lt. 0.0001) then
cc     qqf=1000000.0
cc      else
cc      qqf=(1.d0-qqa)/((1.d0+qqa)*thkf)
cc      endif
c     if(abs(qqa-1.d0).lt. 0.0001) then
c      qqf=1e10
c      else
c      qqf=(1.d0+qqa)/(1.d0-qqa)*thkf
c      endif
      call stiffrb (iaf(lnodef),iaf(lcoordf),iaf(ladresf),
     +iaf(lekb),iaf(llelеb),qqf)
c
999   continue
```

```
c
c....reading of earthquake data from fluid input file
c....in the coupled system data already stored in ia(i).
c
      if (icouple.eq.1) go to 200
        leqdtf=llastf
      call eqdatf (iaf(leqdtf),llastf,mtotf,eqvelo,neqcomp,icouple)
c
C
200   continue
      lloadf=llastf
c     lwindof=lloadf+neqqf*2
c     lwetf=lloadf+neqqf*2
      ldummyg=lloadf+neqqf*2
c     ldummyg=lwetf+numnpf
      ldummyh=ldummyg+neqqf*2
      ldispf=ldummyh+neqqf*2
      lvelof=ldispf+neqqf*2
      laccef=lvelof+neqqf*2
      llastf=laccef+neqqf*2
c
c....place of ldummyc if there is no boundary and
c    no reservoir energy absorption
c
      if (neletb.lt. 1) then
      lekd=llastf+1
c     leletb=lekd+1
c     ldummyc=leletb+1
c     llastf=ldummyc+1
      llastf=lekd+1
        if(nelerb.ge.1) then
        ldummyc=llastf+1
        llastf=ldummyc+neqqf*2
        endif
      endif
c
c.....reservoir bottom absorbtion
c
      if (nelerb.lt.1) then
      lekb=llastf+1
c     lelerb=lekb+1
c     leletb=lekb+1
      llastf=lekb+1
      endif
c.......
```

```
c
      if((neletb.lt.1).and. (nelerb.lt.1)) then
c.....this is for the formation of the couple matrix if
c       there is no boundary or reservoir absorption
      nint=4
      call pgausstb (nint,sg,tg,wg)
c       write(nfo,*)'@@@@@@llastf',llastf
c       if (llastf .gt. mtotf) call termif (llastf,mtotf)
c
c       ldummyc=llastf+1
c       llastf=llastf+1
      endif
c
      if (llastf .gt. mtotf) call termif (llastf,mtotf)
      lavailf=mtotf-llastf
      write (nfo,2004) llastf,lavailf
c
c.....Check for eigen solution
c
      if (ieigf .eq. 0) go to 100
        write (nfo,3001)
        write (*,3001)
c         call eigsol (ia(ladres),ia(lstiff),ia(llast),neq,nsto,0.D0,
c     +   meig,mavl,imass,ia(lwindo),prd1)
  100 continue
c
c       write (nfo,2011)
c       write (*,2011)
c
c          call nseisf (iaf(lnodef),iaf(lleleb),
c     +    iaf(lekh),iaf(lekg),iaf(lekhg),iaf(ladresf),iaf(lcoordf),
c     +    iaf(leqdtf),iaf(lloadf),iaf(lwetf),iaf(ldummyg),
c     +    iaf(ldummyh),iaf(ldispf),iaf(lvelof),iaf(laccef),
c     +    iaf(lekd),iaf(ldummyc),rho,thkf,eqvelo,neqcomp,axgrvf)
c
c
c   ----------------------------------------------------------------
 2000 format(//' PROGRAM STARTS READING THE INPUT FLUID FILE '/)
 2001 format (a80)
 1998 format (/' THE FLUID DATA FILE SEPERATOR WITH  KEY WORD FLUD
     .IS MISSING'/
     .' PROGRAM STOPS. CHECK THE FLUID INPUT FILE')

 2002 format (//' THE CONTROL INFORMATION AS READ FROM THE INPUT FILE'/
     +/' Number of fluid nodal points:                    ',8X,i10,
```

```
     +/' Number of fluid elements:                          ',8X,i10,
     +/' Number of surface element on the accelerated boundary:',8x,i10,
     +/' Number of element on the free surface boundary:          ',8x,i10,
     +/' Number of element on the tank bottom:            ',8x,i10,
     +/' Number of nodes on liquid-tank boundary:            ',8x,i10,
     +/' Unit weight of water:                          ',8x,f10.3,
     +/' Coordinates are scaled by:                       ',8x,f10.3,
     +/' Velocity of sound in water:                      ',8x,f10.3,
     +/' Code for staggered solution schemes:                  ',8x,i10,
     +/' istag=1     displacement method                     ',
     +/' istag=2     pressure     method                     ',/)
 2003 format (//10X,'GOING TO STORE THE GEOMETRY OF FLUID DATA')
 2004 format (/' Required storage space(fluid domain): ',I10/'
    +Remaining storage space(fluid domain):',I10/)
 2007 format (//10X,' GOING TO GENERATE FLUID GLOBAL STIFFNESS [H] AND
    +MASS [G] MATRICES')
 2011 format (//10x,'** GOING FOR TIME DOMAIN SEISMIC ANALYSIS **')
 3001 format (//10X,' GOING TO SOLVE THE EIGENVALUE PROBLEM')
c
      return
      end
c     ----------------------------------------------------------------------INPU
      subroutine inpuf (ndof,coord,iele,ileleb,factor,nelerb)
      implicit double precision (a-h, o-z)
      common /cntrlf/ numnpf,numelf,nleleb,neletb,mband,nsto,neq,istag
      common /iolist/ ntm,ntr,nin,not,nsp,nfl,nt7,nt8,nt9,nt10,nt11(4)
     +,nfi,nfo,nfe
      dimension ndof(1,1),coord(3,1),iele(8,1),ileleb(5,1)
c
c     This routine reads the FLUID geometry, material, and other input data
c      from the specified input file and stores them either in the main
c      array Iaf or in the scratch files.
c
      iflag=0
c
c....Input nodal coordinates
      call findf ('NODE',kn)
      if (kn .ne. 0) then
        iflag=iflag+1
      else
        call nodeinf (coord,numnpf,factor)
      endif
c
c
c.....Input boundary conditions
```

```
c
      call findf ('BCON',kb)
      if (kb .ne. 0) then
        iflag=iflag+1
      else
        call bounf (ndof)
      endif
c
c
c.....Input element data
c
      call findf ('ISOP',ke)
      if (ke .eq. 0) then
        call eleinf (iele,numelf)
      else
        continue
      endif
      if (iflag .ne. 0) then
        write (ntm, 1001) iflag
        write (not, 1001) iflag
      else
        continue
      endif
c
c...Input surface element data  (this module was line element in previous ver.)
c
      call findf ('SELE',ke)
      if (ke .eq. 0) then
        call seleinf (ileleb,nleleb)
      else
        continue
      endif
      if (iflag .ne. 0) then
        write (ntm, 1001) iflag
        write (not, 1001) iflag
      else
        continue
      endif
c
c
c.....Echo print of the nodal data
c
      write (nfo,2002)
      do 200 i=1,numnpf
        write (nfo,2003) i,(coord(k,i),k=1,3),ndof(1,i)
```

```
  200 continue
c.....Echo print of element data
      write (nfo,4001)
      do 300 m=1,numelf
        write (nfo,4002) m,(iele(i,m),i=1,8)
  300 continue
c
c.....Echo print of surface element data
c
      write (nfo,4003)
      ii=0
      jj=0
      kk=0
      ll=0
      nn=0
      do 400 m=1,nleleb
        write (nfo,4004) m,(ileleb(i,m),i=1,5)
      if (ileleb(5,m).eq.1) ii=ii+1
      if (ileleb(5,m).eq.2) jj=jj+1
      if (ileleb(5,m).eq.3) kk=kk+1
      if (ileleb(5,m).eq.4) ll=ll+1
      if (ileleb(5,m).eq.5) nn=nn+1
  400 continue
      write(nfo,401) ii,jj,kk,ll,nn
401   format(2x,'Number of surface elements only have acceleration=',i7,
     + /,   2x ,'Number of surface elements on the truncated boun.=',i7,
     + /,   2x ,'Number of surface elements on the absorbtiv boun.=',i7,
     + /, 2x ,'Number of surface elements on the acc. + abso.boun.=',i7,
     + /, 2x ,'Number of elements on free surface=',i7)
      mm=kk+ll
      if(jj.ne.neletb) then
      write(nfo,4005) jj,neletb
      write(ntm,4005) jj,neletb
      stop
      endif
c
      if(mm.ne.nelerb) then
      write(nfo,4006) mm,nelerb
      write(ntm,4006) mm,nelerb
      stop
      endif
c     ------------------------------------------------------------
c
 1001 format (' ****** DATA READ ERROR ******',i2,/
     +' Material/nodal/element data starting with card identifier '
```